A New Integrated Approach for Modeling Green Passive Cooling Systems

by

Ali Gholami

B.Sc., Sharif University of Technology, 2011

Thesis Submitted in Partial Fulfillment of the
Requirements for the Degree of
Master of Applied Science

in the
School of Mechatronics System Engineering
Faculty of Applied Sciences

SIMON FRASER UNIVERSITY

Summer 2014

Approval

Name:	**Ali Gholami**
Degree:	**Master of Applied Science**
Title:	***A New Integrated Approach for Modeling Green Passive Cooling Systems***

Examining Committee: **Chair:** Behraad Bahreyni
Assistant professor

Majid Bahrami
Senior Supervisor
Associate Professor _____

John Jones
Supervisor
Associate Professor _____

Krishna Vijayaraghavan
Internal Examiner
Assistant Professor _____

Date Defended: August 11, 2014

Partial Copyright License

Abstract

A new one-dimensional thermal network modeling approach is proposed that can accurately predict transient/dynamic temperature distribution of passive cooling systems. The present model has applications in a variety of electronic and power electronic systems. The main components of any passive cooling solution are heat spreaders, heat pipes, and heat sinks as well as thermal boundary conditions such as natural convection and radiation heat transfer. In the present approach, all the above-mentioned components are analyzed, analytically modeled and presented in the form of resistance and capacitance (RC) network blocks. The proposed RC model is capable of predicting the transient/dynamic as well as steady state thermal behavior of the targeted passive cooling systems with significantly less cost of modeling compared to conventional numerical simulations. Furthermore, the present method takes into account thermal inertia of the system and is capable of capturing thermal lags in various system components under all applicable operating conditions. To validate the proposed model, a number of custom-designed test-beds are also built and a comprehensive experimental study is conducted.

Keywords: Thermal management of power electronic and telecom systems; Passive cooling system; Resistance capacitance (RC) network modeling; Dynamic loading; Anisotropic heat spreader

I would like to dedicate my thesis to my beloved family

Acknowledgements

I wish to express my sincere thanks to my senior supervisor, Dr. Majid Bahrami, for his expert, sincere and valuable guidance and encouragement extended to me. Without his guidance and persistent help this dissertation would not have been possible.

I would like to thank my senior colleague; Mr. Mehran Ahmadi, who helped me a lot during my study with his knowledge and valuable experience.

I also thank Mr. Marius Haiducu, our research group passionate lab engineer, for his absolute and unconditional help throughout the experimentation of my study.

I take this opportunity to record my sincere thanks to all my friends and colleagues who directly or indirectly, have lent their helping hand in this venture.

Table of Contents

List of Tables

List of Figures

Glossary

A, B	Temperature solution coefficients
$A_{source/sink}$	Sources or sinks area (m^2)
C	Capacitance (J/K)
F	View factor
L	Length (m)
L_e, L_c	Heat pipe evaporator and condenser length (m)
Q	Heat flow (W)
R	Resistance (K/W)
Ra	Rayleigh number
T	Temperature (K)
V_i	Volume of component I (m^3)
W	Width (m)
X_i, Y_i	Source/sink center coordinates (m)
a_i, b_i	Source or sink's length and width (m)
c_p	Specific heat capacity (J/kg.K)
g	gravity (m/s^2)
h	Convective heat transfer coefficient ($W/m^2.K$)
k	Thermal conductivity (W/m.K)
m, n	Number of eigenvalues
m_i	Mass of component I (kg)
n_f	Number of heat sink fins
p	Fin depth (m)
q	Heat flux (W/m^2)
r	Radius (m)
s	Fin spacing (m)
s_{ij}	Auxiliary coefficients of temperature solution
θ	Dimensionless temperature
α	Thermal diffusivity (m^2/s)
β	Thermal expansion coefficient (1/K)
ε	Width to length ratio of plate
ε_H	Height to length ratio of plate

ε_i	Emissivity of surface i
κ_x, κ_y	In-plane to through-plane thermal conductivity ratio in x and y directions
λ, δ, β	Temperature solution eigenvalues
σ	Stefan-Boltzmann constant ($W/m^2.K^4$)
v	Kinematic viscosity (m^2/s)

Executive Summary

Efficient thermal management in electronics and high power electronics is essential for optimum performance and durability. Generated heat inside the components must be dissipated effectively to eliminate the heat build-up and improve the reliability by preventing premature failure. More than 65% of system failures in high-power electronics and telecom systems have thermal roots. In optoelectronics, photonics and microelectronics, the ability to understand, predict and possibly minimize the thermal stresses, e.g. brittle fracture, thermal fatigue, thermal shock and stress corrosion is of crucial importance. Among different cooling techniques, passive cooling methods are widely preferred since they provide low-cost, no-parasitic power, quiet operation and reliable cooling solutions. One efficient method to model transient thermal systems is using thermal resistance-capacitance (RC) networks that are analog to electrical circuits. In this analogy, voltage and current stand for temperature and heat flow rate, respectively. The focus of this study is on development, experimental validation and industrial application of such methods.

Motivation

Laboratory for Alternative Energy Conversion (LAEC) at Simon Fraser University in a collaborative project with Alpha Technologies Company, plans to: i) improve the performance, reliability and operating cost of the cooling systems of Alpha's telecommunication and power electronics systems; ii) transform Alpha's cooling systems from the current active fan-cooled systems, which consume considerable amount of electricity, to fully passive systems; and iii) assist Alpha to redesign its next-generation sustainable 'green' high-power electronics and telecom systems. Alpha's 1.2kW AC/DC rectifier current design has 7 heat-generating components, including MOSFETs and diodes. Each module is cooled by a single 6W fan which blows air over the heat sinks that are attached directly to the MOSFETS, Preliminary a. In the proposed 'green' design, all the heat sinks and fan are removed and replaced by passive cooling components, i.e., a series of heat spreaders and heat pipes that take the heat from MOSFETs to the enclosure walls with no parasitic power consumption nor noise. The enclosure walls are finned and work as natural convection heat sinks which

dissipate the heat to the ambient passively (Preliminary Figure 1b). Other features of the proposed passive cooling system include its robustness and superior reliability compared to existing active cooling system that uses fans. Electrical fans will eventually fail and lead to thermal and electrical failure, which means costly repair and maintenance.

To achieve this project's goals, our research team started with performing a thorough study on different passive cooling system components, i.e. heat pipes, heat sinks, and heat spreaders, and developed compact models that can predict thermal behavior of the system for optimizing the cooling design.

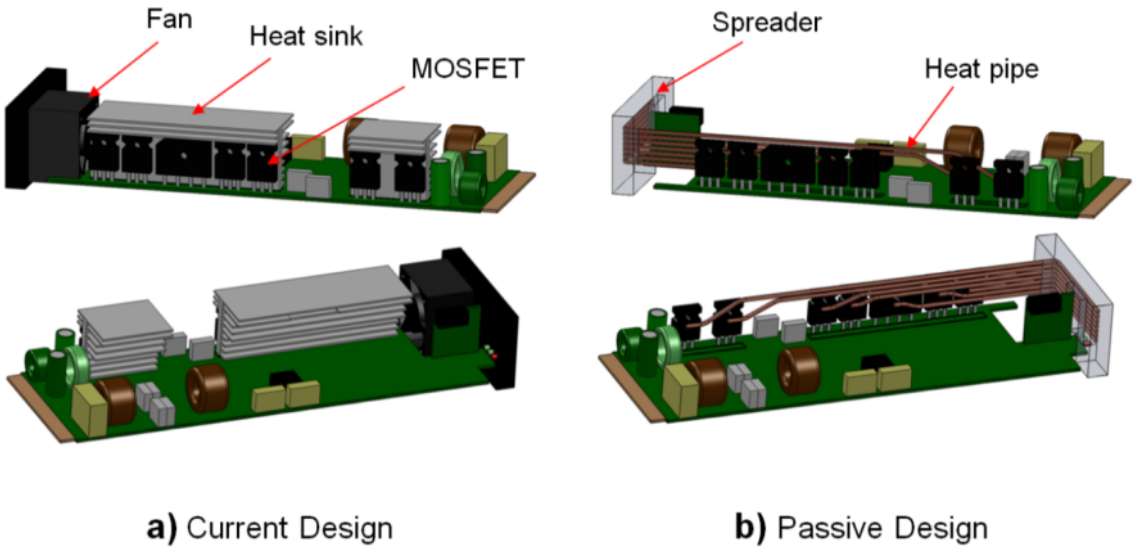

Preliminary Figure 1: 1.2kW AC/DC rectifier cooling systems; a) current design, b) passive-cooled design

Research objective

The objective of this research can be summarized as following,

- To remove all the active cooling components, i.e. rectifiers' primary fans, heat exchanger fans, and the air-to-air heat exchanger from Alpha enclosures and to replace them with fully passive cooling systems.
- Integrating heat pipes in the cooling system to transfer the heat from the hotspots to either cold plates or heat sinks.

- Optimizing the heat spreader design and implementing it in the proposed passive cooling system to achieve efficient heat transfer between components and reduce the operating temperature of MOSFETS and other components.
- Developing an analytical model for thermal resistance/capacitance of each component in the passive cooling systems, including heat spreaders, heat pipes and heat sinks.

Methodology

In this thesis an analytical thermal resistance network model which is capable of simulating the entire range of cooling solutions from module/component-level to system-level is presented. To develop the model, first, all the components of the targeted cooling system (including heat sink, heat pipe, heat spreader, etc.) are modeled individually by a network of resistances and capacitances (R and C). Knowing thermal resistances and capacitances, an RC model can be constructed and analyzed rather readily using any appropriate software. RC modeling enables simulation and accurate prediction of the thermal behaviour of any cooling system at any desired time or location in the system, undergoing any arbitrary operation loading scenario. To validate the proposed model a prototype of multi heat source passive cooled system is designed, built and tested. This test-bed is tested under different combinations of constant and dynamic loading of heat sources. The transient and dynamic behavior of the system and the effect of thermal inertia on the system response are also investigated. The test results are used to validate the model with maximum relative difference of 4.5%. The flowchart in (Preliminary Figure 2) presents the summary of this study.

Along with RC modeling approach for passive cooling systems, graphite-based heat spreaders are investigated and their impact on performance improvement of cooling systems is studied. A comprehensive parametric study on thermal resistance of such heat spreaders is performed for optimization purposes.. Using an existing thermal conductivity measurement test-bed, through-plane thermal conductivity of several graphite sheets is measured to investigate their appropriateness and performance for thermal interface material (TIM) and heat spreader applications. A custom-designed test-bed for measurement of in-plane thermal conductivity of anisotropic materials such as graphite-based plates is also designed and built.

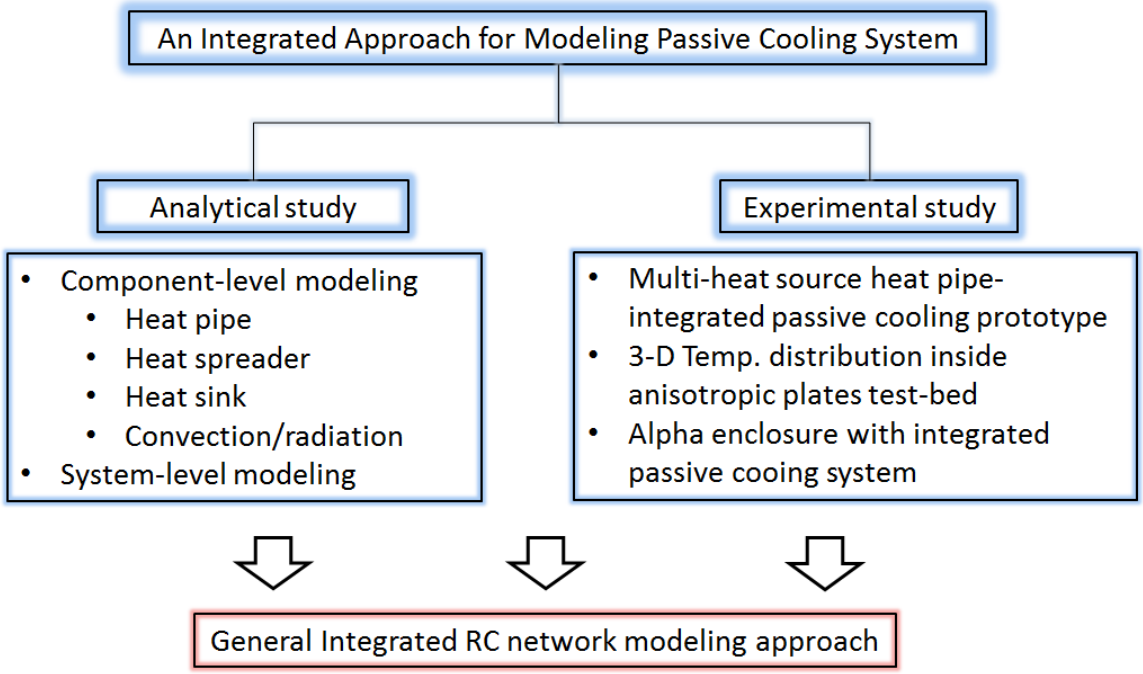

Preliminary Figure 2: research road-map

Chapter 1. Introduction

1.1. Importance of thermal management for electronics and power electronics systems

Efficient thermal management in electronics and high power electronics is essential for optimum performance and durability. Power electronics, as a family of electronic systems, are an essential part of high power systems, which are mainly responsible for converting electrical power from one form to another. Due to high operating currents and voltages thus higher heat generating rates, these systems are more susceptible to thermal stresses and failures and need extra careful cooling solution design. Telecommunications, power generation systems, heavy-duty transportation and aerospace systems are some of main areas for application of power electronics (Figure 1). According to Yole Développement Inc., an international marketing consultant group, the total market for power electronics industry (including power IC, power modules and power discrete devices) was $19 billion in 2011 and is expected to ramp up to more than $35 billion by 2020 [1].

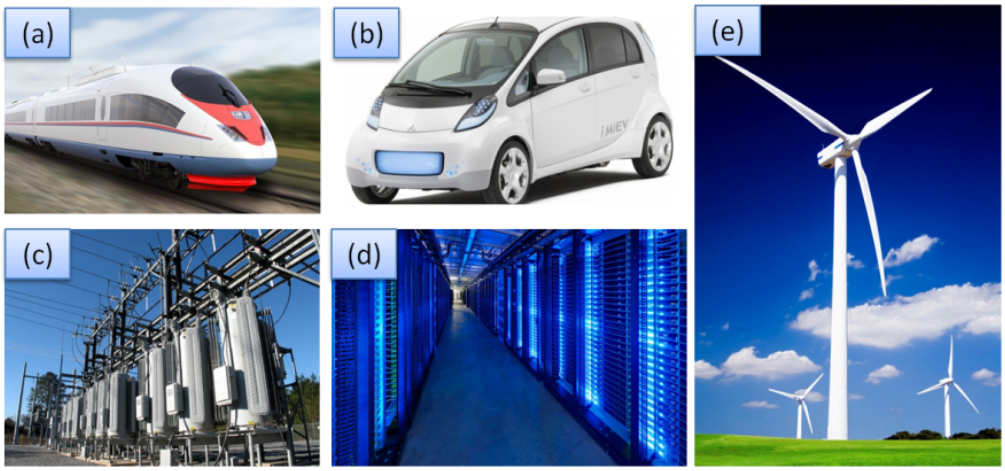

Figure 1: Different applications of power electronics; a) Heavy duty transportation, b) electric vehicles, c) Power plants, d) data centers, e) wind turbines

In electronic and power electronic systems, electrical resistance of components is the main source of heat generation. This generated heat must be dissipated effectively to eliminate the heat build-up and improve the reliability by preventing premature failure. In fact, more than 65% of system failures have thermal roots [2]. Electronic components are observed to fail under prolonged use at high temperatures. A number of failure mechanism which are directly linked to thermal effects are diffusion in semiconductor materials, inter-metallic growth and metal migration caused by chemical reaction, and void formation as a result of creep [3][4]. As shown in Figure 2, the rate of electronic devices failure increases almost exponentially with operating temperature [5], [6]. According to Arrhenius's law, the rate of these failures is approximately doubled with every 10°C increase in the operating temperature of the device [7]. The following paragraphs are dedicated to some facts about the importance of thermal management in different industrial applications.

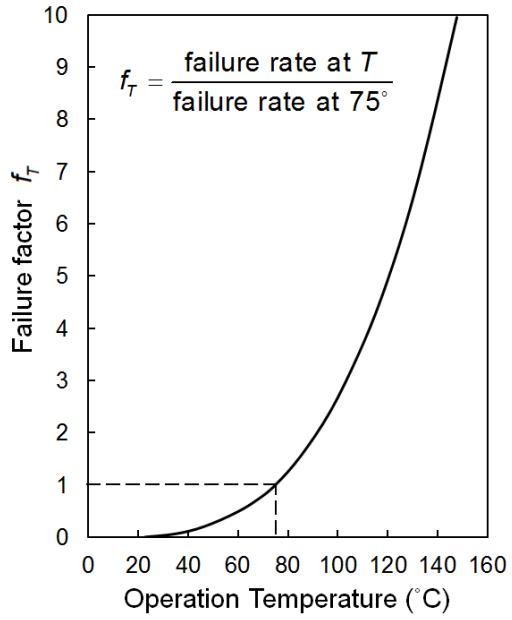

Figure 2: Arrhenius law: Failure rate of electronics at different operating temperatures [5], [6]

Telecommunications systems and data centers: The tremendous amount of energy consumption, approximately 40% for cooling purposes, has become a major concern for thermal engineers [8]. The worldwide electricity usage of data centers excluding the contribution of external networking (i.e., the transport of information between a broader network of data centers) has increased between 2000 and 2005 from

71 billion kWh per year (0.53% of the worldwide total electricity usage in all sectors) to 152 billion kWh per year (0.97% of the worldwide usage), representing a growth of about 10% per year. In terms of the annual electricity consumption for 2005, data centers rank between the national consumption of Mexico and Iran [8].

Hybrid Electric Vehicles (HEVs), Electric Vehicles (EVs) and Fuel Cell Vehicles (FCVs): Thermal management of the batteries has been a major challenge for the automotive industry since the invention of such technologies. Making a national commitment to building HE/E/FC vehicles and most of their components in the United States, the federal government has invested $2.4 billion in electric battery production facilities and nearly $80 million per year for the battery research and development. It is expected that 1 million plug-in electric vehicles would be sold by 2015 with estimated battery cost of $8,000 to $18,000 per vehicle [9]. As all batteries, depending on their type, have specific temperature ranges within which the optimum performance occurs, providing efficient thermal management techniques for such expensive components will have a huge impact on ever-growing HE/E/FCV market [10].

The global market for thermal management products is expected to grow from $10.1 billion in 2013 to $10.6 billion in 2014 and $14.7 billion by 2019, a compound annual growth rate increase of 6.4% (Figure 3). Specifically for power electronics, this value is expected to reach $4.8 billion in 2020 [11]. Thermal management hardware, e.g. fans and heat sinks, accounts for about 84% of the total market. Other main cooling product segments, e.g. software, interface materials, and substrates, each account for between 4% and 6% of the market, respectively. The North American market will maintain its number-one position throughout this period, with a market share of about 37%, followed by Asia-Pacific with approximately 23% to 24% [12].

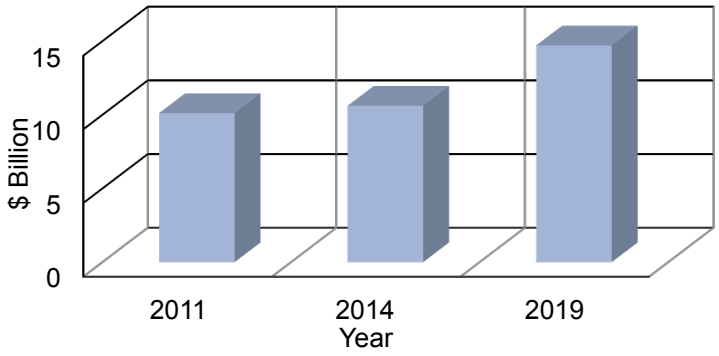

Figure 3: World thermal management market trends, 2011-2019 [12]

The above-mentioned economic statistics clearly demonstrate the critical significance of proper thermal management and efficient cooling strategies for electronics and power electronics especially in the future of this industry.

1.2. Miniaturization and heat flux density

Another issue that intensifies the challenges of thermal management for electronic and power electronic devices is the ever-continuing trend of miniaturization and compactness of such systems, which consequently leads to increasing heat flux at component and system level. If these cooling requirements are left unchecked, it will result in thermal failure, reduced life and reliability which is not acceptable by the industry and the market.

After the introduction of transistors in 1948 and integrated circuits (IC) in 1959, the development of microprocessors in 1970s pioneered by Intel Corporation marked another beginning in the industry of compact electronic chips which have been continued until now. According to Moore's Law, named after Gordon Moore, the co-founder of Intel Corporation, the number of transistors on ICs doubles approximately every two years [13]. As shown in **Error! Reference source not found.**, the Moore's law has been held since 1965 until recently. This ever-increasing trend in power density and compactness of ICs which are the fundamental of electronics and telecommunication industries leads to higher power consumption and consequently a crucial need for efficient thermal management and cooling solutions.

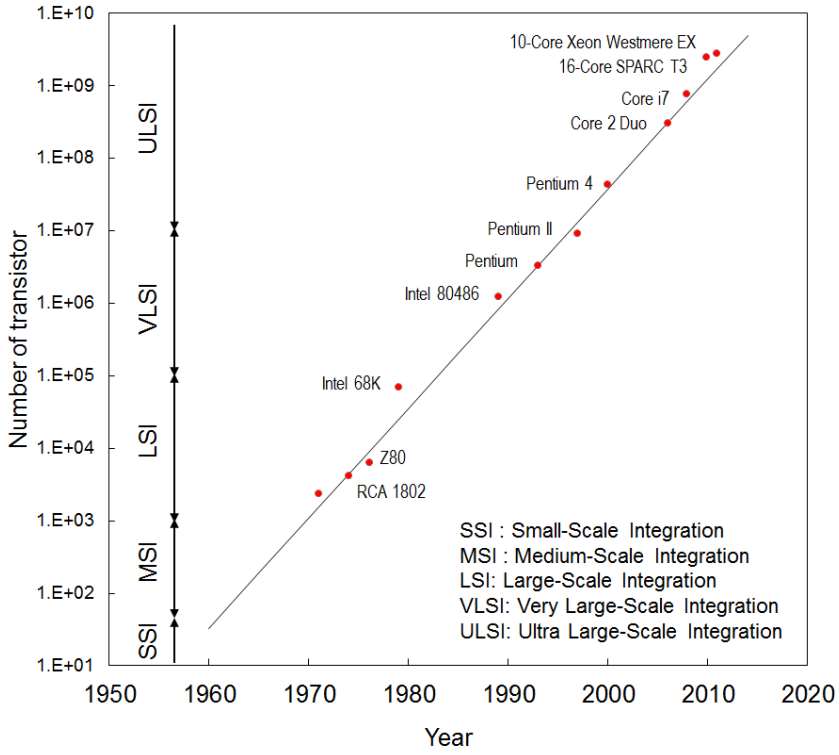

Figure 4: Microprocessor enhancement over the past 50 years [13]

The similar trend is observed in power electronics and telecom systems. The evolution of power electronics can be categorized into four generation based on the specified design rules as indicated in Figure 5 [14], [15]. The first generation starting in 1958 was when thyristor-type devices dominated and lasted around 17 years. In the second generation, lasting about 10 years, self-controlled power devices (BJT[1]s, power MOSFET[2]s, and GTO[3]s) appeared along with power ICs. In the third generation, the most dominant power device, the IGBT[4], was introduced and became an important milestone in power electronics history. Currently, in the fourth generation, new devices such as IGCT[5]s and cool MOSs emerged with the design rule length of less than 1μm.

1 Bipolar Junction Transistor
2 Metal–Oxide Semiconductor Field-Effect Transistor
3 Gate Turn-Off thyristor
4 Insulated Gate Bipolar Transistor
5 Integrated Gate-Commutated Thyristor

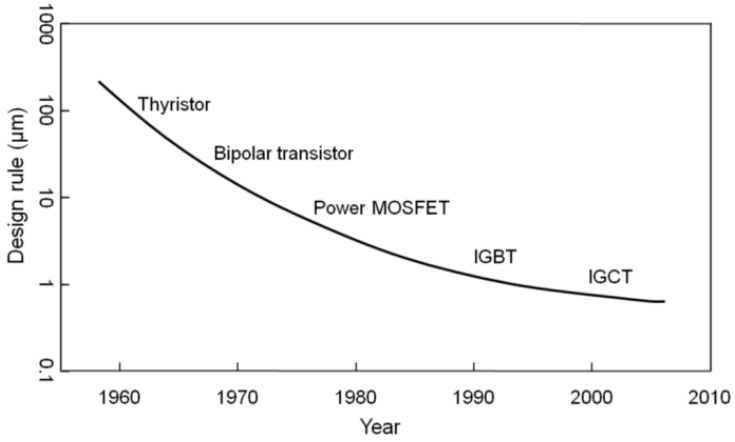

Figure 5: Power electronics enhancement over the past 50 years [14], [15]

The continued growth in performance and functionality of telecom, microelectronics, power electronics, and photonics systems combined with miniaturization trend in the industry have resulted in a significant increase in heat generation rates [3], [16], [17], and presents a great challenge to thermal engineers. Currently typical heat flux densities are in the range of 5 to 500 W/cm^2 for power semiconductor devices, 0.1 to 5 W/cm^2 for magnetic components and below 0.1 W/cm^2 for capacitors [18], [19]. High-power systems such as supercomputers, high power devices and electric vehicles have reached heat generation rate of around 1,000W/cm^2 and higher and this trend is only expected to continue [20], Figure 6. The extreme case occurs in ultra-high heat flux systems where heat fluxes increase by an order of magnitude [21]. As an example, electronic components of fusion reactors or multi-megawatts continuous-wave magnetrons used for short-pulse lasers and radars produce approximately 10-15 kW/cm^2 and higher [21].

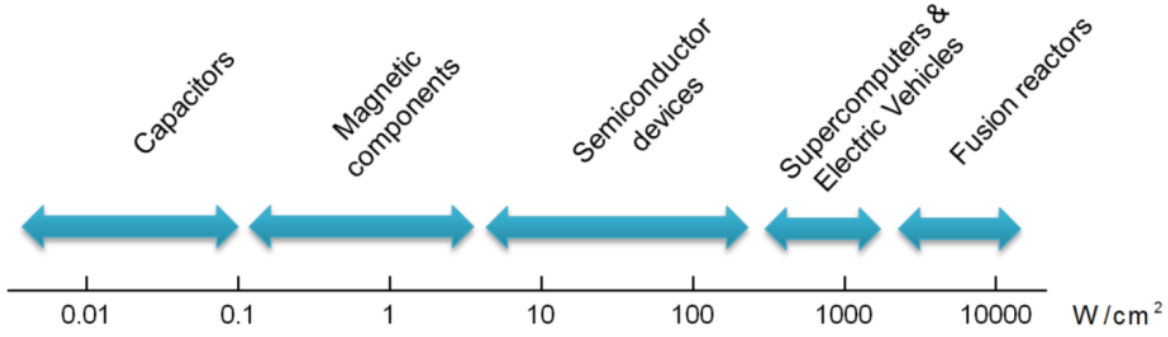

Figure 6: Heat flux density range for power systems [18], [19], [22]

The ever-increasing trend for power density and compactness of power electronics implies that thermal management is becoming the limiting factor in the design and development of higher power electronic devices. Therefore, new reliable and cost effective methods of cooling are required. To achieve this goal, a strategic approach along with a strong knowledge of heat transfer and energy systems is required.

1.3. Non-steady thermal load

Most of electronics and power electronics equipment do not work steadily and experience some fluctuations and transitions in their operation. Such systems require to continuously adjust their output based on the imposed demand. For example, the demand in telecommunication systems could be the number of simultaneous subscriptions to a network, or the amount of data traffic through a specific equipment. Most of these devices also experience an unsteady loading during start-ups and shut-downs. In addition to that, some other environmental effects such as ambient temperature fluctuation and solar gain impose an extra unsteady thermal load on such systems. Researchers at MIT Senseable City Lab in 2012 [23] conducted a major study analyzing 12 huge datasets corresponding to 12 networks from 3 different continents consisting of 33GB of data, and reported weekly and daily pattern of data consumption. In Figure 7, the average total weekly pattern of the data usage in Asia is depicted. As seen, the consumption pattern is transient and dynamic rather than being steady-state in the scale of days. Having a closer look at the data consumption on Monday, a similar unsteady trend in the scale of hours can also be observed. This constantly varying data transfer in communication systems requires the electrical components to function accordingly in a transient manner, which results in unsteady heat generation in the system. This behavior can almost be extended to any electronics and power electronics devices, e.g., stop-start driving cycles in hybrid electric vehicles, earth orbital cycle and climate changes in photovoltaics (PV) systems, etc. The unsteady operation leads to a transient heat generation profile at the component and device level, which should be carefully considered in any successful cooling solution to provide a reliable and efficient operation.

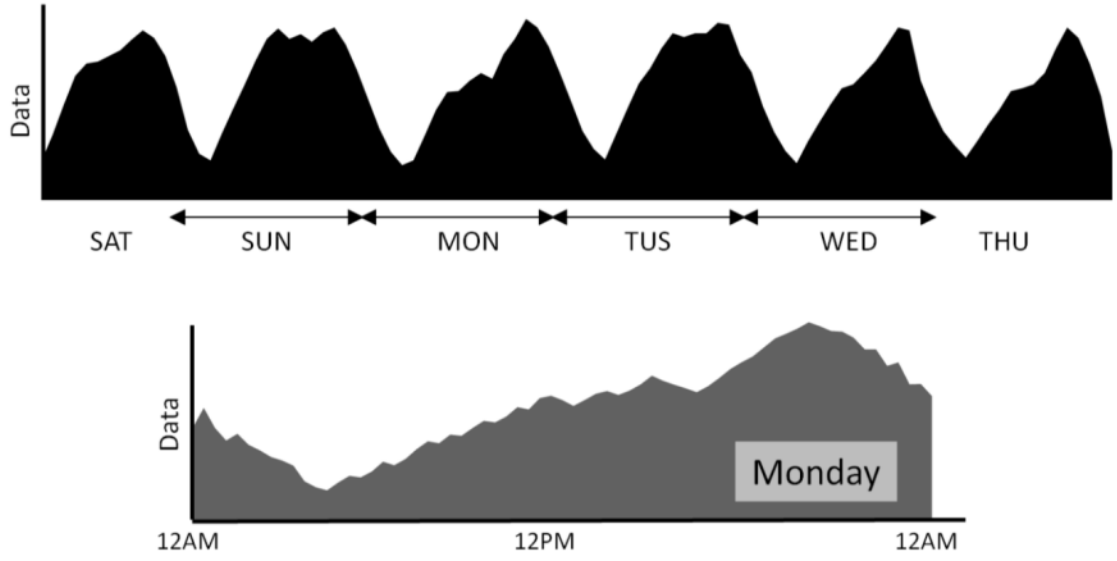

Figure 7: Qualitative map of weekly (top) and daily (bottom) data consumption of Asian [23]

1.4. Cooling mechanisms

There are different cooling techniques available for electronics and power systems whose applications depend on different factors. Required cooling capacity, physical confinements, environmental conditions, cost and compatibility requirements are some of the most important criteria that can determine which method to use for a particular system. Cooling methods in general can be categorized in two major groups; active cooling and passive cooling. Active methods are the ones in which a power source is required to run the cooling system. There are different types of active cooling mechanisms, such as fan-assisted cooling, spray cooling, refrigeration cycles, jet-impingement cooling, and electro-wetting cooling. Each of these methods has its own range of applicability in term of heat dissipation capacity. Among mentioned methods, two-phase cooling mechanisms due to very large value of boiling latent heat of coolant have much higher capacity than single-phase methods. In most of the high and ultra-high heat flux systems single phase methods do not meet the requirements and two-phase should be implemented.

Another major group of cooling systems are passive methods which do not require a power source to operate. These methods have generally less heat dissipation capacity compared to active ones but they are widely preferred for electronic and power electronic devices since they provide low-cost, no parasitic power, quiet operation and reliable cooling solutions. Due to the absence of moving parts in most of the passive cooling systems, they do not need regular maintenance and are very reliable. The most important component of a passive-cooled system is heat sink which is in direct contact with the ambient. Such passive techniques are drawing more attention because they are "green" and air is the most accessible coolant, particularly for applications in hostile environments, e.g. contaminated air, vibrations, noise, and humidity. Other components of such systems may include heat spreaders, heat pipes, and thermal energy storage systems that may include phase change materials (PCM).

Heat pipes come in different shapes and geometries depending on their application. By taking advantage of thermo-syphon and capillary effects, they can effectively transport the heat through their special interior structure. Figure 8 shows the comparison between the supporting range of effectiveness for each cooling method for two most common fluids; air and water [21].

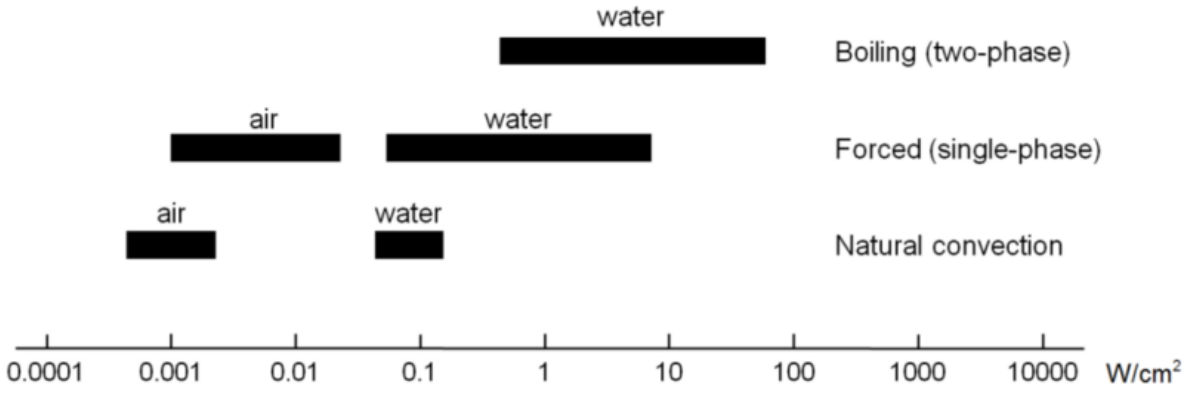

Figure 8: Cooling capacity of different cooling mechanism for air and water [21]

1.5. Alpha project

In 2013, Laboratory for Alternative Energy Conversion (LAEC), at Simon Fraser University (SFU), in close collaboration with a local industrial partner, Alpha Technology

Ltd., planned to design and build a novel fully passive cooling system for Alpha's Outside Plant (OSP) power system supplying a nominal power of 14.4 kW, with the long-term plan of extending the design to bigger high-power systems. The dimensions and weight of the enclosure are 60cm×55cm×110cm and 65 kg, respectively. Figure 9 shows the 14.4 kW OPS with its current active air-forced cooling system.

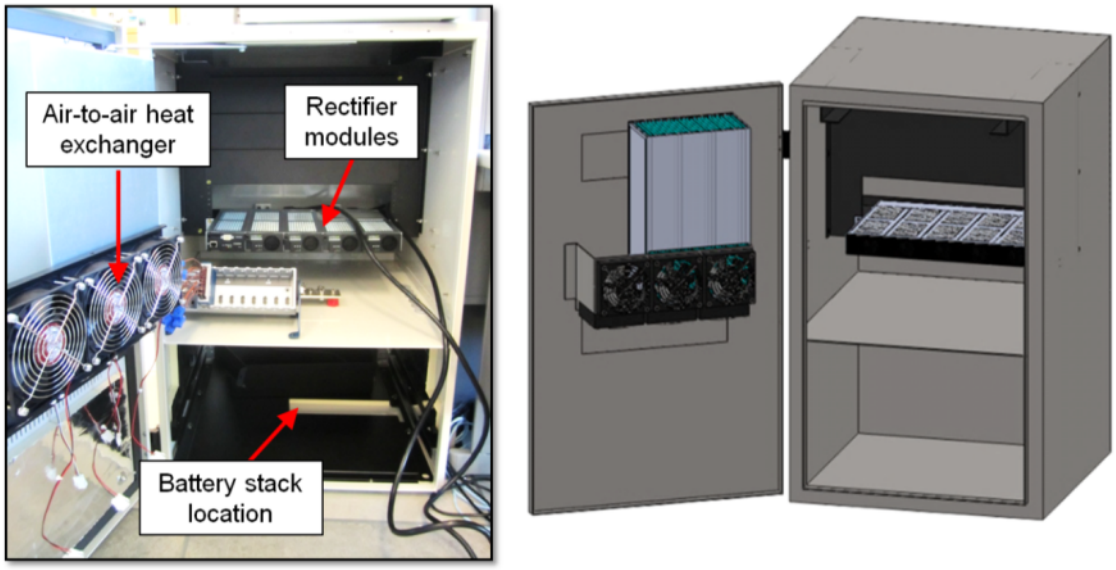

Figure 9: Alpha Technology Company's Outside Plant power system

Inside the enclosure, there are three racks of rectifier modules each containing four 1.2 kW rectifiers, located approximately at the center. There is also a battery compartment at the bottom of the enclosure, accommodating two emergency lead-acid battery packs (Figure 9). Each rectifier consists of a densely populated printed circuit board (PCB), enclosed in an aluminum casing. The critical components inside the rectifiers that require thermal management are 6 MOSFETs, one diode, and one transformer (Figure 10). The design parameters of these components are presented in Table 1.

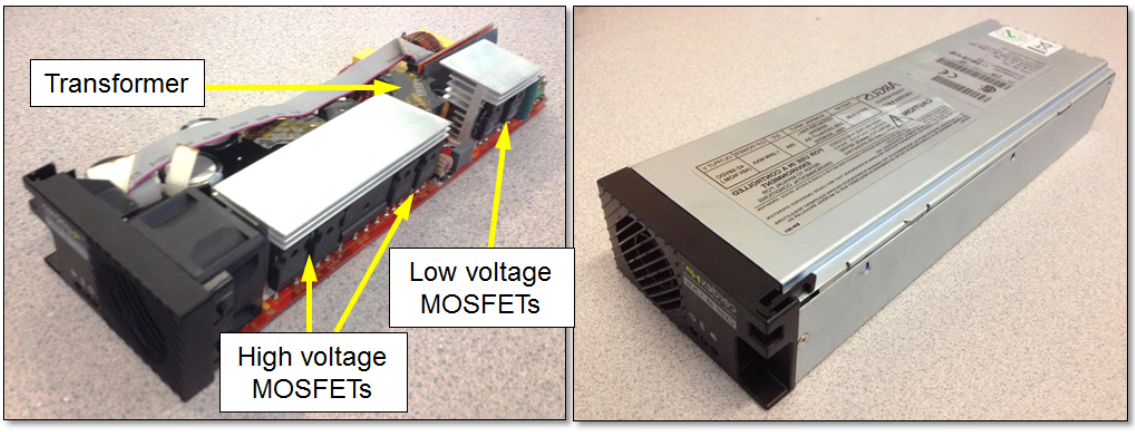

Figure 10: Alpha Technologies 1.2 KW rectifiers, fan assisted cooling system

Table 1: Design parameters for Alpha's rectifiers working condition

Parameter	Design value [˚C]
Maximum allowable temperature of MOSFETs	85
Maximum allowable temperature of transformer	145
Highest ambient temperature (for shaded enclosure)	46
Maximum allowable temperature difference between inside-air and ambient	10

The existing cooling system for the enclosure consists of a two-stage active cooling mechanism. As the first stage, each rectifier has one 6 W fan positioned at the front face which sucks the air from the inside of the cabinet and blows it over the heated components producing a forced convection cooling effect. In the second stage, an air-to-air heat exchanger, that consists of three 18 W fans, rejects the heat to the ambient using an air to air heat exchanger that is installed inside the cabinet. The air to air heat exchanger is installed to prevent the dust and humidity of the outside air entering the enclosure.

The method of thermal management used by Alpha, in its current form, has several drawbacks which are listed as follows:

- There is not a uniform cooling effect for all the hotspots. The components closer to the fan receive colder air than the ones downstream as the air temperature rise passing each component. Also, the components on the way of the blowing air act as obstacles so the further components do not receive as much air as the front ones do. The numerical simulation and experimental

results of temperature distribution for one rectifier operating full load, qualitatively depicted in Figure 11, confirms this fact.

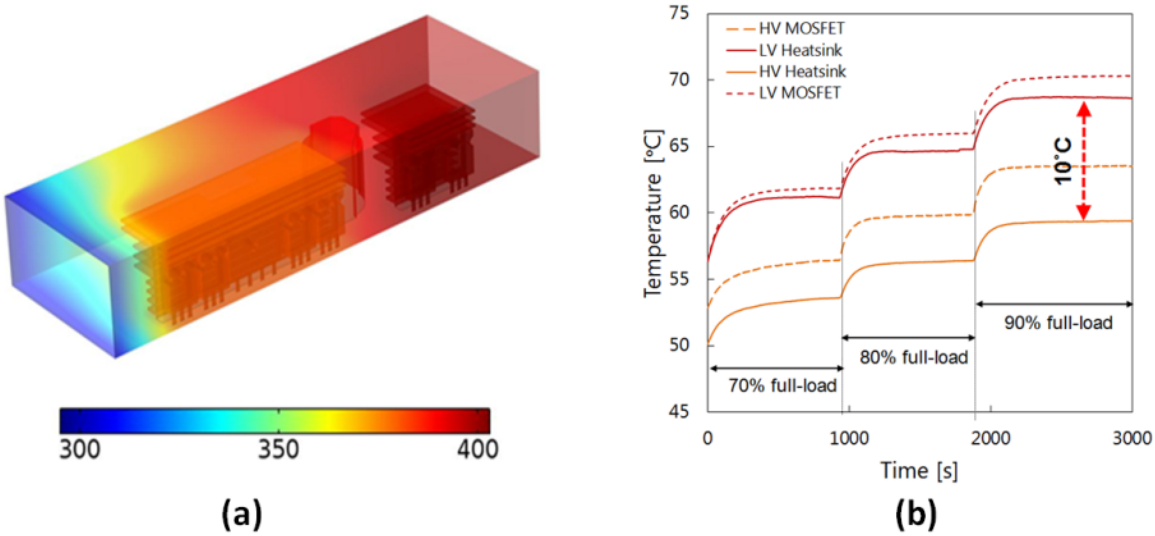

Figure 11: Numerically-modelled temperature distribution of fan cooled full-load rectifier (uniform heat generation is considered) (a); Experimental data of the fan-cooled rectifier (b)

- This cooling mechanism consists of two sets of fans which consume a considerable amount of parasitic power to the system resulting in lower overall efficiency.
- Due to the existing fans as an essential part of the cooling mechanism, the whole system requires regular maintenance which adds an additional cost and reduces reliability.
- The system cannot be sealed as the electronics has to be exposed to the surrounding medium to be cooled. This imposes limitation for installing such system in some certain environments such as marine application.
- Fans also produce noise, which might be undesirable in some locations that the equipment is installed.

To overcome the above-mentioned drawbacks, the present research project aims to replace the existing active cooling method with a passive mechanism. In the proposed solution, the heat will be passively removed from the hotspots using a series of optimally-designed heat pipes and heat spreaders, and transferred to the walls of enclosure which will serve as a heat sink.

The generated heat at the hotspots must pass through a complex network of thermal resistances from the junction (heat generation source) to be dissipated to the surroundings. As will be shown later in the literature review section, the complex mechanisms involved in passive heat transfer solutions, under dynamic loads, are not well studied, and thus require a thorough and systematic characterization prior to industrial implementation. To achieve this goal, it is intended to model the whole heat transfer phenomena in both component and system-level, and also test and prototype the system to develop a general optimized design for the cooling system.

1.6. Objectives and methodology

The objective of this study is to remove all the active fans in the cooling system (rectifier primary fan and secondary air to air heat exchanger fan) and replace them with a fully passive cooling system. Table 2 shows a comparison between the passive and active solution for Alpha enclosures. In order to achieve this challenging goal, a systematic analytical-experimental approach is adopted that includes the following:

- Utilizing heat pipe to transfer the heat from the hotspots to either heat spreaders or heat sinks.
- Optimizing heat spreader design and implementing it in the passive cooling mechanism to improve heat transfer between components.
- Maximizing the efficiency of the natural cooling from the surface of the enclosure by optimized designing of the heat sinks and hotspots distribution on the base plate of heat sinks.
- Proposing a comprehensive and easy-to-implement model that can predict the transient/dynamic response of the cooling systems to arbitrary thermal loads.

Table 2: Comparison between active and passive cooling system for Alpha's enclosures

Active cooling system	Passive cooling system
parasitic power	no parasitic power
noisy	noise-free
regular maintenance required (moving part)	no regular maintenance needed (no moving part)
electronics vulnerable to dust (open system)	can be designed isolated from ambient

Chapter 2. Literature review

Cooling methods of electronics and power electronics ranging from conventional methods such as forced and natural convection to advanced methods including: jet cooling [24], spray cooling [25], piezo-fans [26], electro-wetting [27], and liquid metal cooling [28][29], that have been extensively studied in the literature. A number of these works have been devoted to analysing passive cooling techniques as these methods are preferred due to their advantages over active methods. In this Chapter, the pertinent literature related to, i) passive cooling methods; ii) heat spreaders; and iii) heat pipes are reviewed.

2.1. Modeling of passive transient cooling systems

To model a thermal system, it is necessary to first categorize the system into different levels and sub-levels depending on the complexity of the mechanism and then choose appropriate approach to thermally manage each of the levels. Zuo *et al.* [17] proposed a thermal architecture concept for analysis of thermal problems in electronics and power electronics systems and categorized them into a total of seven levels from the chip to system level which can be applied to all systems including passive systems. They also discussed the existing advanced thermal technologies for cooling of all seven levels. These seven levels are listed in

Table 3.

Table 3: Definition of thermal architecture levels [17]

Level	description	Cooling techniques
1	Heat spreading within components	heat conduction through thin layers of Thermal Interface Material (TIM) or graphite-based interface materials
2	heat spreading through interface between components and circuit card	metallic spreaders with embedded heat pipes, vapor chamber heat spreaders
3	heat transfer from circuit card to rack/chassis	Metallic-based chassis (some with embedded heat pipe), vapor chamber based chassis, cold plates
4	heat transfer from card-rack interface to system heat exchanger	forced airflow over the heat sinks attached to card/rack, pumped liquid flow through cold plates attached to rack, heat pipe/spreader structure
5	heat exchange between cabinet inside and outside	air/air or liquid/air heat exchanger, refrigeration/air conditioning systems
6	direct thermal link between high power components and thermal bus	air or liquid flow directed to high power components, e.g. spray cooling, jet cooling, liquid metal cooling, etc.
7	thermal control of equipment room	air/air or liquid/air heat exchanger, refrigeration/air conditioning systems

In 2004, McGlen *et al.* [16] reviewed the development of high power electronic devices and presented a passive cooling mechanism in a case study using the concept of two-phase heat transfer and heat pipe technology as well as spreading conduction and forced convection. In their design, as shown in Figure 12, the generated heat at several hotspots on the board is transferred to a thermal connector, which is a cold plate with embedded heat pipes, and then through the same process is transferred to the outside heat exchanger or heat sink. Although they did not present any model for prediction of the performance of the introduced cooling mechanism, they discussed the feasibility and applicability of such cooling systems across a range of electronic cooling problems.

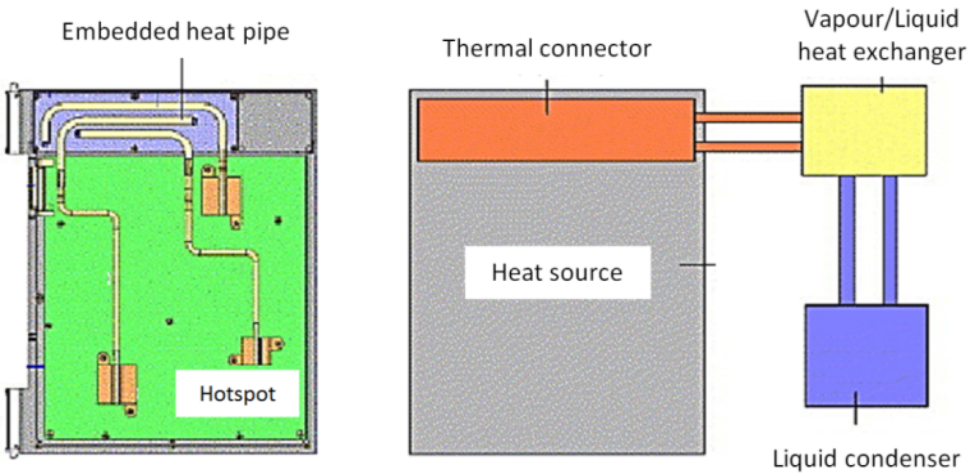

Figure 12: Architectural design of a passive cooling system using spreaders and heat pipe for an electronic board [16]

Heat spreaders, heat pipes, phase change materials (PCM) and heat sinks are the most important components of passive cooling systems. Any possible combination of these components in the form of a cooling mechanism is of interest to thermal engineers. In an interesting study, Gurrum [3] investigated the effective utilization of the board side of electronics as a significant heat flow path for the purpose of passive heat rejection of chips through spreading and dissipating to the ambient. He claimed that by efficient design of circuit board components, optimizing the PCB and integrating vapor chamber if possible and more importantly by using additional solder balls heat can be removed from the board efficiently and potentially lead to a reduction in package heat sink size or its total elimination.

Implementing PCM in the form of thermal storage medium in cooling systems is a passive method to absorb the rejected heat from electronics and cool down the system. These materials by absorbing the heat in the high non-steady modes such as thermal pulsations or sparks prevent sharp temperature variations, leading to smooth performance of the system and less thermal stress. Vesligaj *et al.* [30] in a numerical case study of cooling of a mobile device demonstrated that proper application of PCM can reduce the 7˚C fluctuation band down to less than 1˚C. Gurrum *et al.* [31], and Tan *et al.* [32] also modeled the same phenomenon using numerical methods. Despite the advantages of PCM in cooling solutions most of them still suffer from relatively low

thermal conductivity and bulkiness which make their application a challenge for many cooling solutions. In this study, PCMs are not investigated.

2.1.1. Thermal network modeling

To model passive cooling systems, first the components have to be identified and modeled. Different modeling approaches for such heat transfer systems exist. These approaches range from expensive numerical models to compact and efficient analytical-based models such as lumped modeling and thermal network approach, which is the focus of this work. A number of important studies employing thermal network modeling approach and their shortcomings are presented in Table 4. Steady state thermal resistance network models have been extensively studied in the literature, see e.g., [33]–[41]. There are also a number of studies that include the capacitive behaviour of the components to account for transient heat transfer. Barcella *et al.* [42] presented a resistance-capacitance (RC) modeling method for architecture-level simulation of Very-Large-Scale-Integration (VLSI) chips. Following Barcella's work, Stan *et al.* [43] introduced a thermal RC modeling approach applicable to microprocessor dies and the attached heat sink. Magnone *et al.* and Cova *et al.* [44], [45] presented Cauer RC network model for transient conduction inside silicon power devices and power device assemblies. A thermal RC network model was introduced by Lopez-Walle *et al.* [46] that was capable of modeling heat transfer in micro thermal actuators for both static and dynamic modes. Miana *et al.* in [47] and [48] presented a transient thermal network modeling for prediction of temperature distribution in multi-scale systems subjected to convection at one end. The method was based on dividing the geometry into isothermal elements according to characteristic length and length scale obtained by scale analysis. The RC network modeling concept also has been used in transient modeling of building solar gain [49]–[51].

Table 4: A summary of important existing studies on thermal network modeling approach

Authors	Modelling type	Component modelled	System type	Architecture	Shortcomings
Moghaddam *et al.* [33]	R	Conduction in slab (spreading model implemented) Convection (average *h*)	Multi-component	Chip package	• Did not consider transient analysis • Neglected radiation effects
Luo *et al.* [34]	R	Conduction in slab and solders (spreading model implemented) Convection (average *h*)	Multi-component	Chip-heat sink	• Did not consider transient analysis • Neglected radiation effects
Zhao *et al.* [36]	R	1-D conduction (no spreading model) Convection (average *h*)	Multi-component	Electrolytic cells	• Did not consider transient analysis • Performed a case study (Not a general approach)
Romary and Caldeira [40]	R	1-D conduction (no spreading model)	Single-component	PV module	• Did not consider transient analysis • Did not perform convection-radiation analysis • No 2-D conduction model (spreading)
Del Valle and Atienza [41]	R	Unit cell 1-D conduction in solid	Multi-component	System-on-chip	• Did not consider transient analysis • Components meshing was required (Coding is necessary) • Performed a case study (Not a general approach)
Barcella *et al.* [42]	RC	Unit cell 1-D conduction in solid	Single-component	Chip	• Components meshing required (Coding is necessary) • Did not perform convection-radiation analysis • Resistance calculations were based on numerical simulation (FloWorks) – no analytical approach presented
Bagnoli *et al.* [30]	RC	conduction (experimental data required)	Single-component	electronic devices	• Experimental data was needed to define the circuit components' parameters • No correlation for resistance calculation was presented
Stan *et al.* [43]	RC	Unit cell 1-D conduction in solid Convection (average *h*)	Multi-component	Chip-heat sink	• Components meshing was required (Coding is necessary) • Numerical software was needed (Floworks)

Authors	Modelling type	Component modelled	System type	Architecture	Shortcomings
Magnone *et al.* [44]	RC	Unit cell 1-D conduction in solid (cylindrical)	Single-component	Silicon power device	• Components meshing was required (Coding and numerical software is necessary) • No 2-D conduction analysis was performed • Did not perform convection-radiation analysis • It was only applicable to conduction in thin slabs
Cova *et al.* [45]	RC	1-D conduction (no spreading model) Convection (average *h*)	Multi-component	Power assembly device	• Components meshing was required (Coding and numerical software was necessary) • No correlation for R and C calculation was presented • Performed a case study
López-Walle *et al.* [46]	RC	Conduction in slab (spreading model implemented)	Single-component	Thermal micro-actuator	• Did not perform convection-radiation analysis • appropriate for single component (spreader)
Miana and Cortés [47], [48]	RC	Conduction in solid	Multi-component	Multi scale systems	• Division of geometry in isothermal elements was required (Coding and numerical software was necessary)
Ramallo-González *et al.* [49] Buonomano and Palombo [50] Athienitis [51]	RC	1-D conduction (no spreading model) Convection (average *h*)	Multi component,	Building solar gain	• The models were only applicable to solar gain heat transfer systems • The models generally were meshing-based and require coding
[52]–[55]	RC	Conduction in solid Convection (average *h*)	Multi component	Chip package	• Components meshing was required (Coding and numerical software was necessary)

The above studies are mostly limited to component-level modeling and component temperature distribution prediction. Most of them do not consider the components' thermal inertia and its impact on dynamically loaded systems. In addition, in most of the existing models listed in Table 4, because of the lack of analytical solutions for temperature distribution inside the components, the components have to be divided into sub-sections of isotherm regions.

The above literature review indicates that there is no system-level analysis in the literature which does not require component meshing. As such, one of the goals of this study is to devise a robust, system-level, and transient thermal network modeling approach implementing component-level analytical solutions. This will cover a broad

range of applications such as building cooling system, automobile, and aerospace. In this study an efficient compact thermal network model is proposed that can accurately predict real-time transient and steady-state behaviour of electronic, power electronic and photonic systems.

2.2. Spreading resistance

Spreaders are one of the principal components in both passive and active cooling systems and are available in different geometries and materials (Figure 13). Due to relatively high thermal resistance of spreading and constriction phenomenon it has been the focus of a number of numerical and analytical studies. These studies have been performed for different types of heat spreaders with different materials, geometries and boundary conditions. Most of the existing works have focused on isotropic materials, whereas only a few studies have focused on anisotropic heat spreaders. The existing studies are summarized in .

Table 5.

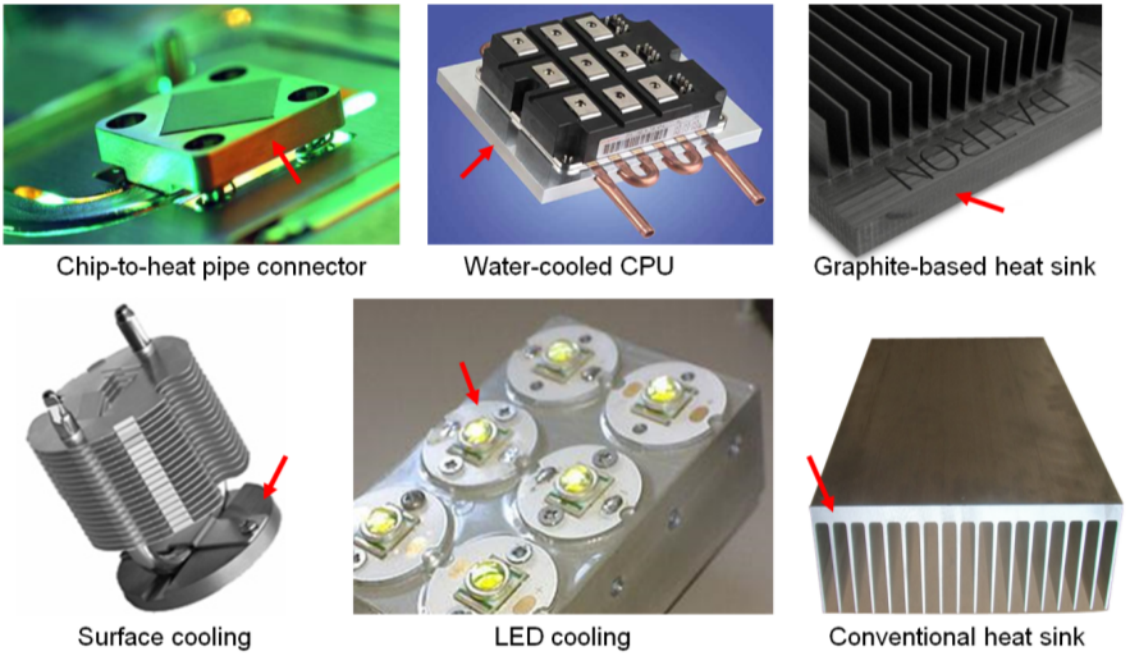

Figure 13: Different industrial applications of thermal spreaders

2.2.1. Isotropic models

Kokkas [56] obtained a general quasi-equilibrium Fourier/Laplace transform solution for a rectangular slab with heat sources on top and convective cooling on the bottom. Kadambi and Abuaf [57] developed an analytical solution to axisymmetric as well as 3-D steady-state and transient heat conduction equations for a convectively cooled slab with a heat source at the center of the top surface. A numerical technique was presented by Albers [58] to solve for surface temperature of a stack of rectangular layers for both isotropic and anisotropic materials. Yovanovich *et al.* [59] reported a general expression for spreading resistance of a heat source centered on a rectangular double layer plate with either conduction or convection on the bottom surface. They also presented closed-form spreading resistance relationships for several special cases. Culham *et al.* [60] reported a more general solution to the 3-D Laplace equation for the rectangular plate with centered heat source on the top and edge cooling instead of insulation on the side walls. Later, Muzychka *et al.* [61] extended Culham *et al.* [60] work and solved the same problem in cylindrical coordinates for a circular slab. In another study [62], they reported a general solution for thermal spreading resistances of

convectively cooled rectangular flux channel with eccentric heat sources on top. Using a superposition technique, Muzychka [63] generalized the solution for problems with multi-heat sources on the top. He introduced the “influence coefficient”, which defines the contribution of each heat source on the temperature rise of other hotspots. Employing an asymptotic approach, Karmalkar *et al.* [64] proposed a closed-form expression for spreading resistance for all rectangular and circular hotspot contact conditions. Recently, Dan *et al.* [65] presented a solution to temperature distribution inside a multi-layered isotropic rectangular tube with discrete isothermal hotspots on both top and bottom surfaces. To overcome the complexity of the mixed boundary conditions they employed an approximate technique to convert this boundary condition into a Neumann boundary condition.

2.2.2. Anisotropic models

Despite the isotropic models there are only a few analytic studies on 3-D conduction heat transfer in anisotropic materials subjected to discrete heat flux in the literature. In 1995, Albers [58] presented a general solution for surface temperature of multilayer materials. Later, Ying and Toh [66] developed an anisotropic spreading resistance model in cylindrical coordinates for a disc with centric heat source on the top and convective cooling on the bottom. Lam *et al.* [67] performed a parametric study on geometrical parameters of a 2-D rectangular orthotropic material. Muzychka *et al.* [68] brought a summary of all the previous studies for isotropic materials and by transforming the boundary conditions and governing equations for anisotropic systems, obtained a new solution for convectively cooled rectangular flux channels as well as circular flux tubes with centralized heat source on the top. He recently [69] developed a model for spreading resistance in compound orthotropic flux tubes and channels with interfacial resistance.

Table 5: A summary of existing studies on analytical modeling of thermal resistance of spreaders

Author	Orthotropic	Eccentric source	Compound	Geometry	cooling Boundary condition	Note
Kokkas [56]	×	✓	✓	rectangular	convective-cooled	• a general quasi-equilibrium solution for 3-D Laplace equation was presented
Kadambi and Abuaf [57]	×	×	×	circular & rectangular	convective-cooled	• Iso-flux single source was considered
Albers [58]	×	✓	✓	rectangular	convective-cooled	• General power functions for sources were considered
Yovanovich *et al.* [59]	×	×	✓	rectangular	convective or conductive cooled	• Iso-flux single source was considered, • Effect of heat source flux distribution studied
Culham *et al.* [60]	×	✓	✓	rectangular	convective-cooled	• An approximate method for modelling complex IC geometries was proposed
Ying and Toh [66]	✓	×	×	circular	convective-cooled	• A numerical validation was presented
Muzychka *et al.* [70]	×	×	✓	circular	convective-cooled	• Geometric transformation from circular to rectangular was investigated
Muzychka *et al.* [61]	×	×	×	rectangular	convective-cooled & edge cooled	• Approximations for edge cooling cases were presented
Yovanovich [71]	×	×	×	circular	convective-cooled & edge cooled	
Muzychka *et al.* [62]	×	✓	✓	rectangular	convective-cooled	• Iso-flux sources were considered
Muzychka *et al.* [68]	-	-	-	circular & rectangular	-	• Review paper
Lam *et al.* [67]	✓	×	×	rectangular	convective-cooled	
Karmalkar *et al.* [64]	×	✓	×	rectangular	convective-cooled	• An equivalent rectangular-based solution for circular geometries was presented
Muzychka [63]	×	✓	×	rectangular	convective-cooled	• Equivalence Coefficient Method for analyzing multi-heat source geometries was presented
Dan *et al.* [65]	×	✓	✓	rectangular	Iso-thermal heat sinks	• The solution for isothermal multi-source/sink was presented
Rahmani and Shokouhmand [72]	×	×	×	half-space	half-space	• The effect of temperature functionality of thermal conductivity was studied
Muzychka [73][69]	✓	×	✓	circular & rectangular	convective-cooled	• Interfacial resistance between layers was considered

In some applications heat spreaders work as an interconnection between two components rather than being completely exposed to natural (or forced) convection on one side. Good examples are chip-to-heat pipe connectors or the substrate in the package of electronic chips (Figure 13). In these applications the spreader is in contact with neighbouring components rather than being convectively cooled on one side. In the open literature there is no model that can predict the temperature distribution inside anisotropic materials which are subjected to discrete sources and sinks on both sides. Therefore, this study aims to develop a new analytical solution for 3-D temperature distribution inside interconnecting anisotropic spreaders with multiple source/sinks on both faces.

2.3. Heat pipes

Another component that is widely used in cooling systems is heat pipe. Heat pipe simply is a sealed tube made of a highly heat conductive material with special interior wall structure (wick) which produces capillary effect for the purpose of liquid transportation and consequently heat transportation between two ends. There are different types of heat pipes available including: round, micro grooved, variable conductance, diode and pulsating heat pipes all of which work based on a similar concept [74]–[76]. Heat pipes in the last two decades have been extensively studied and different analytical and numerical models have been proposed that can predict their behaviour under different conditions. Dr. A. Faghri is one of the pioneers who has more than 100 publications on this topic [77]. In this study, the aim is to analyze heat pipe from system-level perspective and the details of heat and mass transfer inside the heat pipe tubes will not be discussed.

From the system level point of view, heat pipes are intermediary components in thermal systems. As such, it is crucial to propose an effective thermal resistance that represents the thermal behavior of heat pipes. El-Nasr *et al.* [37] introduced a thermal resistance network that represents the behaviour of a heat pipe and proposed an effective thermal conductivity. Later, Zuo and Faghri [38] proposed a RC network analysis method for the heat pipe that was capable of modeling transient thermal behaviour. They concluded that the resistance of vapor flow at the core section of a heat

pipe is considerably smaller than those of the other parts and is negligible. In another study, by Zuo *et al.* [78], a 2-D analytical model for cylindrical heat pipes was presented and closed-form correlations for prediction of vapor and liquid velocity, pressure and temperature distribution were developed. They employed liquid-vapor interfacial hydrodynamic coupling and non-Darcian transport through the porous wick in their analysis. The analytical studies of the last two mentioned studies were extended recently by Shabgard *et al.* [39] and Aghvami *et al.* [79]. They proposed two-dimensional models for round heat pipes considering the heat transfer inside the wall and wick, liquid flow and vapor flow in the core. The former presented a resistance network for the heat pipe structure accounting for both axial and radial heat transfer in the wall. Aghvami *et al.* [79] argued that the assumption of uniform evaporation and condensation in the axial direction was valid under certain conditions. In a recent study, Ferrandi *et al.* [80] discussed the concept of lumped model for transient heat pipe by developing an RC definition for different parts of heat pipes.

In this study, the concept of thermal network modeling for heat pipe will be used and a general and easy-to-implement analytical model for both round and flat heat pipe will be presented. This model will later be used as an input for the system-level modeling of Alpha enclosure passive cooling solutions.

Chapter 3. System-level modeling of passive cooling mechanisms

In this chapter, a new thermal resistance modeling approach for passive cooling systems at both component and system level is presented that can accurately predict the behaviour of a heat-pipe integrated passive cooling solution. Then the experimental study on a laboratory version of passive cooling test-bed will be introduced and the effect of different loading scenarios will be discussed. And finally the developed model will be validated using the collected experimental data.

3.1. Introduction

In general, a passive cooling system includes the following main components; i) heat spreaders; ii) heat pipe(s); iii) thermal interface material (TIM) and iv) heat sinks. A schematic of a typical passive cooling system is shown in Figure 14.

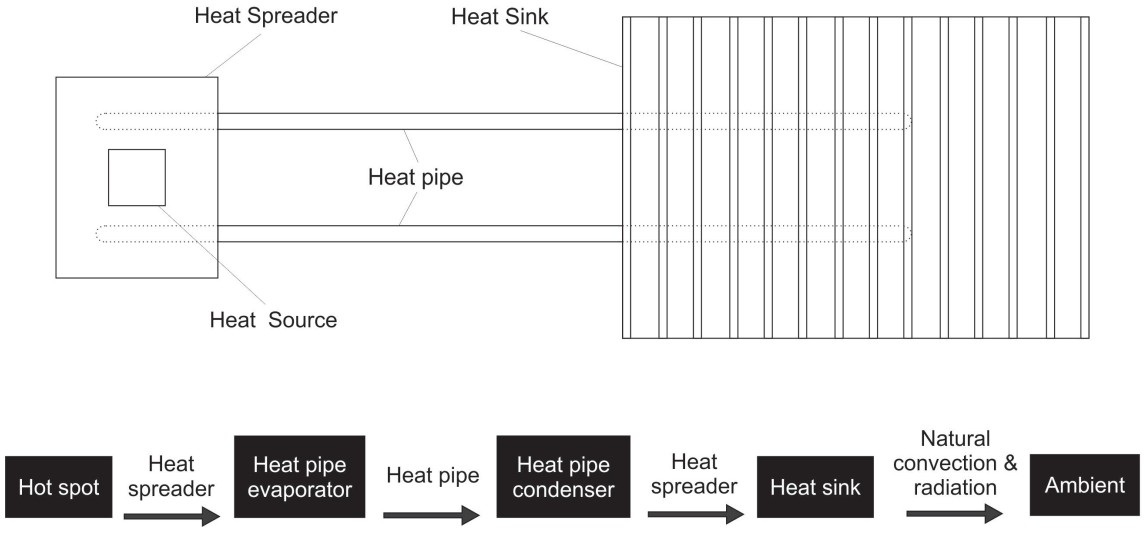

Figure 14: Schematic and block diagram of a typical passive cooling system

Every component on the heat transfer path causes a temperature drop, i.e., introducing resistance against the heat flow. This temperature drop is a function of geometry (dimensions and shape), thermo-physical properties of the component and the heat flow rate. The ratio of the temperature drop over the rate of heat flow is known as thermal resistance [81].

$$R = \frac{\Delta T}{Q} \tag{1}$$

where ΔT is temperature drop and Q is the heat transfer rate. System components also have thermal inertia acting as thermal capacitors that store or release heat during transient operation. This capacitive characteristic results in a “thermal lag” in the system response to variations such as boundary conditions or thermal load. In addition to the components’ resistance and thermal inertia, there are also some thermal phenomena at the system boundaries and components’ interfaces, such as; natural convection, radiation and thermal contact resistance, which should be considered as resistances against the heat flow. It should be noted, no capacitor have to be considered for the boundary phenomena as they do not show any thermal mass effect, thus cannot store or release thermal energy.

There are different methods with different levels of complexity to model a thermal system. Numerical and semi-numerical approaches are popular in modeling the details of thermal systems and can be used for complex geometries with known boundary conditions. However, this high accuracy comes at the cost of tedious numerical procedures and large computation time and cost.

To overcome the high simulation time of the numerical methods, analytical and/or semi-analytical models can be adopted. One method to model transient thermal systems is using the thermal resistance-capacitance (RC) networks, which is analog to electrical circuits [81]. In this analogy, voltage and current stand for temperature and heat flow rate, respectively. Each system component, as well as any surface phenomena, is represented by a network of resistances and capacitance blocks. Then based on the heat flow path, these blocks are connected to form a network, which represents the whole system.

Knowing thermal resistances and capacitances, an RC model can be constructed and analyzed rather readily using software such as MATLAB [82], LTspice [83] or SapWin [84], which enables simulation and accurate prediction of the thermal behaviour of any cooling system over time at each desired location in the system under any arbitrary operating scenario. To calculate the resistances and capacitances in an RC model, all the dimensions and thermal properties of the components as well as the boundary conditions, e.g. ambient temperature should be known. For the radiation thermal resistance, emissivity of the radiant surface should be known as well.

In this chapter a RC thermal model is presented which is capable of covering the entire range of cooling solutions from module/component-level to system-level with arbitrary number of components. One major advantage of the proposed thermal network method is its simplicity, i.e., the transient behaviour of the system under various operating and load conditions can be simulated rather easily without using complicated and time consuming numerical solutions.

The proposed RC model is focused on passive cooling systems; however, the same approach can be used for active cooling systems. The considered passive system includes heat spreader, heat pipe and naturally-cooled heat sink. The model is developed at two complexity levels of 0-D and 1-D which support both transient and steady state conditions. The proposed model is capable of simulating any arbitrary loading and operating scenarios. A custom-designed test-bed is developed and several passive cooling systems are built and tested. The model is successfully validated with experimental data and an excellent agreement between the modeling results and experimental data is observed.

3.2. Component-level modeling

The resistive behaviour of components of a thermal system against heat transfer is independent of the neighbouring components as well as the heat flux profile with respect to time. This characteristic postulates that every component or contact phenomenon can be separately modeled and then all components are integrated to form a system-level model that represents the thermal behaviour of the device.

Unlike resistance that is a strong function of geometrical characteristics of the component, the capacitance of each component can be estimated knowing only the mass and specific heat capacity of that piece [5]. It is calculated using Eq. (2) which is the summation of all sub-components' capacities.

$$C = \sum_n m_n c_n = \sum_n \rho_n c_n V_n \tag{2}$$

where m is the mass of each part, c is the specific heat capacity and ρ and V are the density and the volume of each part, respectively. However, the approach to define the resistance of each component is different. In the Sections, a resistance model for each component is developed.

3.2.1. Heat spreaders model

Heat spreaders come in variety of shapes and materials with various types of boundary conditions as well as different number of arbitrary-shaped heat sources and sinks attached to them. Most of them are, or can be simplified to circular or rectangular plates with a number of hot/cold spots on faces. Heat spreader faces can be exposed to different number of cold/hot spots or natural convection and/or radiation heat transfer. As will be explained in Chapter 4, most of these cases have been already studied by others and thermal spreading resistances are available.

To define thermal resistance two temperatures and the amount of heat flow is required [61]–[63], [65]. In this study, the difference between average temperatures over the heat sources and heat sinks are considered as the temperature difference required for the thermal resistance definition. Total heat flow also can be derived by integrating the heat flux over the heat sources or heat sinks domain. It should be noted that the total heat transferred to the plate is equal to the total heat removal from the plate under steady-state condition, which is the case in our solution. As such, the spreading resistance can be defined as:

$$R^* = \frac{\left|\overline{\theta}_{Sources} - \overline{\theta}_{Sinks}\right|}{Q^*} \tag{3}$$

where,

$$\bar{\theta}_{Sources} = \frac{1}{\sum_{Sources} a_i^* b_i^*} \sum_{Sources} \int_{Y_i^* - \frac{b_i^*}{2}}^{Y_i^* + \frac{b_i^*}{2}} \int_{X_i^* - \frac{a_i^*}{2}}^{X_i^* + \frac{a_i^*}{2}} \theta_{Sources} dx^* dy^* \tag{4}$$

$$\bar{\theta}_{Sink} = \frac{1}{\sum_{Sinks} a_i^* b_i^*} \sum_{Sinks} \int_{Y_i^* - \frac{b_i^*}{2}}^{Y_i^* + \frac{b_i^*}{2}} \int_{X_i^* - \frac{a_i^*}{2}}^{X_i^* + \frac{a_i^*}{2}} \theta_{Sink} dx^* dy^* \tag{5}$$

$$Q^* = \left| \iint_{Sources/Sinks} q_i^* dx^* dy^* \right| \tag{6}$$

For the case of uniform heat fluxes, Q^* can simply be calculated by the summation of dimensionless heat fluxes multiplied by their dimensionless source areas. To calculate the average temperatures at both sources and sinks, the steady state temperature distribution at those locations needs to be known. A general solution for the temperature distribution inside rectangular blocks with multiple heat sources and sinks on the faces of spreaders is presented in detail in chapter Chapter 4.

3.2.2. Heat pipes model

The following simplifying assumptions are made to model the heat pipes:

- The vapor resistance is neglected.
- Axial resistances through wall and wick due to their comparatively large values are assumed as open circuit in the RC network.

Heat pipe is a passive heat transfer device that takes advantage of both conduction and two-phase flow heat transfer that occurs in a thermodynamic cooling cycle inside the heat pipe core. The mechanism of heat transfer, in brief, is evaporation of the refrigerant at one end (evaporator section) as a result of heat absorption from the surrounding and dissipating it to the ambient through condensation at the other end (condenser section), see Figure 15. The moving force for the refrigerant through the

cycle is the local pressure difference in the vapor and the capillary force for the liquid phase.

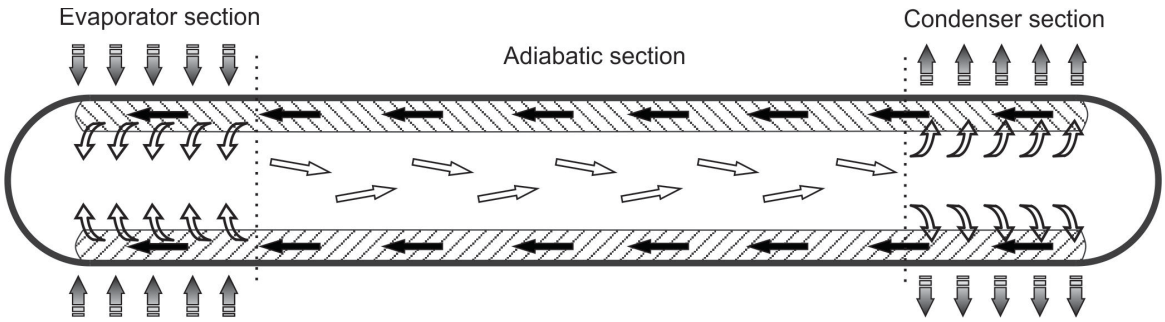

Figure 15: Schematic of a heat pipe, the interior cooling cycle and different regions

Heat pipes work perfectly within their designed temperature range. Working in temperatures other than this range result in malfunction and low efficiency of the device due to dry-out, sonic limit, viscous limit or entrainment limit [37], [80], [85].

In a heat pipe heat is transported through three paths. The main path is the inner hollow through which the vapor is transported by the means of pressure difference between its two ends. Going further in detail, for the heat to vaporize the refrigerant in the evaporator end, it has to radially pass through the wall and the wick. At the condenser end, after the heat is released by condensation it has to be radially transferred through the wick and the wall to the outside. As a result, a main path of heat transfer in heat pipes can be modeled using five thermal resistances corresponding to the radial conductions through wall and wick at each of the heat pipe's ends and one corresponding to the vapor transportation [80]. The two other paths are axial conduction through the wall and wick and are comparatively less important. Figure 16 shows the thermal resistance circuit for a heat pipe under steady-state condition.

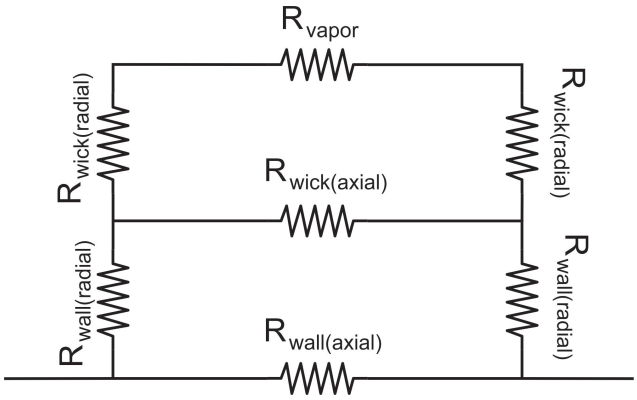

Figure 16: Thermal resistance network model for a heat pipe (steady state)

Based on definition, R_{vapor} is a function of temperature and pressure drop of the travelling vapor between two ends of the heat pipe. Looking through the existing theoretical models for heat pipe and the available experimental data in the literature [38][80][78], it is confirmed that the temperature drop of the vapor inside a heat pipe is relatively small which means that the resistance corresponding to the vapor can be neglected. On the other hand, due to the large ratio of heat pipe's length to its wall and wick thickness, the thermal resistances associated with axial conductions through the wall and wick are comparatively large. This means that the contribution of the heat transfer through the wall and wick is significantly smaller than that of the vapor channel. As such, axial conduction resistances in the RC model can be assumed as open-circuit without losing accuracy. Applying the above mentioned simplification and considering the thermal storage of the heat pipe, thermal resistant network of a heat pipe can be represented as shown in Figure 17 [38][80][78].

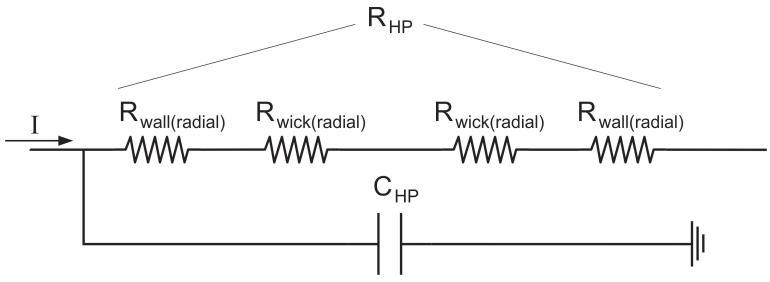

Figure 17: Simplified thermal network model for a heat pipe

The radial thermal resistance for a cylinder wall with inner and outer radii of r_1 and r_2 and length of L with thermal conductivity of k is [86]:

$$R_r = \frac{\ln\left(\frac{r_2}{r_1}\right)}{2\pi kL} \tag{7}$$

Thus, the resistance of a cylindrical heat pipe is simply the summation of all the resistances shown in Eq.(8):

$$R_{HP} = \frac{L_e + L_c}{2\pi L_e L_c}\left(\frac{\ln\left(\frac{r_{out}}{r_{wall}}\right)}{k_{wall}} + \frac{\ln\left(\frac{r_{wall}}{r_{wick}}\right)}{k_{wick}}\right) \tag{8}$$

where r_{out} is the pipe outer radius, $r_{wall}$and r_{wick} are inner radii of the wall and the wick, L_e and L_c are the length of the evaporator and the condenser sections, and k_{wall} and k_{wick} are thermal conductivities of the wall and the effective thermal conductivity of the wick, respectively. This resistance for a flat heat pipe of width w_{HP} is,

$$R_{HP} = \frac{L_e + L_c}{w_{HP} L_e L_c}\left(\frac{t_{wall}}{k_{wall}} + \frac{t_{wick}}{k_{wick}}\right) \tag{9}$$

Effective thermal conductivity of two commonly used types of wick structure are listed as examples below (Figure 18) [37][80],

$$k_{wick} = \frac{k_l[(k_l + k_s) - (1-e)(k_l - k_s)]}{[(k_l + k_s) + (1-e)(k_l - k_s)]} \quad \text{wrapped screen wick}$$

$$k_{wick} = \frac{k_s[2 + (k_l / k_s) - 2e(1 - (k_l / k_s)]}{[2 + (k_l / k_s) + e(k_l / k_s)]} \quad \text{sintered wick} \tag{10}$$

Where k_l and k_s are thermal conductivities of liquid and wick material respectively, and e is the wick porosity. The capacitance of the heat pipe can be calculated using Eq. (2).

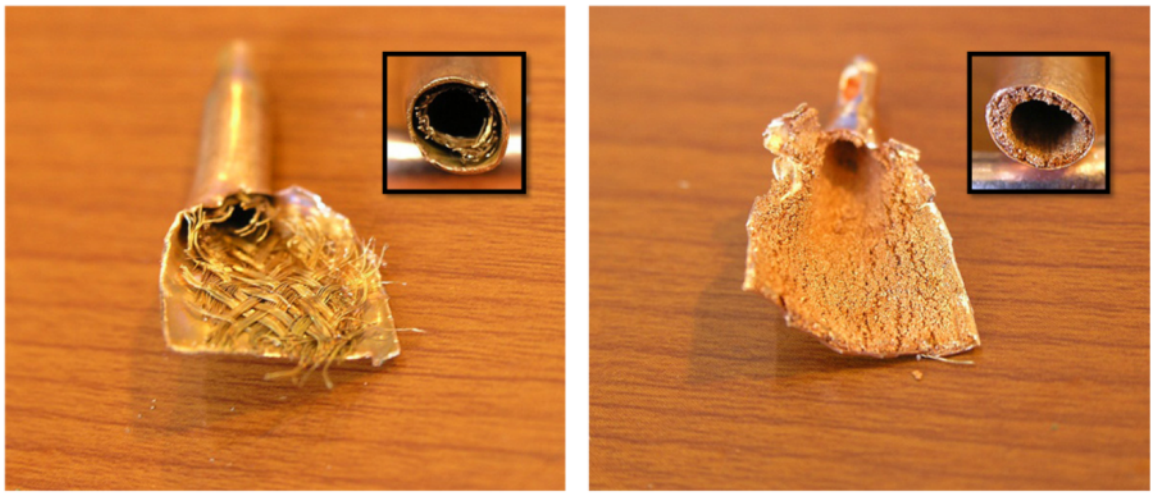

Figure 18: Two common types of heat pipe wick structure [87]

3.2.3. Heat sinks model

The following simplifying assumptions are made to model the heat sinks:

- Only the spreading resistance in the base plate is considered and the effect of fins' resistance is neglected. According to Eq. (11) which provides the temperature difference between the base and the tip of the fin in typical heat sinks [86], this assumption has little impact on the accuracy. For typical natural convection aluminum heat sinks with fin thickness of around 2-5 mm and fin depth of 1-5 cm, the temperature difference percentage between the base and the tip of the fin is 12% in the worst case scenario that can be neglected.

$$\frac{T_{base}-T_{tip}}{T_{base}}=\frac{\cos(mp)-1}{\cos(mp)} \qquad \text{where} \qquad m^2=\frac{hP}{kA_c} \tag{11}$$

- Isothermal heat sinks. Although this assumption may introduce some inaccuracy in the model, it is not far from reality for most engineering applications.
- Uniform averaged convective heat transfer coefficient over the heat sink surface.

Heat sink spreading resistance

Neglecting the fins resistance simplifies the heat sink's thermal resistance into the resistance of a rectangular block whose thickness is equal to the thickness of the

base plate. In this block heat sources are the projected area of the hotspots on the back face, and sinks are a series of alternate rectangular strips with the length of the block width, the width of fin thickness and the fin spacing which cover the whole surface of the block, as shown in Figure 19. Assuming a uniform averaged convective heat transfer coefficient over the heat sink surface, the dissipated heat through each strip sink can be readily determined using its corresponding area in the real heat sink. For a heat sink with n_f fins, fin spacing of s, fin thickness of t and fin depth of p, the heat transfer will be,

$$Q_{fin} = \frac{2p + t}{2n_f p + L} Q_{in} \qquad \text{one fin strip}$$
$$Q_{base} = \frac{s}{2n_f p + L} Q_{in} \qquad \text{one base strip} \tag{12}$$

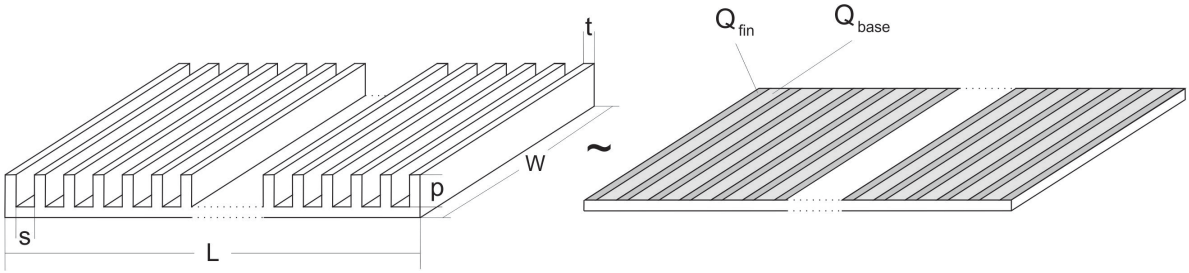

Figure 19: Rectangular finned heat sink and its base rectangular shape equivalent spreader

Having the heat sink simplified to the above-mentioned geometry which is a multi-hotspot rectangular heat spreader, the spreading resistance can be calculated using the approach explained in section 3.2.1.

Convective and radiative heat transfer resistances

On the surface of a heat sink, heat is dissipated to the ambient through two parallel mechanisms: i) natural convection and ii) radiation [86]. Using the definition of the thermal resistance, Eq.(1), the thermal resistance of a heat sink can be defined as:

$$R = \frac{\Delta T}{Q_{convection} + Q_{Radiation}} \tag{13}$$

where ΔT is the temperature difference between the surface of the heat sink and the ambient. The amount of convective heat transfer is the summation of heat transfers from the fins and the base,

$$Q_{Convection} = h_f A_f \Delta T + h_b A_b \Delta T \tag{14}$$

where the subscripts *f* and *b* refer to 'fin' and 'base plate', respectively. The following correlations are used for calculating the convective heat transfer coefficient in rectangular finned heat sinks [86],

$$h_b = \frac{k}{L} 0.59 Ra_L^{0.25} \qquad \text{Single plate } (\text{base plate}) \tag{15}$$

$$h_f = \frac{k}{s}\left[\frac{576}{\left(\frac{Ra_s s}{L}\right)^2} + \frac{2.873}{\left(\frac{Ra_s s}{L}\right)^{0.5}}\right]^{-0.5} \qquad \text{Parallel plates } (\text{fins}) \tag{16}$$

where

$$Ra_x = \frac{g\beta}{\nu\alpha}(T_s - T_{amb})x^3 \tag{17}$$

In the above correlations, *L* and *s* are the fin length and fin spacing of the heat sink, respectively. Other types of heat sinks can be modeled using a similar approach.

For radiation heat transfer, the following correlation is used [86],

$$Q_{Radiation} = \sigma\left(T_s^4 - T_{amb}^4\right)\left(\sum_i \frac{1}{\frac{1-\varepsilon_i}{A_i\varepsilon_i} + \frac{1}{A_i F_{i\infty}}}\right) \tag{18}$$

where σ, ε and F are the Stefan-Boltzmann coefficient, emissivity and the view factor of surface i, respectively. The view factor of a single duct of heat sink for comparatively small fin aspect ratios can be calculated using the following approximation,

$$F = \frac{s}{s + 2p} \tag{19}$$

Substituting the correlations for both natural convection and radiative heat transfers, Eq. (14) and (18), into the resistance definition, Eq.(13), the following relationship for the thermal resistance of a rectangular heat sink is derived,

$$R_{HS} = \frac{1}{h_f A_f + h_b A_b + \sigma\left(T_s^2 + T_{amb}^2\right)(T_s + T_{amb})\left(\sum_i \frac{1}{\frac{1-\varepsilon_i}{A_i \varepsilon_i} + \frac{1}{A_i F_{i\infty}}}\right)} \tag{20}$$

Equation (20) shows that the heat sink resistance is a function of thermo-physical properties as well as the temperature of both the heat sink and the environment.

3.3. System-level modeling

Using the component-level thermal resistance models, in the following sections, two general network models, 1-D and 0-D, are developed to predict the behaviour of thermal systems under any arbitrary operating and environmental conditions. The one-dimensional (1-D) model is more comprehensive and considers more details. The lumped or zero-dimensional (0-D) model is a simplified version of the 1-D model, and is less accurate but faster and easier to apply. Contact resistances due to their comparatively small values are neglected in both models; however, it can be readily included in the models wherever the contact resistance is important.

3.3.1. 1-D thermal network model

In this model, the resistance and capacitance of every component or contact phenomena are considered. Following the heat flow path from the source to the sink, the RC blocks corresponding to each component are connected to form the circuit. The 1-D thermal network model for a typical cooling system is demonstrated in Figure 20. The present model is general and can be constructed for any other passive (or active) cooling system with any number of components.

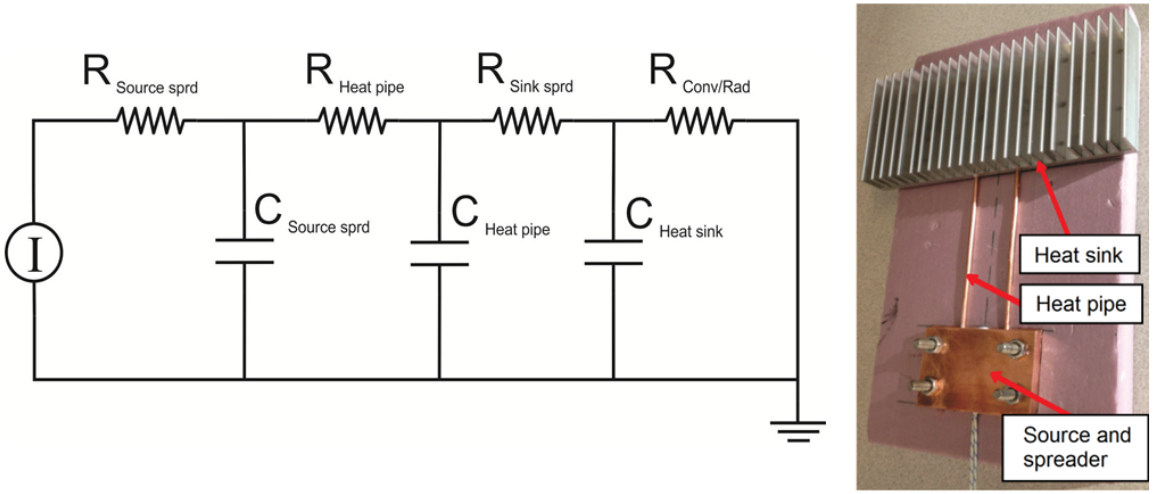

Figure 20: 1-D RC model of the passive cooling system including: heat source, heat spreader at the heat source, heat pipes and naturally cooled heat sink

3.3.2. 0-D thermal network model

In systems where the components' resistance is smaller than the convective resistance of the heat sink, approximately by an order of magnitude or higher, the whole system can be treated as a lumped body with no internal resistance. This means that ideally the system does not have any internal thermal resistance and the only resistance against heat transfer from the source to the ambient happens at the boundaries of the system. According to [86], this criteria can be quantified and stated in the form of the Biot number. The lumped system analysis is applicable where $Bi \leq 0.1$ [86].

$$Bi = \frac{hL_c}{k} \tag{21}$$

where h is the convective heat transfer coefficient, k is the thermal conductivity of the body and L_c is the characteristic length which is commonly defined as the volume of the body divided by the convection surface area (L=V/A). For systems with Biot numbers smaller than 0.1, the corresponding RC circuit consists of one capacitance and one convective-radiative resistance, see Figure 21. For a passive cooling system shown in Figure 14, the resistance network shown in Figure 21 represents the convection and radiation on the heat sink surface and the capacitance represents the thermal capacity of the entire system.

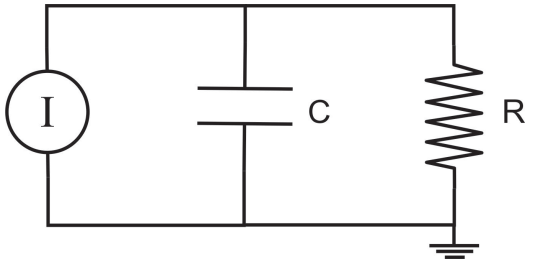

Figure 21: 0-D RC thermal network model for the passive cooling system shown in Figure 14

3.4. Experimental study

3.4.1. Test-bed design

To investigate the effect of thermal inertia and transient performance of passive cooling system a prototype was built. This test-bed consists of one rectangular fin heat sink, two round heat pipes, two electric cartridge heaters (120V AC, 30W) supplied by OMEGA (Toronto, ON) each connected to the heat sink via one heat spreader and heat pipe as shown in Figure 22. The thermo-physical specifications of the components are presented in

Table 6. As shown in Figure 22, to reduce contact resistance, heat pipes were sandwiched between two rectangular plates and thermal paste was used. Heat had to pass through these heat spreader plates to be transferred to heat pipes. The electrical heaters were insulated with a layer of foam with thickness of 1.5 cm to prevent heat loss to the surroundings.

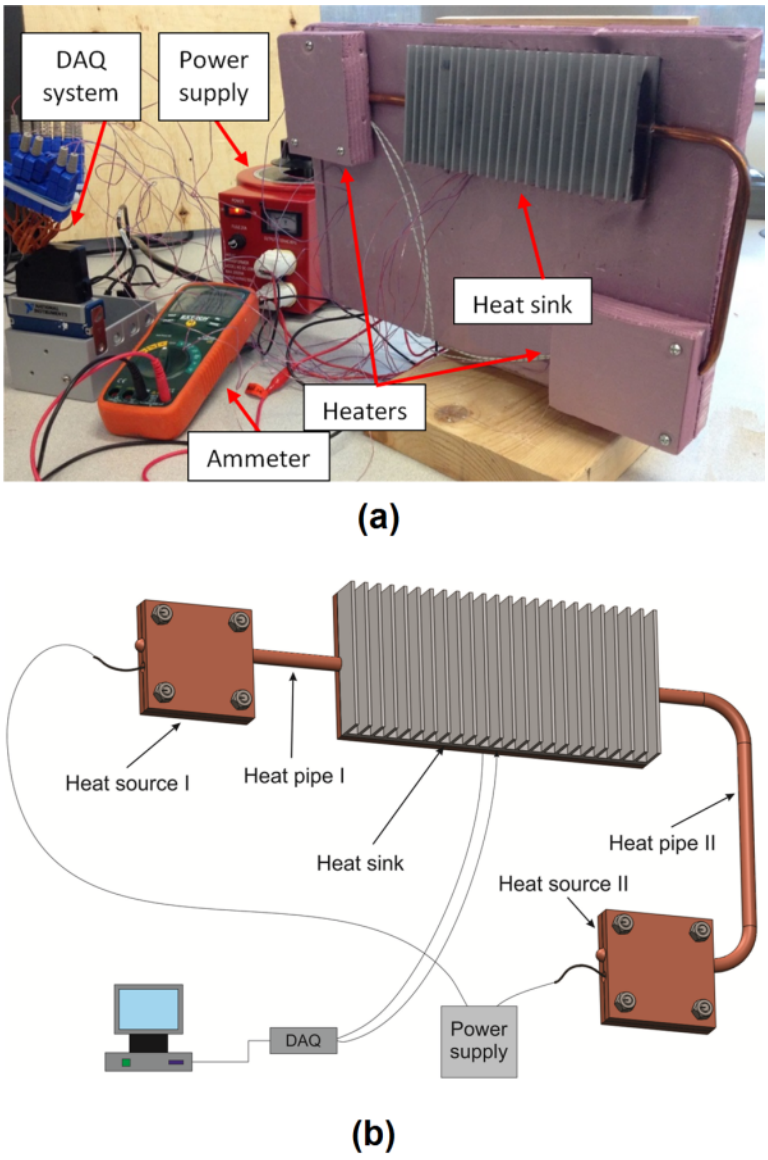

Figure 22: (a) Custom-designed test-bed and (b) schematic of the experimental test-bed

Table 6: Test-bed thermo-physical specifications

	Heater I & II	Spreader I & II	Heat pipe I & II	Heat sink
Material	304 stainless steel	Copper	Copper	Aluminum
Length [mm]	63.5	63	$L_{HP\text{-}I}$= 200 $L_{HP\text{-}II}$= 300 L_eL_e = 30 L_c = 30	185
Width [mm]	-	63	--	86
Thickness [mm]	-	6	t_{wall}= 0.8 t_{wick} = 1.2	t_{base} = 5 t_{fin} = 2
Diameter [mm]	6.35	--	D_{out} = 8	--
Fin depth [mm]	--	--	--	17
Fin spacing [mm]	--	--	--	6
Thermal conductivity [W/m.K]	18	400	k_{Copper} = 400 k_{wick} = 50	120
Density [kg/m^3]	8030	8960	8960	2700
Specific heat [J/kg.K]	490	386	386	900

To measure and monitor the temperature, 16 thermocouples (T-type, with accuracy of ±0.5˚C) were attached to different locations of the test-bed. All the temperature readings were collected and stored using a National Instrument DAQ system (model number: NI 9213). The input power to the heaters was supplied by an adjustable AC power supply (VARIAC, China) and both voltage and current were measured using an EXTECH 430 digital multi-meter.

All the machining, such as milling, cutting, lathing and finishing were done in the SFU Machine Shop using available equipment such as, milling machine, band saw, laser cutter, lathe machine and grinder. Activities such as heat pipe bending, tapping and drilling as well as data collections were performed in Dr. Bahrami's lab at SFU, the Laboratory for Alternative Energy Conversion (LAEC).

3.4.2. Test procedure and data collection

In the passive cooling prototype experiment, different step and oscillatory loading scenarios are imposed to the passive cooling test-bed by heaters, and the temperature

at various locations are monitored and stored. Each test is carried out for the transition time starting from the initial equilibrium state in which all the components are in equilibrium with the ambient, to the final steady state (Appendix B). At the steady state, the temperature becomes either statically or “dynamically” steady depending on the load profile of the heaters. To investigate the thermal behavior of the system in different load cycles and validate the present 0-D and 1-D models, the experiments are conducted for the following two different loading scenarios:

I. Static loading; each heater has a constant power.
II. Dynamic loading; each heater has a cyclic heat load profile.

Four thermal loading scenarios were selected arbitrarily to validate the model; these scenarios are specified in Table 7 and depicted in Figure 23.

Table 7: Thermal loading scenarios for multi heat source passive cooling test-bed

	Heater I / Heater II			
	Type of thermal load	**Load pick [W]**	**period of dynamic load [min]**	**off ratio of dynamic load [%]**
Scenario 1	step / step	14 / 10	-	-
Scenario 2	step / step	9 / 5	-	-
Scenario 3	step / pulse	13 / 20	20	0 / 50
Scenario 4	off / 2-step pulse	0 / 17 and 30	15	- / 33

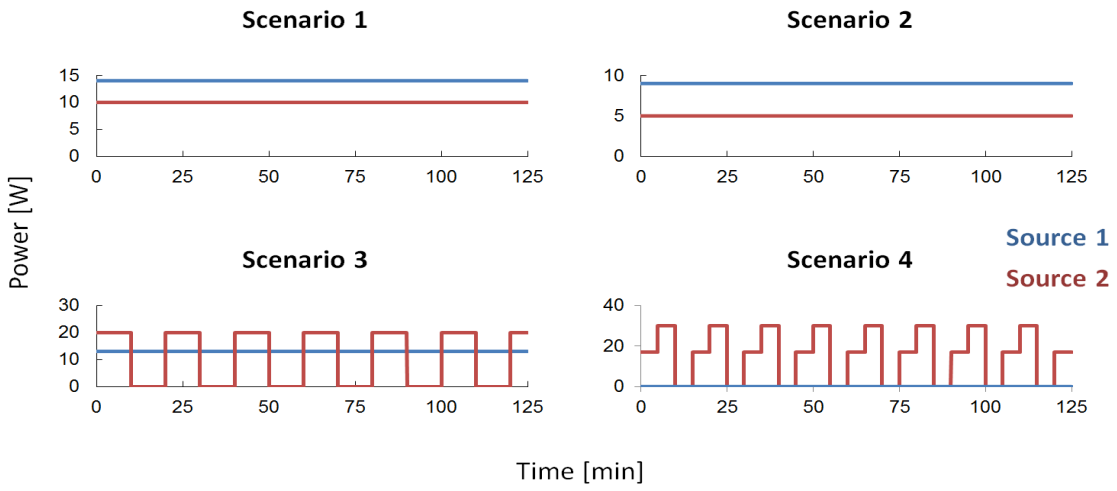

Figure 23: Multi heat source test-bed thermal loading profiles

Applying the methodology described in section 3.3, the 1-D RC model of the multi-heat source test-bed (Figure 22) is shown in Figure 24. For the 0-D RC model, the RC network has the form shown in Figure 21. The values of the components are listed in Table 8.

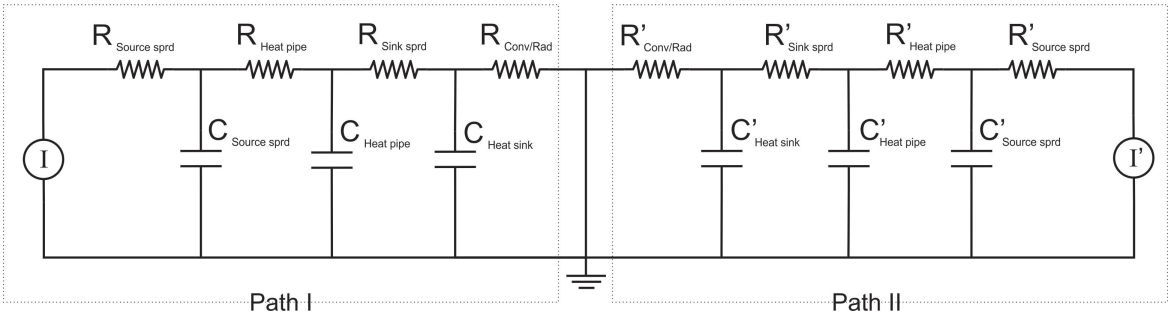

Figure 24: 1-D model of the two-path experimental test-bed

Table 8: Component values of the 1-D RC model of the two-path experimental test setup

	Resistance [K/W]				Capacitance [J/K]		
	Heat source Spreader	Heat pipe	Heat sink spreader	Convection/ radiation	Heat source Spreader	Heat pipe	Heat sink
1-D (path I)	0.052	0.014	0.19	1.5	140	18	350
1-D (path II)	0.052	0.014	0.19	1.5	140	27	350
0-D	R_{total}=1.5				C_{total}=1025		

3.5. Model validation and discussion

To validate the proposed models, experimental data recorded for different heating scenarios are plotted and compared with their corresponding model simulations. Three important locations, two on the heat sources and one on the heat sink, are chosen as benchmarks for comparison and validation. In Figure 25 the temperature at these three spots are compared with the 1-D as well as the 0-D model for the loading scenario #1, static loading of 10 watts for heater I and 14 watts for heater II, Figure 23.

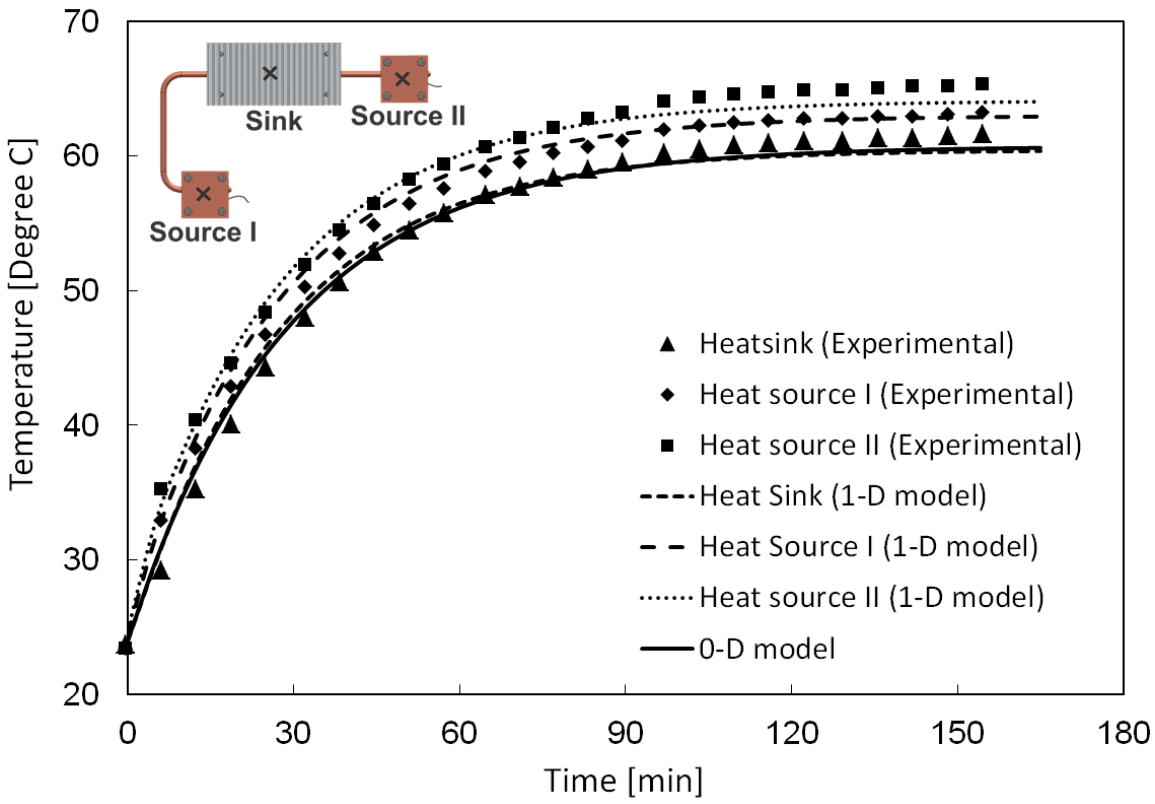

Figure 25: 0-D model validation with experimental data at three locations of heat sink and two heat sources for the heating scenario of constant 14W for heater I and 10W for heater II

As the 0-D model only provides one temperature for the whole test-bed as a lumped mass, it is not capable to detect the temperature difference between the heat sinks and heat sources. Therefore, in Figure 25, it can be seen that the 0-D model captures the heat sink temperature reasonably well with less than 2% relative difference. However; it is not capable of predicting other components temperature such as heat sources. The present 1-D model however is capable of accurately predicting temperatures at different spots as it considers the thermal resistance between the components. The maximum relative difference with the experimental data with the 1-D model is approximately 4%. Figure 26 depicts another static loading case (Heater I, 5W and heater II, 9W) in which again the heat sink temperature is accurately predicted by both 0-D and 1-D model whereas the temperature of the heat sources can only be predicted by the 1-D model.

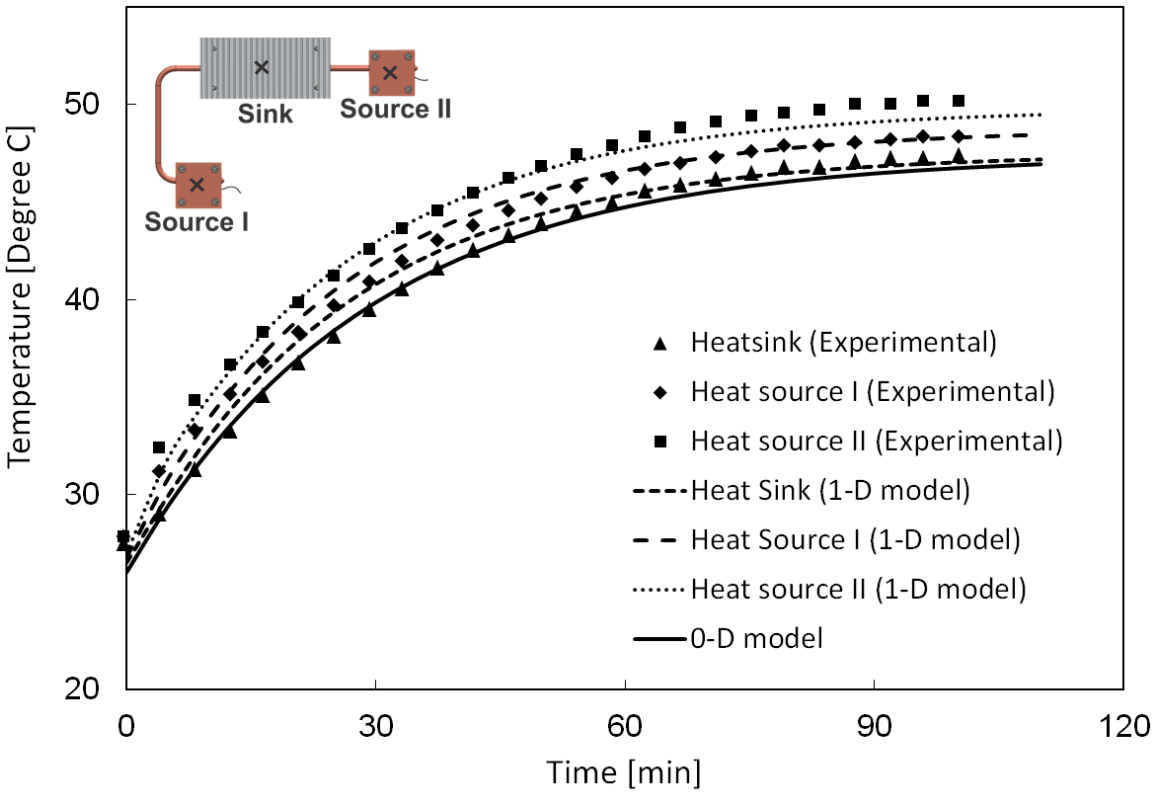

Figure 26: 0-D model validation with experimental data at three locations of heat sink and two heat sources for the heating scenario of constant 9W for heater I and 5W for heater II

Figure 25 and Figure 26 indicate that the temperature of other locations in the test-bed has almost the same trend as the temperature of the heat sink with a small offset. It can be interpreted that for cases with no sharp variation in heat source power, the 0-D model is sufficient if the purpose is only to predict an estimation of the system temperature. Obviously, for variable loading situations in which the internal thermal resistances and thermal inertia become important, a 0-D model cannot provide detailed information.

The following two dynamic loading scenarios (see Table 7) are selected arbitrarily: i) heater I with a constant heat generation of 13W and heater II with a pulsating heat generation with a maximum of 20W and a minimum of 0 and the period of 20 minutes; and ii) heater I with a two-step pulsating heat generation with the profile shown in Figure 23 and heater II turned off.

Figure 27 presents the measured temperatures over time at three specified spots as well as the both models results for heat sink temperature. Both 0-D and 1-D models have predicted the heat sink temperature accurately. As it is seen, unlike the static form of loading, the shape of temperature variation for dynamic loading is different at various locations. These differences are due to thermal inertia effects and the 0-D model is unable to detect them. The 1-D model results for the two heat sources are shown in Figure 28. It is indicated that the 1-D model performs very good and captures the trend of the temperature fluctuation at the two hotspots. The relative difference between the model and experimental data in this case is less than 4%.

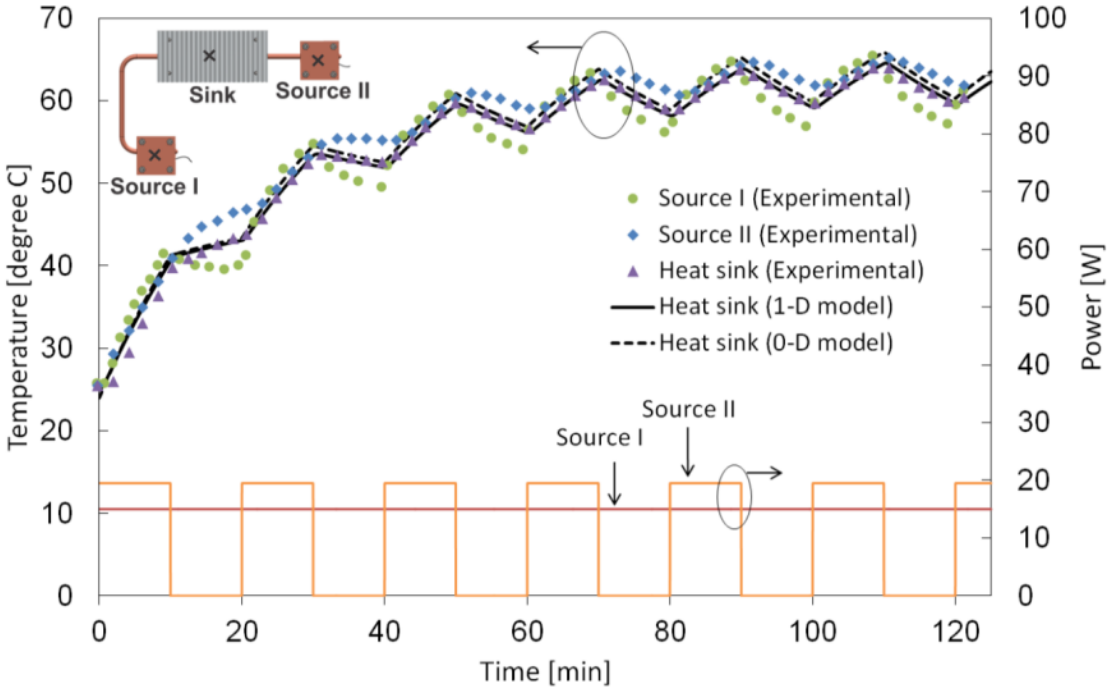

Figure 27: Comparison of 0-D model with experimental temperature of three different locations on the test bed for the applied dynamic loading of shown in the figure

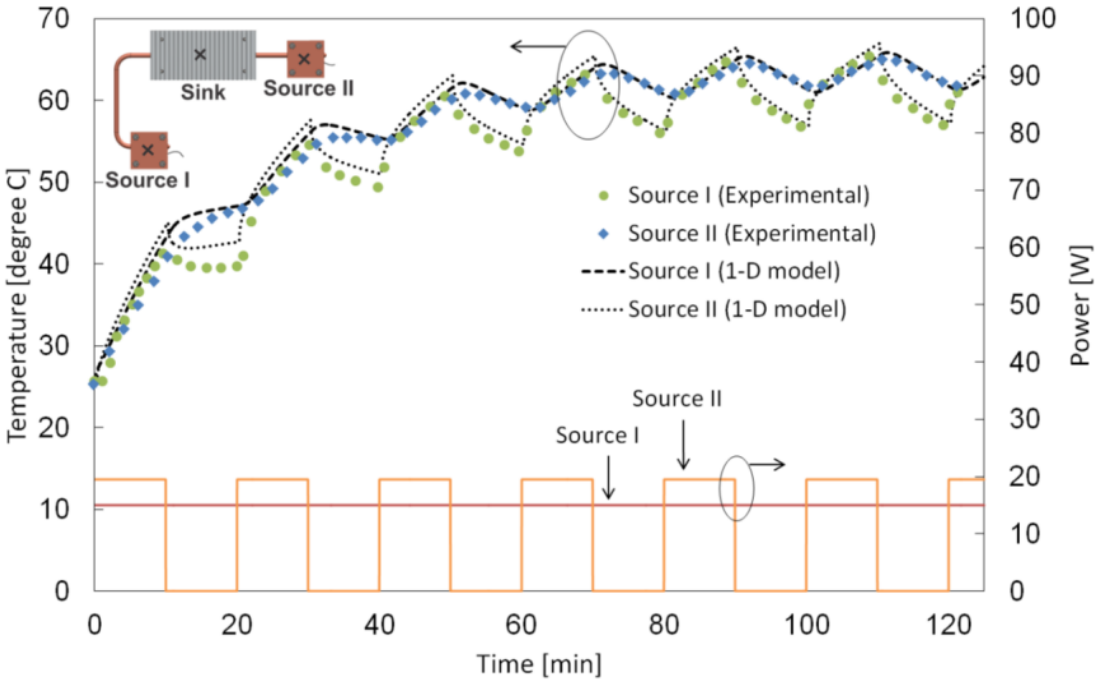

Figure 28: 1-D model validation with experimental data at two heat source locations for the imposed dynamic loading shown in the figure

The comparison for the second scenario is shown in Figure 29 and Figure 30. This loading scheme represents the worst case in terms of fluctuation and thermal inertia effect on the thermal behavior of the system. As it is seen in Figure 29, both models capture the heat sink temperature very well. It is worth noting that the temperature variation at the pulsating heater is very sharp while at the other heat source the temperature fluctuates much smoother with a lag in responding to the power changes, which is due to the damping effect caused by thermal inertia of the system components. This effect is completely captured by the 1-D model and the results for these two temperatures are plotted and compared with our experimental data in Figure 30. The maximum relative difference between the model and experimental data is approximately 4.5%.

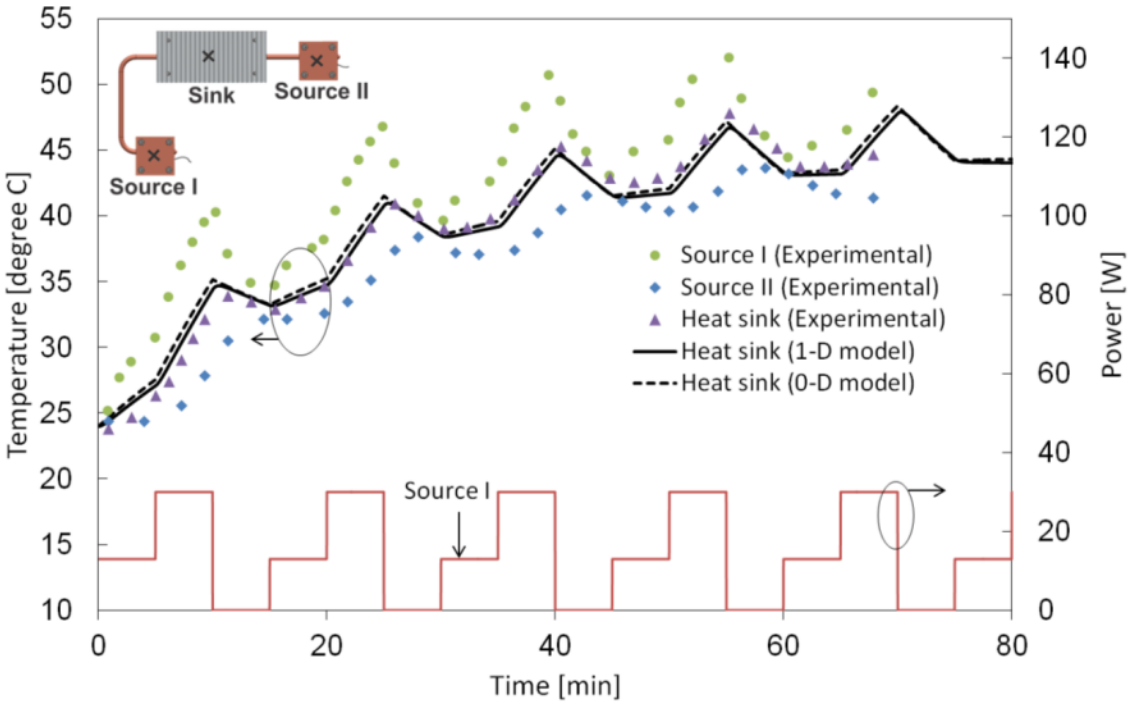

Figure 29: Comparison of 0-D model with experimental temperature of three different locations on the test bed for the imposed dynamic loading

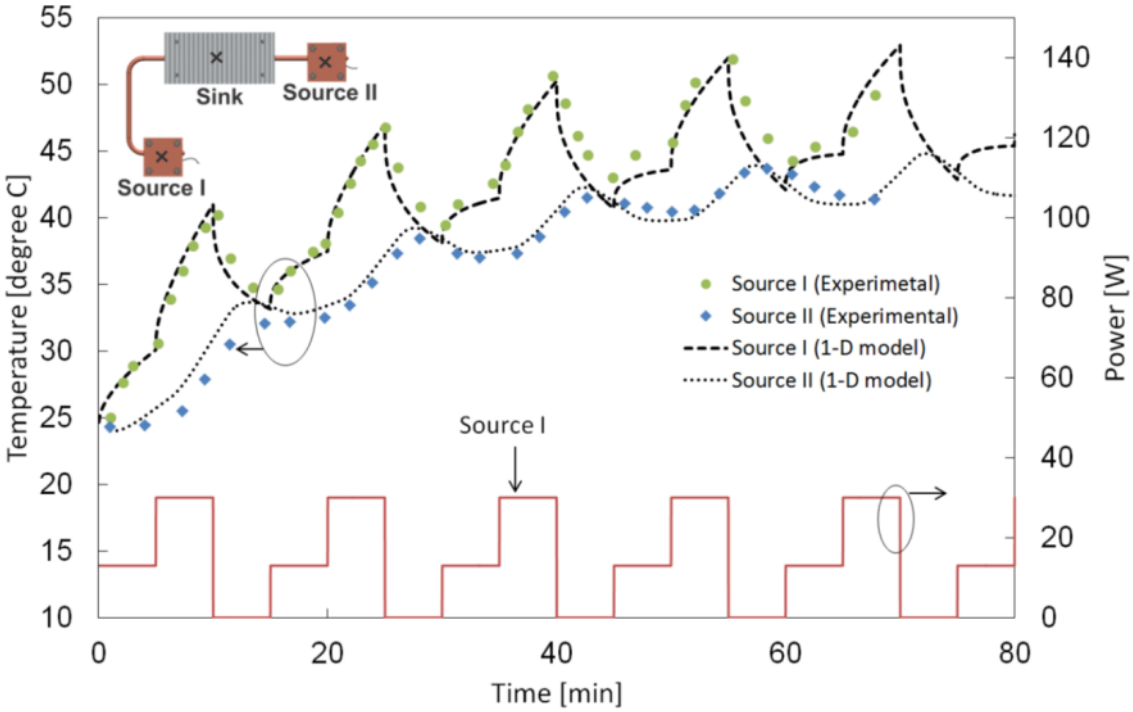

Figure 30: 1-D model validation with experimental data at two heat source locations for the imposed dynamic loading shown in the figure

3.6. Conclusion

In this chapter passive cooling systems and their essential components were introduced. A general and comprehensive thermal network modeling approach was presented for: i) component-level and ii) system-level analyses. Equivalent thermal resistance and capacitance of the components including heat spreaders, heat pipes, heat sinks, convection and radiation were analytically presented. A general and robust method to construct the system-level R-C network representing the entire system was also demonstrated. The summary of Section 3.2 is presented in Table 9.

Table 9: A summary of final correlations for thermal resistance of different components of passive cooling systems

Component	Thermal resistance correlation	Required parameters
Spreaders	Eqs. (3) and (27)	• Geometrical parameters of spreaders and sinks and sources • Directional thermal conductivities
Heat pipes	Round heat pipe: Eq. (8) Flat heat pipe: Eq. (9)	• Geometrical parameters of heat pipe • Thermal conductivities of wall material and wick • Evaporator and condenser sections' length
heat sinks	Base plate: Eqs. (3) and (27) Fins convection/radiation: Eq. (20)	• Geometrical parameters of heat sink and hotspots on its back • Thermal conductivity of heat sink material • surrounding convective heat transfer coefficient • Emissivity

To validate the presented model a custom-designed multi-heat source passive cooling mechanism was built and tested. The components of the test-bed were two heat sources connected to one heat sink through a series of heat spreaders and heat pipes. The test-bed was exposed to different types of transient thermal loads from step heat flux to multi-stage pulsating heat flux and the junction temperatures recorded during the transient performance of the system until it reaches the steady state condition (appendix B). The experimental results were compared to that of analytical model and a very good agreement (less than 4.5% maximum relative difference) was observed.

Chapter 4. Anisotropic heat spreaders

This chapter is dedicated to developing and validating a new analytical model for predicting the temperature distribution inside an anisotropic rectangular plate subjected to multiple heat sources and sinks on both faces. After a brief introduction, the analytical model is presented and numerically validated. Then a comprehensive parametric study on thermo-physical properties of the heat spreaders is performed. Finally, a new method for the measurement of in-plane thermal conductivity of anisotropic plates is introduced and the experimental results are presented.

4.1. Introduction

Anisotropic materials are becoming the key component of next-generation cooling systems in electronics and telecommunication industries. Proper use of these materials in the form of thermal spreaders as compared to conventional metallic ones can significantly reduce the thermal stresses in the system as well as thermal resistance. The high in-plane thermal conductivity of these materials can be taken advantage of, to efficiently spread the heat over a larger area with the minimum possible thickness of the plate. Heat spreaders come in different shapes and materials.

Recently, graphite-based anisotropic materials have received a significant attention due to their exceptional thermo-physical properties [88]–[90]. They are widely used in electronic devices such cell phones, battery modules, and notebooks. Graphite-based materials are one of the well-known anisotropic materials which have in-plane thermal conductivity, up to 1500 W/m.K, and through-plane thermal conductivity around 2-10 W/m.K. [90]–[93]. This property is mainly due to their especial atomic structure. They are generally, a stack of graphite flakes piled upon each other (Figure 31). The interlayer cohesive energy of graphite flakes which is due to the covalent bonding is much stronger than intralayer van der Waals atomic attraction [94]. This structural

feature causes large anisotropy in graphite sheets, which make them ideal candidate for heat spreaders where higher heat transfer rates are desired in the in-plane than in the through-plane direction. Proper use of graphite-sheet can lead to significant heat flux reduction at hotspots by spreading the heat over larger areas. [59], [64]. It should be noted that the spreading (or constriction) resistance causes an extra resistance against the heat flow which should be considered in the design of the spreader.

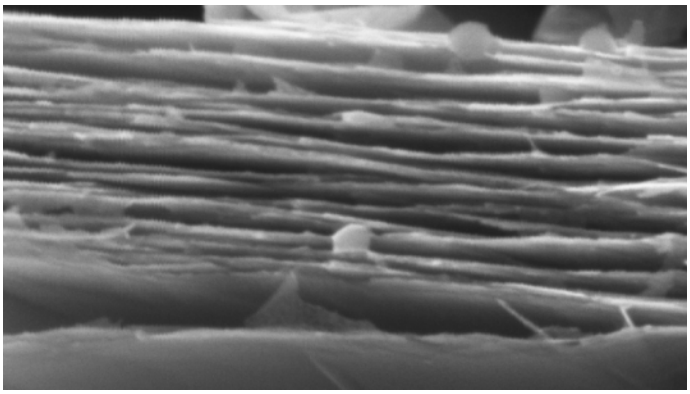

Figure 31: SEM image of graphite plate – side view

In this chapter, the author presents a new analytical model for 3-D temperature distribution inside anisotropic materials subjected to multiple hot/cold spots following by model validation and parametric study. At the end, an in-plane thermal conductivity measurement approach will be presented and the obtained results will be discussed.

4.2. Analytical Modeling

Spreaders come in a variety of shapes and materials with various types of boundary conditions as well as different numbers of arbitrary-shaped heat sources and sinks attached to them. Most of them are, or can be simplified to, circular or rectangular plates with a number of hot/cold spots on faces. Heat spreader faces can be exposed to different number of cold/hot spots or natural convection and/or radiation heat transfer. As will be explained in Chapter 4, most of these cases have been already studied by others and thermal spreading resistances are available.

In this section, a new general analytical solution is presented for steady-state temperature distribution inside anisotropic rectangular blocks subjected to multiple heat

sinks and sources on both top and bottom faces. An anisotropic rectangular plate ($k_x \neq k_y \neq k_z$) of $L \times W$ with thickness of H (Figure 32.a) is considered for the following two scenarios:

i) Subjected to a single rectangular source and sink arbitrary-located on both top and bottom surfaces and,

ii) More generally, subjected to '*M*' and '*N*' arbitrarily located sinks and sources on the top and bottom surfaces, respectively.

As boundary conditions, it is assumed that the lateral faces of the plate are insulated, i.e., no heat transfer through the side walls. All the top and bottom surfaces except the sources (sinks) are also considered to be insulated. Sources have arbitrary heat flux, $q_{i(x,y)}$ (*i* is the number assigned to a hotspot), positive values are considered for heat sources and negatives for sinks, which are functions of *x* and *y*. Each source (sink) is centrally positioned at x coordinate of *X* and y coordinate of *Y* with length and width of *a* and *b*, respectively, as shown in Figure 32.b. The objectives are to:

i) find the temperature distribution inside the plate with any arbitrarily arrangement of hotspots on the top and bottom surfaces analytically, and
ii) define corresponding spreading resistance.

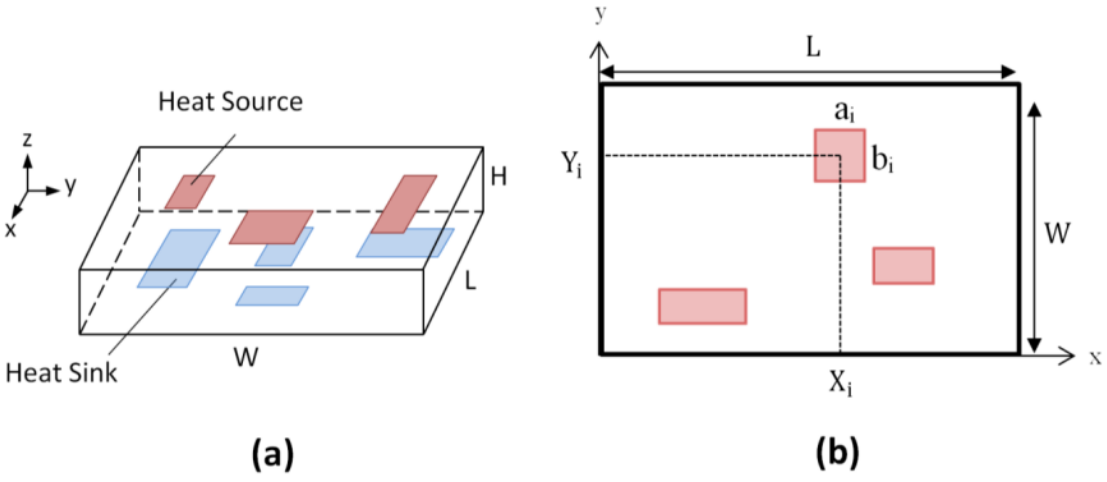

Figure 32: Schematic of an anisotropic rectangular spreader with multiple hotspots on the top and bottom surfaces (a) Size and location of the hotspots (b)

4.2.1. General solution

Dimensionless parameters are defined as follows and the governing equation and boundary conditions are expressed accordingly.

$$\varepsilon = \frac{W}{L}, \qquad \varepsilon_H = \frac{H}{L}, \qquad x^* = \frac{x}{L}, \qquad y^* = \frac{y}{L}, \qquad z^* = \frac{z}{L}$$
$$a_i^* = \frac{a_i}{L}, \quad b_i^* = \frac{b_i}{L}, \quad q^*_{i(x,y)} = \frac{L^2 q_{i(x,y)}}{Q_{ref}}, \qquad \theta = \frac{Lk_z}{Q_{ref}}(T - T_0) \tag{22}$$
$$\kappa_x = \sqrt{\frac{k_z}{k_x}}, \qquad \kappa_y = \sqrt{\frac{k_z}{k_y}}, \qquad R^* = Lk_z R$$

where Q_{ref} is an arbitrary reference heat flux and T_0 is a reference temperature. Using the parameters in Eq. (22) the dimensionless form of the governing equation and the boundary conditions, are:

$$\nabla^2\theta = \frac{1}{\kappa_x^{\,2}}\frac{\partial^2\theta}{\partial x^{*2}} + \frac{1}{\kappa_y^{\,2}}\frac{\partial^2\theta}{\partial y^{*2}} + \frac{\partial^2\theta}{\partial z^{*2}} = 0 \tag{23}$$

$$\begin{aligned} &\frac{\partial\theta}{\partial x^*} = 0 && \text{at } x^* = 0,\ x^* = 1 \\ &\frac{\partial\theta}{\partial y^*} = 0 && \text{at } y^* = 0,\ y^* = \varepsilon \end{aligned} \tag{24}$$

$$\text{at } z^* = 0 \rightarrow \begin{cases} \dfrac{\partial\theta}{\partial z^*} = q_{i(x,y)}^{\,*} & \text{at spot 'i' domain} \\ \dfrac{\partial\theta}{\partial z^*} = 0 & \text{at remainder} \end{cases} \tag{25}$$

$$\text{at } z^* = \varepsilon_H \rightarrow \begin{cases} \dfrac{\partial\theta}{\partial z^*} = q'^{\,*}_{i(x,y)} & \text{at spot 'i' domain} \\ \dfrac{\partial\theta}{\partial z^*} = 0 & \text{at remainder} \end{cases}$$

Using a separation of variable technique, Eq. (23) has the general solution in the form of below [95]:

$$\theta = \sum_{\lambda}\sum_{\delta} C_{(\lambda,\delta)}\, e^{\lambda \kappa_x x^*} e^{\delta \kappa_y y^*} e^{i\sqrt{\lambda^2+\delta^2}\, z^*} \tag{26}$$

witch, λ, δ and $C_{(\lambda,\delta)}$ are unknown coefficients that should be defined through applying the boundary conditions. Applying the first boundary conditions, Eq. (24) and expanding the solution into trigonometric form results:

$$\begin{aligned}\theta = {} & A_0 z^* \\ & + \sum_{m=1}^{\infty} \cos\left(\lambda \kappa_x x^*\right) \times \left[A_m \cosh\left(\lambda z^*\right) + B_m \sinh\left(\lambda z^*\right)\right] \\ & + \sum_{n=1}^{\infty} \cos\left(\delta \kappa_y y^*\right) \times \left[A_n \cosh\left(\delta z^*\right) + B_n \sinh\left(\delta z^*\right)\right] \\ & + \sum_{n=1}^{\infty}\sum_{m=1}^{\infty} \cos\left(\lambda \kappa_x x^*\right)\cos\left(\delta \kappa_y y^*\right) \times \left[A_{mn} \cosh\left(\beta z^*\right) + B_{mn} \sinh\left(\beta z^*\right)\right]\end{aligned} \tag{27}$$

where λ, δ and β are eigenvalues in the form of below:

$$\lambda = \frac{m\pi}{\kappa_x}, \qquad \delta = \frac{n\pi}{\kappa_y \varepsilon}, \qquad \beta = \sqrt{\lambda^2 + \delta^2} \tag{28}$$

In the Eq. (27) '*A*'s, '*B*'s are coefficients which should be defined by applying the boundary conditions on the top and bottom surfaces. As it is shown in Eq.(25), the Neumann boundary conditions on these two surfaces have a discrete form that cannot be applied. To apply the boundary conditions, Eq.(25), a 2-D Fourier expansion technique is used [59]. Using this technique, the temperature distribution inside the heat spreader is derived for single and multi-hotspots cases.

4.2.2. Single heat source and heat sink

For a plate with one heat source on one surface (subscript *t*) and one heat sink on the other side (subscript *b*), the coefficients of the solution, Eq.(27), are as follows:

$$A_0 = \frac{s_{00}^t}{\varepsilon} = \frac{s_{00}^b}{\varepsilon} \tag{29}$$

$$B_m = \frac{2s_{m0}^t}{\varepsilon\lambda} \tag{30}$$

$$B_n = \frac{2s_{0n}^t}{\varepsilon\delta} \tag{31}$$

$$B_{mn} = \frac{4s_{mn}^t}{\varepsilon\beta} \tag{32}$$

$$A_m = \frac{2}{\varepsilon\lambda}\left(s_{m0}^b \operatorname{csch}\left(\lambda\varepsilon_H\right) - s_{m0}^t \coth\left(\lambda\varepsilon_H\right)\right) \tag{33}$$

$$A_n = \frac{2}{\varepsilon\delta}\left(s_{0n}^b \operatorname{csch}\left(\delta\varepsilon_H\right) - s_{0n}^t \coth\left(\delta\varepsilon_H\right)\right) \tag{34}$$

$$A_{mn} = \frac{4}{\varepsilon\beta}\left(s_{mn}^b \operatorname{csch}\left(\beta\varepsilon_H\right) - s_{mn}^t \coth\left(\beta\varepsilon_H\right)\right) \tag{35}$$

In which the auxiliary coefficients, obtained from Fourier expansion, are:

$$s_{00}^{t\ or\ b} = \iint_{t\ or\ b} q_{(x,y)}^* \, dx^* dy^* \tag{36}$$

$$s_{m0}^{t\ or\ b} = \iint_{t\ or\ b} q_{(x,y)}^* \times \cos\left(\lambda\kappa_x x^*\right) dx^* dy^* \tag{37}$$

$$s_{0n}^{t\ or\ b} = \iint_{t\ or\ b} q_{(x,y)}^* \times \cos\left(\delta\kappa_y y^*\right) dy^* dx^* \tag{38}$$

$$s_{mn}^{t\ or\ b} = \iint_{t\ or\ b} q_{(x,y)}^* \times \cos\left(\lambda\kappa_x x^*\right)\cos\left(\delta\kappa_y y^*\right) dx^* dy^* \tag{39}$$

In order for the solution to hold, coefficient A_0 must satisfy both boundary conditions at the top and bottom surfaces. Therefore, considering the definition of A_0, Eq.(29), and the definition of s_{00} in Eq.(36), one can conclude that the energy conservation in the plate is automatically satisfied.

4.2.3. Multiple heat sources and heat sinks

Since conduction heat transfer in a solid is a linear process, the superposition principle is applicable. As such, for cases with multiple sources on each of the surfaces, temperature distribution can be readily obtained by superposing the single source solutions derived in Section above. Using this approach, the solution can be generalized for rectangular plates with 'M' and 'N' sources/sinks on the top and bottom surfaces, respectively. As a result, the solution, Eq.(27), and the coefficients, Eq. (29-35), remain unchanged, however; the auxiliary coefficients take the more general form:

$$s_{00}^{t\ or\ b} = \iint_{t\ or\ b} q^*_{i(x,y)}\, dx^* dy^* \tag{40}$$

$$s_{m0}^{t\ or\ b} = \iint_{t\ or\ b} q^*_{i(x,y)} \times \cos\left(\lambda \kappa_x x^*\right) dx^* dy^* \tag{41}$$

$$s_{0n}^{t\ or\ b} = \iint_{t\ or\ b} q^*_{i(x,y)} \times \cos\left(\delta \kappa_y y^*\right) dy^* dx^* \tag{42}$$

$$s_{mn}^{t\ or\ b} = \iint_{t\ or\ b} q^*_{i(x,y)} \times \cos\left(\lambda \kappa_x x^*\right) \cos\left(\delta \kappa_y y^*\right) dx^* dy^* \tag{43}$$

Using the above auxiliary coefficients, the temperature distribution inside an anisotropic plate can be found for any number and arrangement of heat sources and sinks.

Special case: in a particular case, in which each spot has a constant heat flux q_i, the general auxiliary coefficients take the following simplified form:

$$s_{00}^{t\ or\ b} = \sum_{i=1}^{M\,or\,N} q_i^* a_i^* b_i^* \tag{44}$$

$$s_{m0}^{t\ or\ b} = \frac{1}{\lambda\kappa_x} \sum_{i=1}^{M\,or\,N} q_i^* b_i^* \sin(\lambda\kappa_x x^*)\Big|_{x_i^* - \frac{a_i^*}{2}}^{x_i^* + \frac{a_i^*}{2}} \tag{45}$$

$$s_{0n}^{t\ or\ b} = \frac{1}{\delta\kappa_y} \sum_{i=1}^{M\,or\,N} q_i^* a_i^* \sin(\delta\kappa_y y^*)\Big|_{Y_i^* - \frac{b_i^*}{2}}^{Y_i^* + \frac{b_i^*}{2}} \tag{46}$$

$$s_{mn}^{t\ or\ b} = \frac{1}{\lambda\delta\kappa_x\kappa_y} \sum_{i=1}^{M\,or\,N} q_i^* \sin(\lambda\kappa_x x^*)\Big|_{x_i^* - \frac{a_i^*}{2}}^{x_i^* + \frac{a_i^*}{2}} \times \sin(\delta\kappa_y y^*)\Big|_{Y_i^* - \frac{b_i^*}{2}}^{Y_i^* + \frac{b_i^*}{2}} \tag{47}$$

4.3. Model validation

4.3.1. Numerical validation

To validate the present model, an anisotropic rectangular Pyrolytic Graphite Sheet (PGS) with an arbitrary arrangement of four spots, i.e., two sources on the top surface and two sinks on the bottom is assumed, see Figure 33. The chosen PGS has through-plane thermal conductivity of 4W/m.K and in-plane one of 800W/m.K [91]–[93].

The numerical analysis is performed using COMSOL Multiphysics 4.2a [96]. A sensitivity study on the grid size is performed for two different levels of extra and extremely fine mesh sizes with 7.6×10^4 and 4.2×10^5 elements, respectively. Less than 0.1 percent relative difference for local temperature between the two cases is observed. The computation time for the extra fine mesh size using a typical Pentium Dual-Core PC is around 20 seconds. Using the proposed model, this time is less than 5 seconds for 100 terms in the series solution and fine mesh size.

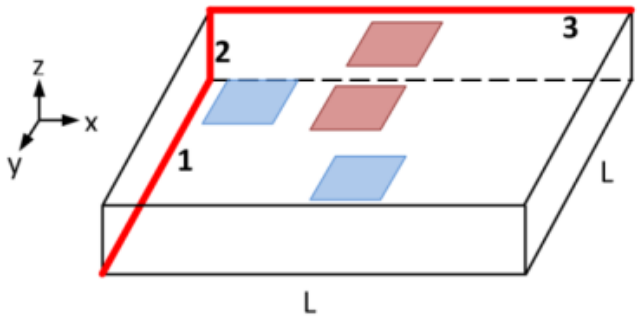

Figure 33: Cut-lines' position inside the rectangular plate for comparison between the analytical and numerical results

To compare the results quantitatively, temperatures along three different imaginary lines in three different directions, labeled in Figure 33, are plotted in Figure 34 for both analytical and numerical results. For this specific example, the characteristic length, L, and Q_0 are equal to 0.1m and 1kW, respectively. The reference thermal conductivity is assumed to be 4W/m.K. The thermo-physical parameters are listed in Table 10.

Table 10: Thermo-physical characteristics of the plate and the spots in Figure 33 used in the numerical analysis

Plate dimensions	Plate material	Source 1	Source 2	Sink 1	Sink 2
L=10cm	k_0=4W/mK		Q_0=1kW		
ε=1	κ_x=0.07	a^*=0.2	a^*=0.2	a^*=0.2	a^*=0.2
ε_H=0.2	κ_y=0.07	b^*=0.2	b^*=0.2	b^*=0.2	b^*=0.2
	κ_z=1	X^*=0.5	X^*=0.5	X^*=0.5	X^*=0.2
		Y^*=0.5	Y^*=0.8	Y^*=0.5	Y^*=0.9
		q^*=1	q^*=1	q^*=1	q^*=1

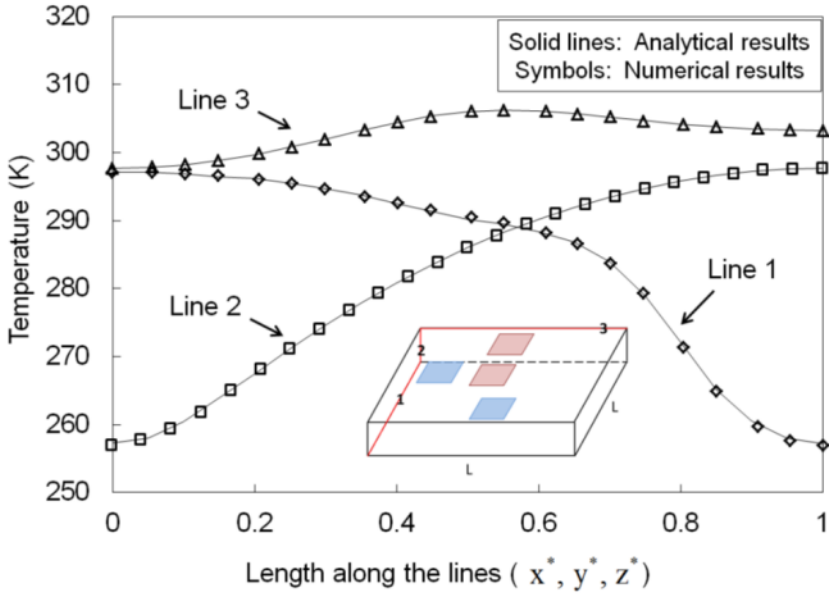

Figure 34: Comparison between the present analytical model and numerical results for temperature along three different cut-lines. The hotspots arrangement of Figure 33 was used

As shown in Figure 34, there is an excellent agreement between the analytical model results and the numerical simulation. A sensitivity analysis on the number of eigenvalue terms in the series solution is performed. Increasing the number of terms in the series from 100 to 400 will not change the solution considerably (less than 0.1%).

4.3.2. Experimental validation - Graphite plate temperature mapping

The 2-D temperature distribution on the top and bottom surfaces of a rectangular graphite slab, exposed to two square heat source and sink each located on one face of the slab at the opposite corners are measured to validate the analytical model developed above in Section 4.2.1. Figure 35 shows the test-bed and graphite block tested. For this purpose, one cartridge heater (120V, 30W) and two 3mm heat pipes are sandwiched separately between two copper plates of 50mm×50mm to form flat heat source/sink, respectively. A wooden frame and a few layers of foam are used to insulate the graphite block. The test should be run long enough to ensure the steady state condition, see Appendix B for more details.

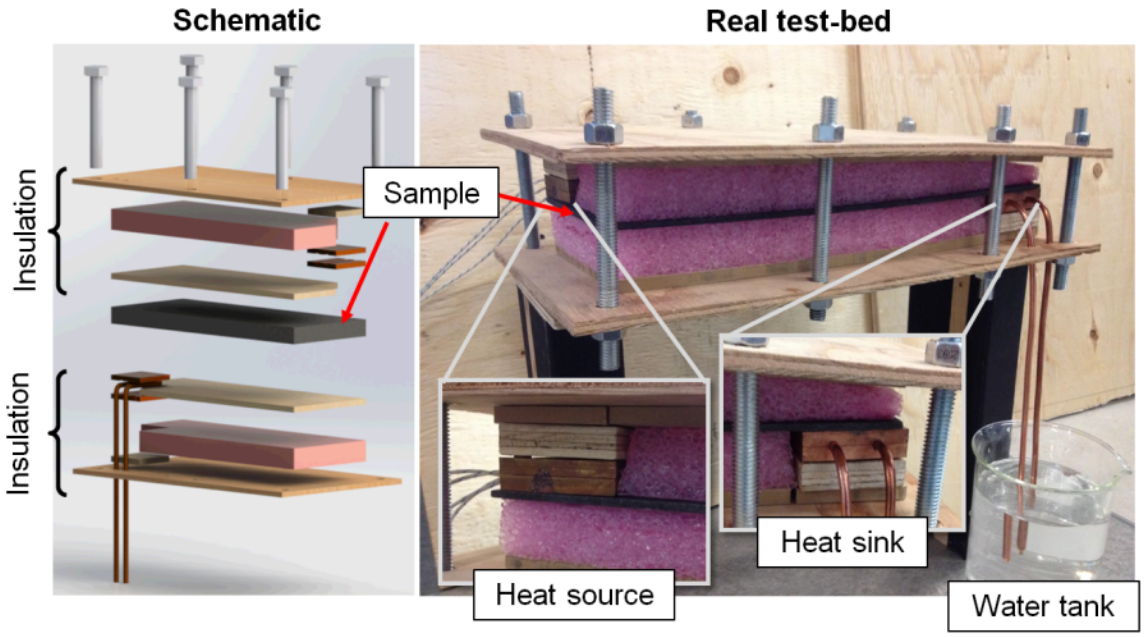

Figure 35: Graphite plate temperature mapping test-bed

14 T-type thermocouples attached to the top and bottom surfaces were used to capture the temperature distribution on the samples (Figure 36). For storing and monitoring the temperatures as well as input power the same equipment as in the in-plane thermal conductivity experiment was used.

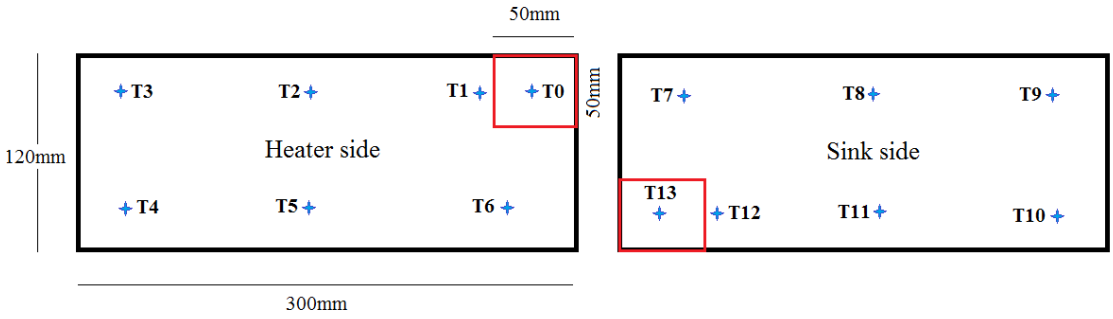

Figure 36: Thermocouple locations on samples of graphite plate

In the following, the comparison between experimental data and the analytical results of the equivalent system for two samples with different thicknesses and thermal conductivities are plotted. The input thermal conductivities to the analytical model were chosen using the experimental measurement values. The maximum relative difference

between the obtained experimental data and the analytical results is less than 5%, which may occur due to the following reasons:

- The heat flux at the heat source and sink in experiment is not completely uniform whereas the model is solved for uniform heat flux.
- Location of thermocouples in experimental setup does not completely match the location of read values in analytical solution.
- Measurement errors and thermocouples uncertainty.

A list of measurement parameters and their corresponding uncertainties are presented in appendix A.

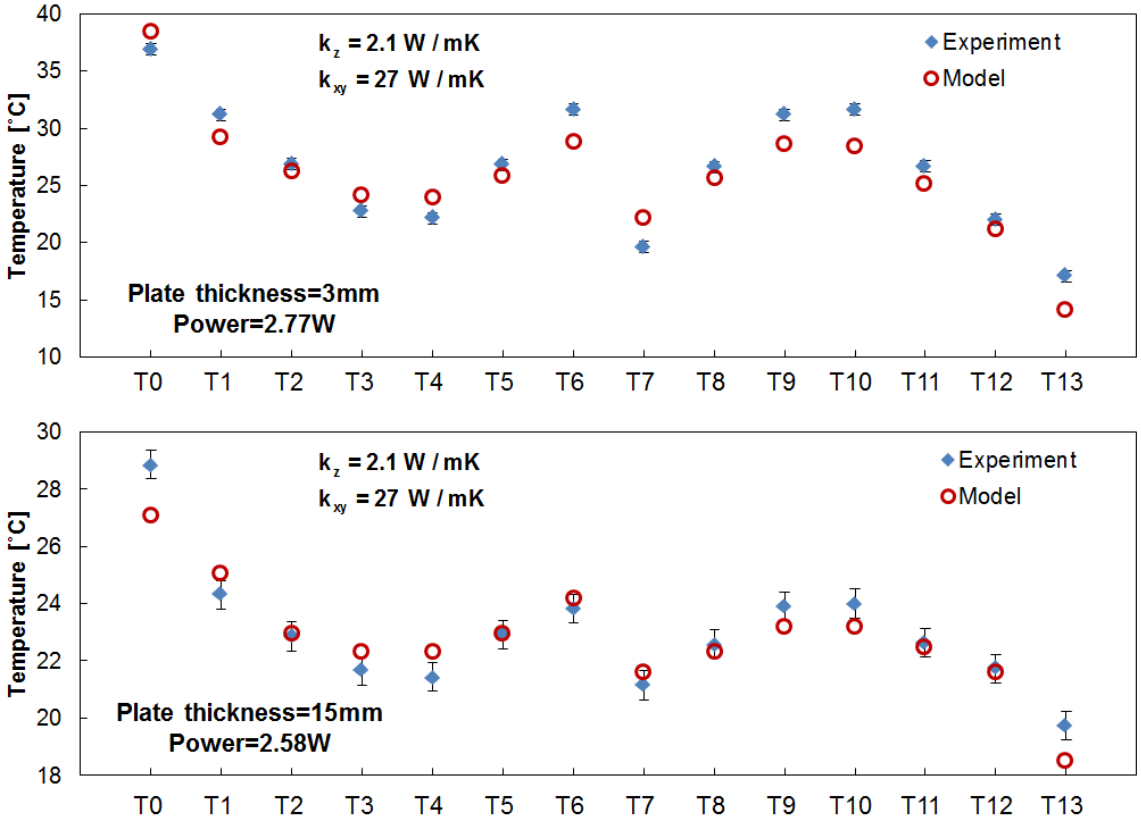

Figure 37: Comparison between experimental and analytical data for temperature distribution on two different rectangular graphite samples.

4.4. Parametric study

A parametric study is performed to investigate the effects of: i) anisotropy and ii) geometrical parameters such as plate thickness, plate aspect ratio, spots relative size and aspect ratio on thermal performance of heat spreaders. This parametric study is performed for spreaders with single heat source and heat sink, each of them placed on one face of the plate. The behavior of the multi-hotspot geometries can be obtained by superposing the effects caused by each single spot.

To cover a wide range of variation in each of the above-mentioned geometrical parameters and see the effect of anisotropy, two different arrangements for source and sink are chosen to represent two extreme cases, as shown in Figure 38. In the first case, a heat source on the top and a heat sink on the bottom are centrally aligned and positioned at the center of the plate. This arrangement (Case I) represents the lowest thermal resistance due to the minimum distance between the source and the sink. In Case II, the heat source on the top surface and the heat sink on the bottom surface are positioned at two opposite corners; thus representing the highest thermal resistance. Heat sources and heat sinks are assumed to be isoflux.

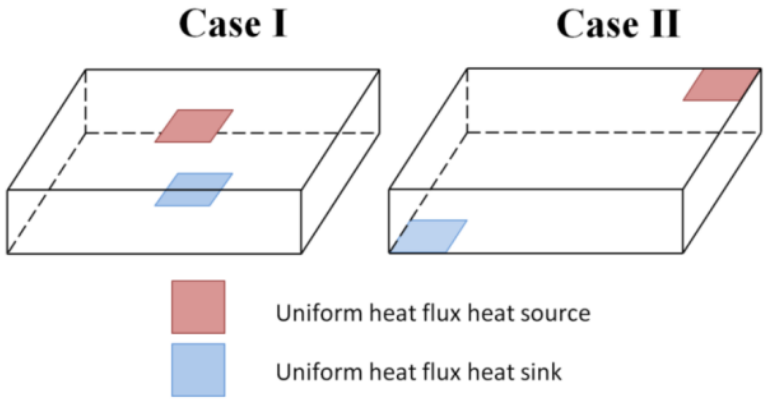

Figure 38: Two different arrangements of hotspots for parametric study (left: Case I, right: Case II)

4.4.1. Anisotropy effect

To study the anisotropy of materials, resistance of square plate with two different arrangements of source and sink, Case I and Case II, Figure 38, is plotted versus

through-plane to in-plane conductivity ratios for four different plate thicknesses in Figure 39 and Figure 41. Conductivity ratio (k_{xy}/k_z) ranges from 0.01 to 100. The source and sink are identical squares with arbitrary side length of *0.2L*. The plate is also set to be square ($\varepsilon=W/L=1$). The effect of spots size will be investigated separately later. For better depiction, the graphs are plotted in logarithmic scale.

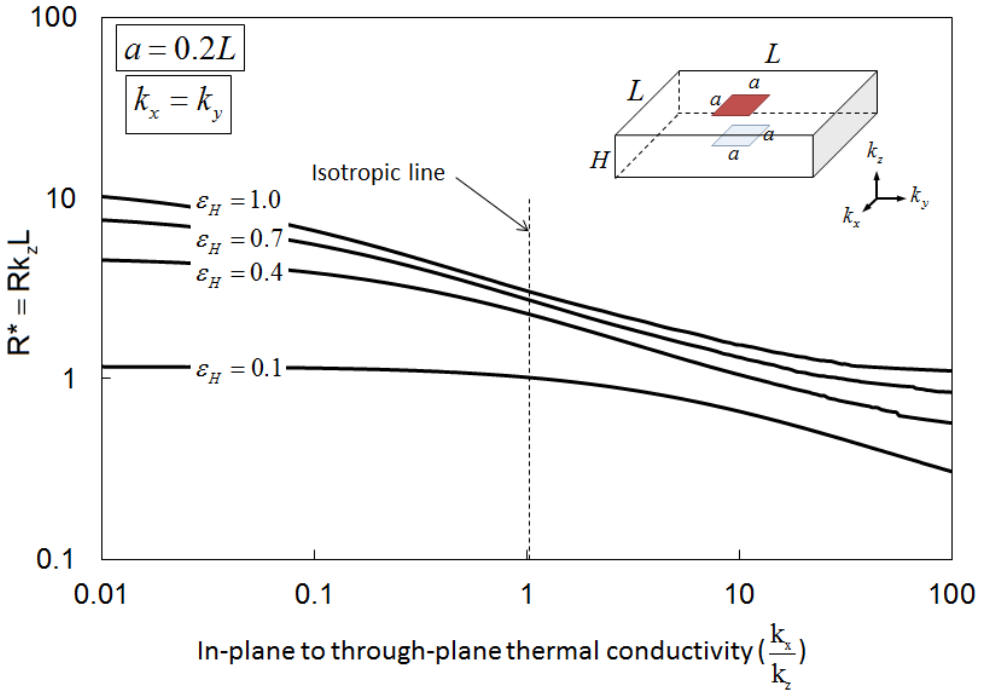

Figure 39: Resistance versus through-plane to in-plane conductivity ratio for four thicknesses (Case I)

Figure 39 shows, in a plate with two centrally-aligned spots on the top and bottom (Case I), as the ratio of the in-plane to through-plane conductivity increases, the thermal resistance decreases. This trend can be explained as follows: as the in-plane conductivity increases, the temperature becomes uniform over the surface much faster due to less in-plane resistance against the heat flow, so the heat spreading/constriction takes place easier with less temperature drop.

For the arrangement of Case I, heat transfer improvement due to increasing the in-plane conductivity is directly related to the size of the spots. As shown in Figure 40, for smaller spot area, the resistance decrease occurs more significantly when the in-plane thermal conductivity increases. This is due to the fact that the

spreading/constriction resistance becomes more considerable with smaller relative spot sizes. Thus, in such spreaders, higher in-plane thermal conductivity results in much better thermal performance improvement of the heat spreader. In other words, for smaller spots it is thermally more efficient to use anisotropic material for spreader. At the limit where the spot's sizes are as big as the plate surface, i.e., 1-D heat conduction, no spreading or constriction exists thus changing the in-plane conductivity has no effect on the plate resistance.

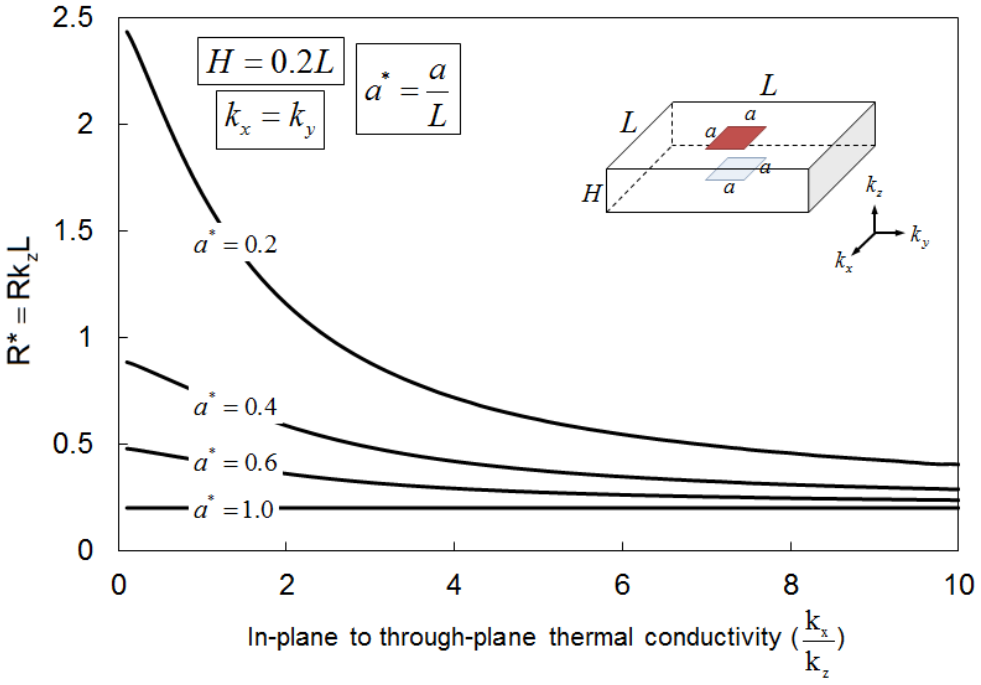

Figure 40: Resistance versus through-plane to in-plane conductivity ratio for four hotspot size (Case I)

For the second arrangement (Case II), anisotropy of the material has a more pronounced effect on the thermal performance of the spreader. Figure 41 presents the resistance variation of the plate as the in-plane to through-plane conductivity ratio changes from 0.01 to 100. It shows, for all the thicknesses, thermal resistance decreases as the in-plane conductivity increases. For thinner plates, this variation is more than thicker ones. For thin plates the heat coming from the heat source at one corner has to pass through a smaller cross-section than the thicker plates to reach the heat sink at the other corner, resulting in higher resistance for thinner plates. But as the in-plane thermal conductivity increases, the effect of in-plane resistance becomes less

important and the thickness becomes the controlling parameter. This phenomenon is clearly shown in Figure 41, where two curves of different thicknesses intersect. These intersection points demarcate the critical conductivity ratios for the two corresponding thicknesses before which the in-plane resistance is dominant, thus thinner plate has larger resistance. However, beyond these points, through-plane heat transfer plays a more important role, and the thicker plate presents more resistance.

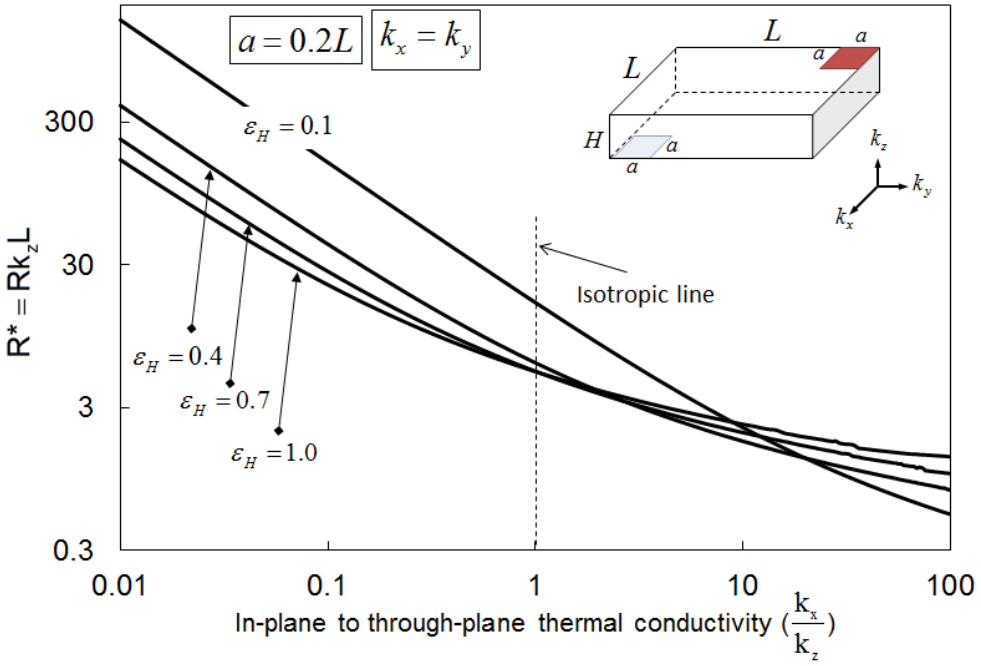

Figure 41: Resistance versus through-plane to in-plane conductivity ratio for four thicknesses (Case II)

The important points can be summarized as,

- Regardless of spots' arrangement and plate thickness, increasing the in-plane thermal conductivity always improves the heat transfer.
- As the relative eccentricity of spots on the top and bottom surface increases, the anisotropy effect becomes more prominent.
- As the relative size of spots becomes smaller, increasing in-plane thermal conductivity has a more pronounced effect on the thermal performance of the plate.
- Changing anisotropy in thinner plates creates more resistance variation compared to thicker ones.
- In 1-D heat transfer, resistance is only a function of through-plane conductivity and the plate material's anisotropy has no effect on its resistance.

4.4.2. Geometrical parametric study

In this section, for convenience, all cases are assumed to be isotropic.

Effect of plate thickness

Dimensionless resistance versus dimensionless thickness for five arbitrary different sizes of spots is plotted for both Case I and II in Figure 42 and Figure 43. Heat source and heat sink in each case are assumed to be square and have the same size. The plate is also set to be square.

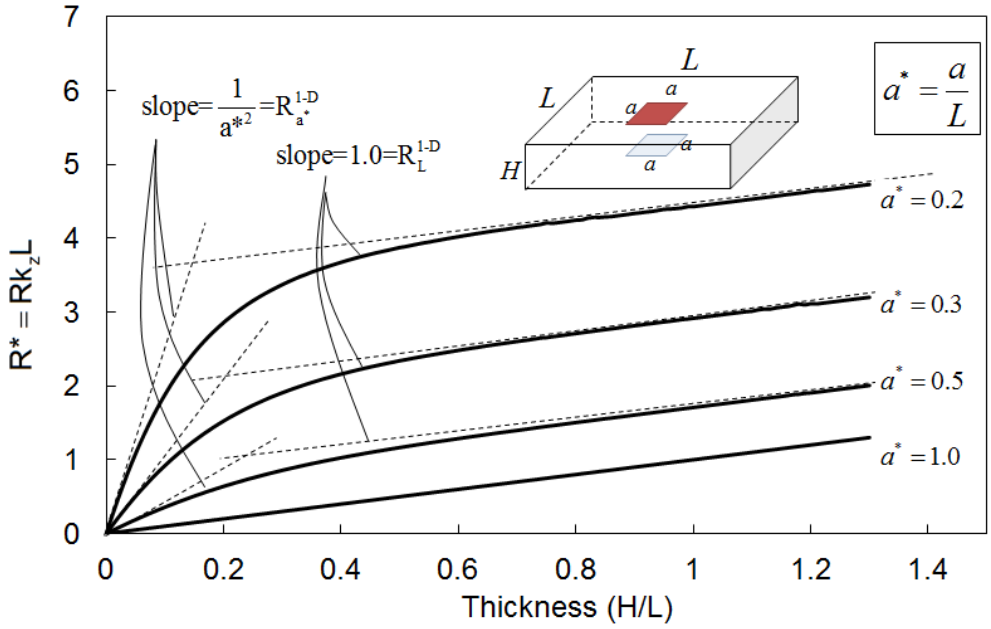

Figure 42: Plate resistance versus plate thickness for hotspot arrangement of Case I

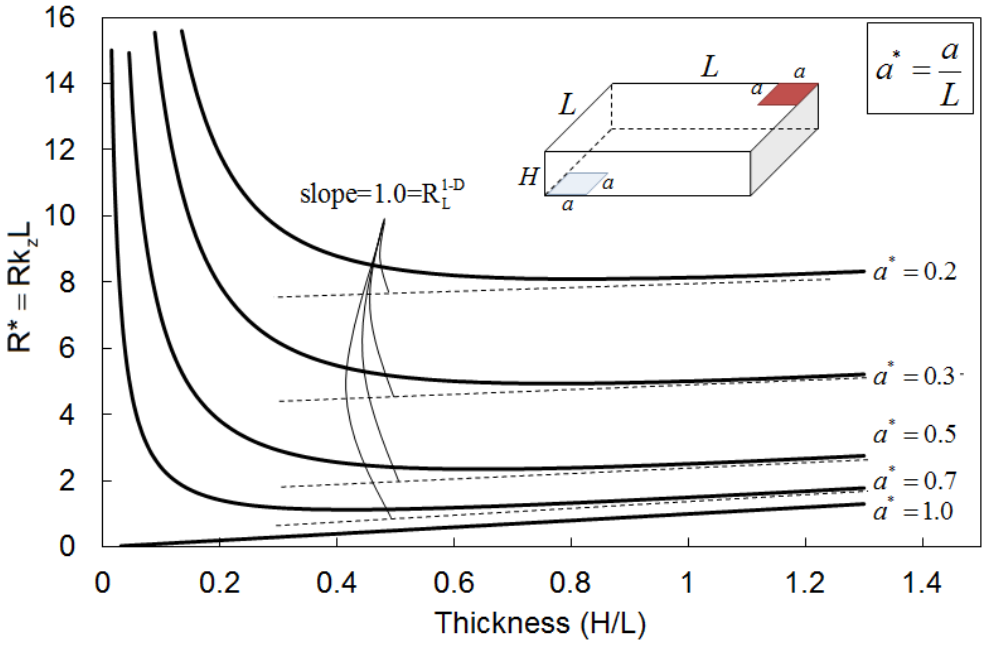

Figure 43: Plate resistance versus plate thickness for hotspot arrangement of Case II

As is indicated in Figure 42 and Figure 43 two asymptotes can be recognized. It is shown that in Case I, in which the source and sink are vertically aligned, as the thickness of the plate approaches zero the resistance with an increasing slope goes to zero. The slope at very small thickness approaches the inverse of the spot area for each spot size. It can be interpreted that for Case I, at smaller thickness the heat transfer approaches a 1-D conduction in which the resistance is proportional to the thickness and the inverse of the area. In other word, if the plate is thin enough, heat passes only through that column between the source and sink, i.e., 1-D heat conduction. However, it is not true for Case II in which the source and sink are positioned at the corners. In this case as the thickness approaches zero, the resistance approaches infinity due to the very narrow heat transfer path, Figure 43.

On the other extreme when the plate thickness increases to large values, similar behavior is observed for both Cases I and II. It is seen that for thick plates, resistance varies almost linearly with thickness and the rate of change approaches unity, which means any increase in the thickness is equivalent to adding the resistance of a 1-D heat transfer in a block with the dimensions of plate area and that increased thickness. This

can be explained as follows: as the thickness increases beyond a certain value, the resistance increase is not a function of spots size and position anymore and it changes only with thickness. To explain more, for such cases, the plate can be divided into three regions of heat transfer; i) the spreading section where the heat flows from the source into the plate; ii) the constriction section where the heat leaves the plate into the sink, and iii) the middle section or bulk resistance where the heat flow takes place almost 1-D. The resistance of the plate is a summation of these three regions as they are in series. As the thickness increases, the corresponding middle-section resistance controls the total resistance and has a linear relation with thickness. Thus, no matter how the arrangements of sources and sinks are at the top and bottom surface, in thick plates, any increase in thickness adds an amount of resistance which is equal to the resistance of that increased thickness as if there is 1-D heat transfer in the plate.

Also note that for the spreaders with eccentric spots there always is an optimum thickness which provides a minimum resistance and is a function of plate geometry and spots arrangement. The following summarizes the effects of plate thickness:

- For large thicknesses, the resistance variation due to the thickness change is not a function of spots arrangements.
- Resistance for plates with non-aligned spots on the top and bottom surfaces approaches infinity as the thickness approach zero.
- Resistance for plate with aligned and equal spots on the top and bottom surfaces becomes independent of plate size and spots position as the thickness approaches zero.
- For plates with non-aligned spots on the top and bottom surfaces, there is an optimum thickness, which gives a minimum resistance. As the size of spots decreases, this optimum value increases.
- Resistance for plates with aligned and equal spots on the top and bottom surfaces has an asymptotic behavior in both very small and very large thicknesses.

Effect of plate aspect ratio

The effect of plate aspect ratio on the resistance for both Cases I and II for different thicknesses are shown in Figure 44 and Figure 45. The area of the plate, $W \times L$, is kept constant, equal to unity. The source and sink dimensions remain constant and equal in both cases, $a=b=a'=b'=0.2L$.

In this specific case, because the goal is to investigate the effect of variation of *L* which has been used as the characteristic length, non-dimensionalizing the resistance with respect to *L* would not lead to any useful results. Therefore, dimensional resistances are plotted.

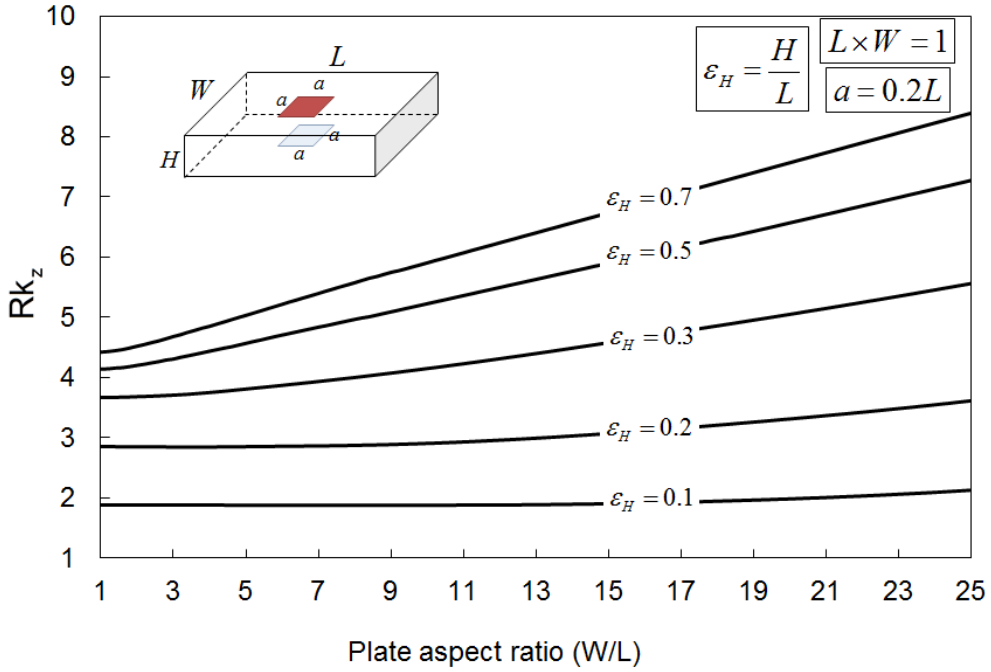

Figure 44: Plate resistance versus plate aspect ratio for different thickness (Case I)

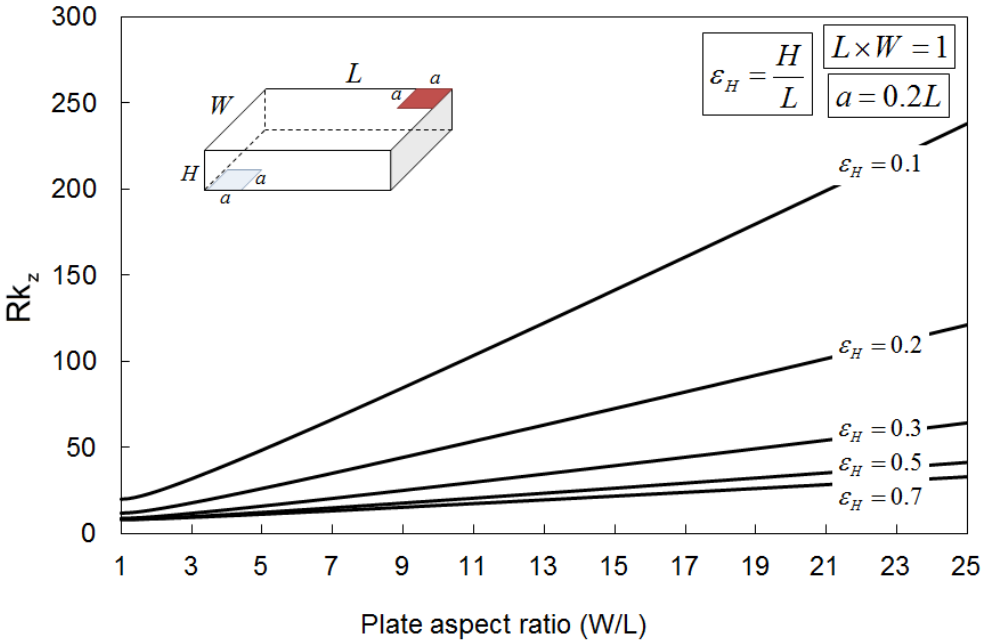

Figure 45: Plate resistance versus plate aspect ratio for different thickness (Case II)

Figure 44 shows the resistance of constant area plate versus its aspect ratio with identical spots in the center. It can be seen that regardless of the thickness, increasing the aspect ratio deteriorate the thermal performance. However, as the thickness of the plate decreases, the effect of aspect ratio variation becomes smaller. The reason is that, heat transfer occurs mainly through the plate bulk which is in between the sink and source. Thus, changing the aspect ratio does not affect the heat transfer noticeably.

Similar to Case I, but more strongly, increasing the aspect ratio for the spots arrangement of Case II increases the resistance, Figure 45. This is reasonable since as the aspect ratio increases, two spots get further away from each other so the heat flow coming from the source has to pass through a longer distance to reach the sink. Thermal performance becomes even worse if the thickness decreases. This is also because the cross section reduces as the thickness decreases, so the heat has to pass through a smaller area which results in a higher resistance. The following are the important conclusions regarding the plate aspect ratio,

- For a fixed area of heat spreader, square shape offers the minimum resistance.

- Changing the plate aspect ratio causes smaller resistance change in thicker plates rather than thinner ones.

Effect of source/sink relative size

In applications where the spot sizes are adjustable, they can be chosen such that thermal resistance is minimized. For this purpose, the effect of spots relative size on the plate resistance is studied on Case I for two different scenarios: i) the square shape source and sink vary in size simultaneously, and ii) the sink size is kept constant at *a'=b'=0.2L* while the source size is varied.

For the first scenario, the resistance versus side length of square source and sink is plotted in Figure 46 for different thicknesses. As can be seen, the spots side length is ranging from small values to unity, i.e. the plate length.

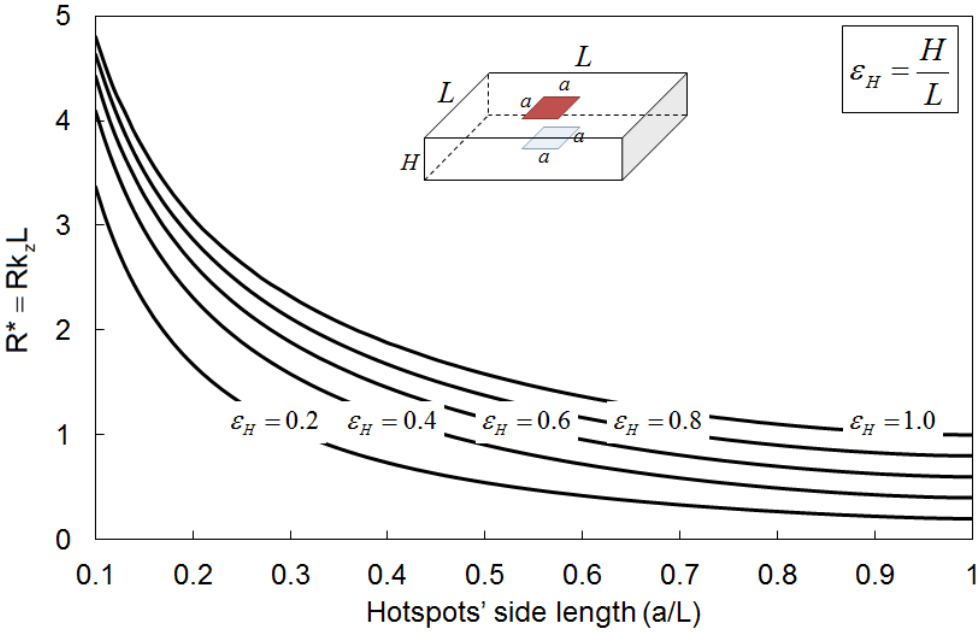

Figure 46: Plate resistance versus hotspots' size for Case I. (Source and sink vary in size equally)

Figure 46 shows that as the heat sink and heat source size increases, the resistance against the heat flow decreases. At the point where the dimensionless spots side length is equal to unity the area of spots are equal to the area of the plate, so the heat transfer is 1-D and the dimensionless resistance is equal to the dimensionless thickness.

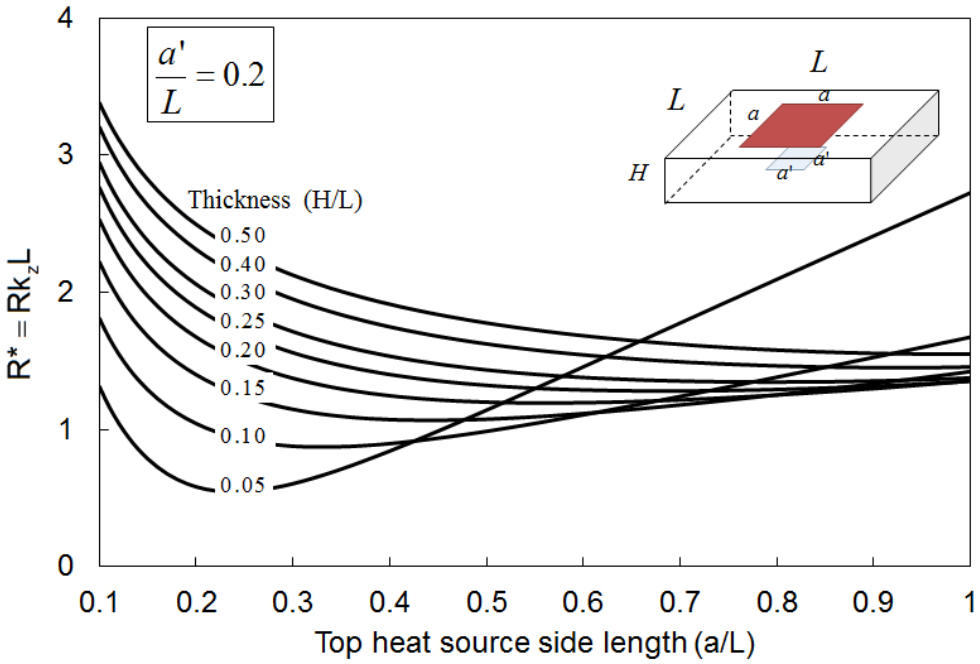

Figure 47: Plate resistance versus heat sink's size for Case I

The second scenario is plotted in Figure 47. When one of the spots has a constant area, increasing the other spot's size does not always cause heat transfer improvement. It shows that the minimum resistance occurs when the sink area is between the heat source and the spreader plate area. This optimum point depends on the geometrical parameters of the plates and the source. One important parameter in defining this optimum point is the thickness of the plate. As indicated in Figure 47, the minimum resistance happens at larger heat source areas as the thickness increases. There is a critical thickness beyond which this optimum resistance occurs where the source has the biggest possible area, i.e., the plate surface area. For instance, when the square heat source has the constant side length of 0.2*L*, this critical thickness is almost 0.3*L*, and beyond this value the minimum resistance happens when the sink area is equal to plate area. The important points regarding the spots size (Case I) can be concluded as,

- For the same heat source and heat sink size, a minimum thermal resistance exists where they have maximum available area.
- If one of the spots area is fixed, there is an optimum size for the other spot that offers a minimum resistance. This optimum size is somewhere between the fixed spot size and the spreader plate size.

- Beyond some thicknesses, the minimum resistance occurs when the spots have the maximum available area.

Effect of source/sink aspect ratio

Spots aspect ratio also can affect the resistance of the plate. Resistance versus heat sink aspect ratio, while its area is kept constant, is plotted in Figure 48 for Case I for different plate thickness. All other geometrical parameters including sink's dimensions are kept constant. The aspect ratio changes from 1 which is a square of 0.2*L*×0.2*L* to 25 which is a strip with the length of the plate width. The plot in Figure 48 shows that if one hotspot is confined to a square shape, the minimum resistance occurs when the other spot has a rectangular shape and its aspect ratio depends on the plate thickness and square spot's size and area. As can be seen in Figure 48, as the thickness of the plate increases the optimum aspect ratio of the source increases.

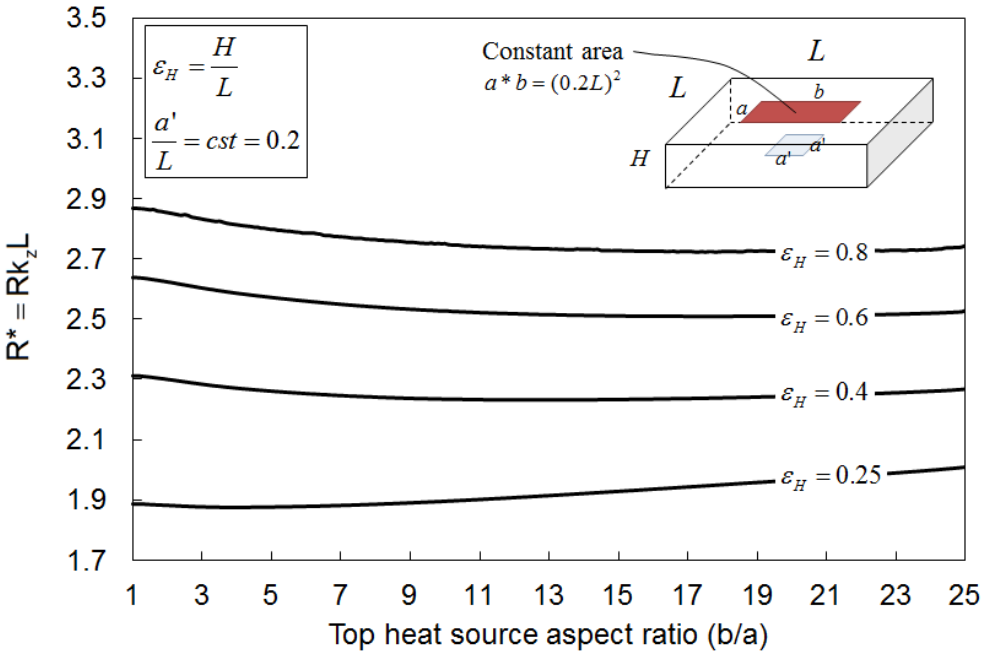

Figure 48: Plate resistance versus heat sink's aspect ratio for Case I. (Source size remains constant)

The following summarizes the trends observed in Figure 48:

- If one spot is confined to a constant square- shape, the minimum resistance occurs when the other spot has a rectangular shape and its aspect ratio depends on the plate thickness and square spot size and area.

- As the plate thickness increases, the optimum aspect ratio for the heat sink while the heat source is in square shape increases.
- Comparing to other parameters spot's aspect ratio has less impact on thermal resistance.

4.5. In-plane thermal conductivity measurement

To assist power dissipation in high-density electronic devices, there has been an increasing demand for materials that are characterized by high thermal conductivity in the given directions only. High in-plane thermal conductivity materials are of interest to many cooling mechanism designers. Despite wide employment of anisotropic materials such as graphite plates, gas diffusion layer (GDL) and different porous materials in heat transfer and cooling industry, companies still are seeking accurate yet simple methods for the property measurement of their products. One of the key properties of such materials which needs to be determined accurately is the in-plane thermal conductivity. Several theoretical and experimental approaches have been proposed to measure electrical and thermal conductivity of anisotropic plates [97]–[101]. Zamel *et al.* [99] developed a numerical model to estimate the through-plane and in-plane effective thermal conductivities of untreated GDL using realistic 3-D pore morphology of the material and solving the governing mathematical equations. Ismail *et al.* [98] measured the in-plane and through-plane permeability of a specific type of GDL using a custom-made experimental set-up. In their setup the sample was compressed with a specific fiber angle between two plates and was exposed to a mixture of gas. The amount of penetrated gas in that specific direction was used to calculate the permeability. In a novel yet simple method, Sadeghi *et al.* [97] measured the in-plane thermal conductivity of GDL. In their experimental method, by using two different length of material exposed to same amount of heat flow from one end to the other, they canceled the end effect resistances and reported the in-plane thermal conductivity with an acceptable accuracy.

The LAEC team in collaboration with their industrial partner, Terrella Energy Systems Company, are designing a technique for the measurement of the in-plane thermal conductivity of the company's products which are different types of graphite plate. In the following sections, a new experimental approach for measuring in-plane

thermal conductivity of graphite (referred to as Two-Length Method) following by the results for different samples is presented. In the end, a new semi-analytical algorithm for measurement of in-plane thermal conductivity using both the presented analytical model and experimental data is introduced.

4.5.1. Two-Length Method

Two-length method is an experimental method for measuring the in-plane thermal conductivity. In this approach, two rectangular strips of the sample material with the same width but different length are exposed to a constant thermal difference at ends as shown in Figure 49. The ratio of samples' length to their thickness have to be chosen large enough (at least 50 times bigger) in order for the heat flow-lines in the middle of the samples to become parallel to each other and form a one-dimensional heat transfer in the longitudinal direction. Since the experimental setup is identical for both sample lengths, it is concluded that the thermal end-effects (including spreading/constriction and contact resistances) in both samples' ends are identical. Hence, it can be deduced that the difference between the measured thermal resistances of the two samples (with different lengths) is due to the difference in 1-D heat transfer in the middle section of samples.

In the experimental custom-designed test-bed shown in Figure 51, the thermal resistance between the source and sink for each sample can be measured rather simply, i.e. the temperature difference between sink and source divided by the heat flow. Considering the equivalent resistance network of each sample, Figure 49, the difference between the resistances will be,

$$R_1 - R_2 = R_1^{1-D} - R_2^{1-D} \tag{48}$$

As the spreading and constriction regions are the same in both samples, the difference between the resistances is equal to the 1-D resistance of a plate with the same cross section (A) and length of $L_2 - L_1$.

$$R_1 - R_2 = R_1^{1-D} - R_2^{1-D} = \frac{L_1 - L_2}{A k_{in-plane}} \tag{49}$$

Rearranging the total resistance in the form of $\Delta T / Q$, the following can be used to calculate the in-plane thermal conductivity of the graphite sheets and any other porous thinned-film samples:

$$k_{in-plane} = \frac{L_2 - L_1}{A}\left(\frac{\Delta T_2}{Q_2} - \frac{\Delta T_1}{Q_1}\right)^{-1} \tag{50}$$

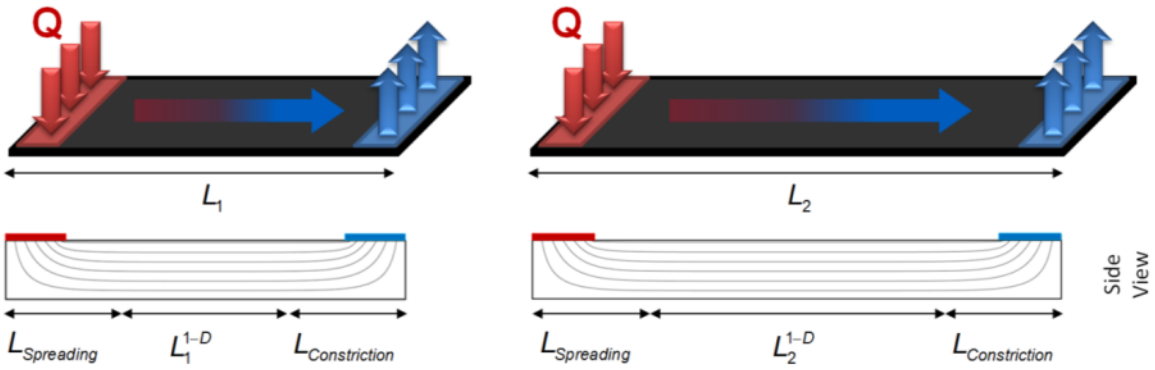

Figure 49: Schematic for the Two-Length Method test-bed used for in-plane thermal conductivity measurements of graphite sheets

4.5.2. Experimentation - In-plane thermal conductivity measurement test-bed

Two important considerations should be satisfied in the test-bed design: i) the exact amount of heat passing through the samples should be measured; and ii) the end effects, i.e, contact and spreading resistances at both ends, should be identical In both test steps. The first issue will be explained at the end of this section. To address the second issue, the pressure on the samples at both ends has to be measured and kept constant for each test. As such, the contact resistance between the holders and samples which is a function of pressure remains constant [102]. The spreading resistance also has to be kept constant by choosing the same cross-section for both samples in each experiment. In the following the custom-designed test-bed that was used in this study is explained.

The test-bed consists of a hot end, cold end, adjustable bed frame, and an iced water tank. In the test-bed, the hot end consists of two identical 2.5inch long cartridge heaters (120V, 30W) embedded symmetrically on the back of the four samples' spot. On the cold end, 5 identical 200mm long heat pipes with radius of 6mm reject the heat to the iced water tank underneath the test-bed. The iced water tank is kept at zero degrees centigrade by refilling the ice during the experiment resulting in a constant cold end temperature (Figure 50). The bed frame of setup allows both source and sink to slide and become adjusted for any sample length in the range of [20mm-200mm].

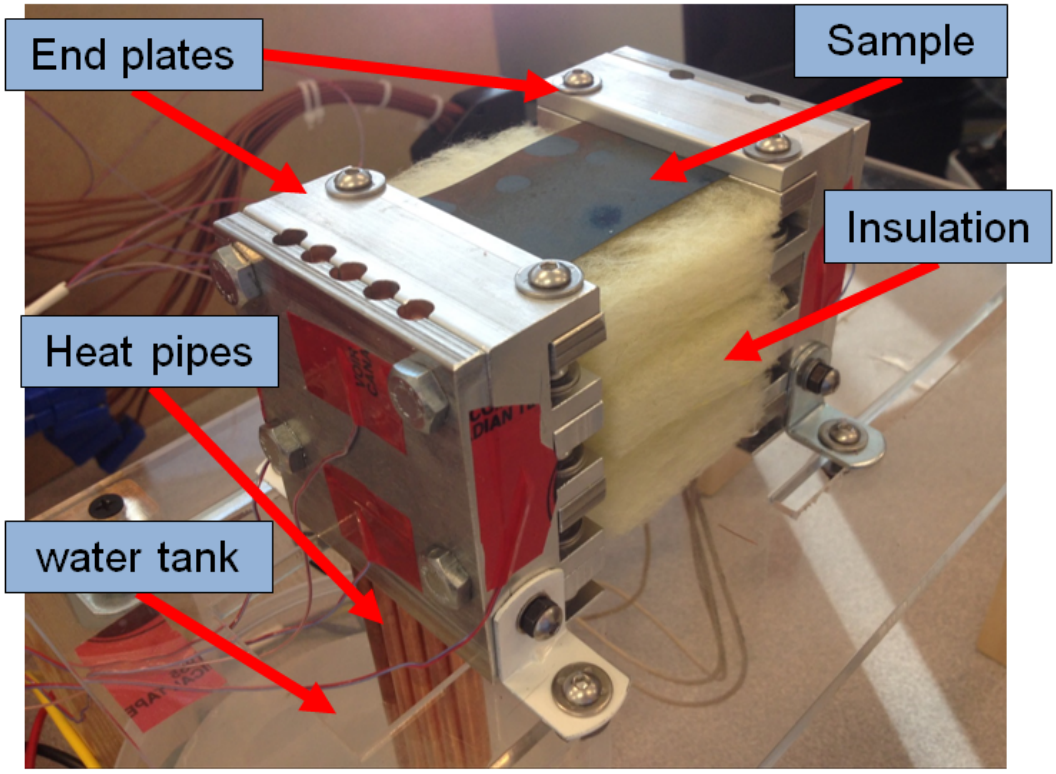

Figure 50: In-plane thermal conductivity measurement test-bed

For very thin samples, the large thermal resistance will hinder the heat flow so the heat leakage through the insulations increases, i.e. the uncertainty of the results increases and the accuracy drops. Therefore, the test-bed is designed in a way to run the experiment for four samples at once, so it reduces the thermal resistance and improve the accuracy of the measurement. According to Appendix A, increasing the number of experimental results by the factor of *n* reduces the uncertainty of the results

by the factor of $\sqrt{n}$, so this test-bed by having four samples tested at once reduces the uncertainty of the final result by half.

The proper design of the test-bed permits the pressure to be adjustable on the sample by controlling the torque applied on the screws of sample holders, Figure 50. The samples and the end plates are insulated to minimize the heat loss to the surrounding. 9 T-type thermocouples read the temperature at different locations such as heat source, heat sink, water tank and ambient. Temperatures are monitored and stored using the NI 4213 module of National Instrument DAQ system. The voltage and power of the heater is supplied and monitored by the Chroma Programmable DC Power Supply (model: 62012P).

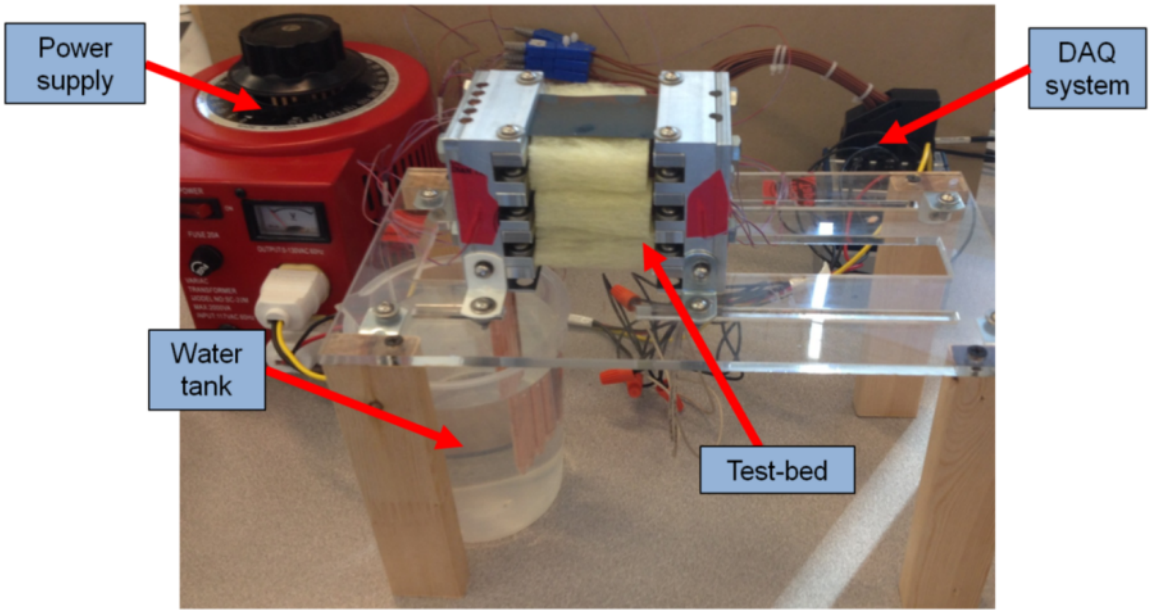

Figure 51: In-plane thermal conductivity test-bed with power supply and DAQ system

All the graphite samples were cut and measured using knife cutter and caliper. The samples for in-plane thermal conductivity measurement are presented in

Table 11.

Table 11: In-plane thermal conductivity measurement samples specifications

sample	short/long length [mm]	Width [mm]	thicknesses [mm]
GT-1	100/150	40	0.57
GT-2	100/150	40	1.17
GT-3	100/150	40	0.38
GT-4	100/150	40	0.80
Battery-1	60/80	40	0.18

The general procedure to run the experiment is to turn on the heaters at a constant heat flow for both sample lengths and let the system reaches the steady state condition (appendix B), then read the temperature difference at each step caused by the total resistance. For the experiment to have more reliable results the temperature difference should be relatively large, but not as large that cause thermal issues to the system. Meeting these criteria leads to find an optimum value for the input power for each specific sample. This value for the graphite samples was chosen to be 20W as an average.

In all the performed experiments, the test-bed and the samples are completely insulated; however, there still is some heat loss. The IR images of the test-bed while functioning (Figure 53) shows a slight temperature difference between the surface of insulation and the ambient, which due to relatively large surface area, may cause considerable heat loss. To account for the heat loss, we can model the test-bed as two parallel resistances (Figure 52) operating between the heat source and heat sink (in this case the heat sink is assumed to be the ambient). The first resistance is the resistance of the samples and the second one represents the resistance of all other heat dissipation paths to the ambient. To calculate the sample's thermal conductivity, one has to know the value of the loss resistance (R_{loss}) of the test-bed. The loss resistance for the test bed is mainly the resistances of the insulation and the bypass paths from the source to sink such as convection of the entrapped air and conduction through the frame bed. To find this resistance a no-sample test has to be performed while having all the insulation on. By applying a known amount of heat flow and reading the steady state temperature difference (appendix B) between heat source and the ambient, the loss resistance can be calculated using Eq. (1). This resistance hardly changes for other tests as it is only a

function of insulation and distance between source and sink. After running the no-sample test for our test-bed, R_{loss} was found to be 25.2 [˚C/W].

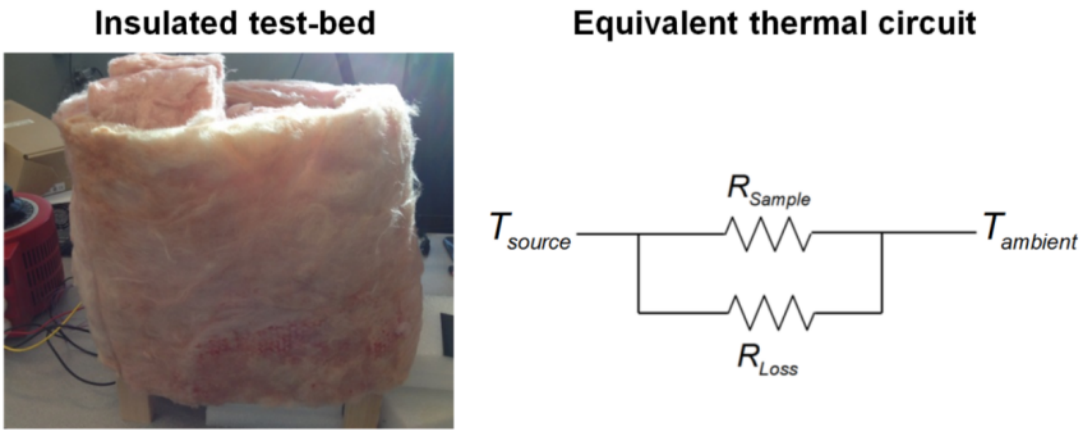

Figure 52: Thermal resistance network of the insulated in-plane thermal conductivity measurement test-beds

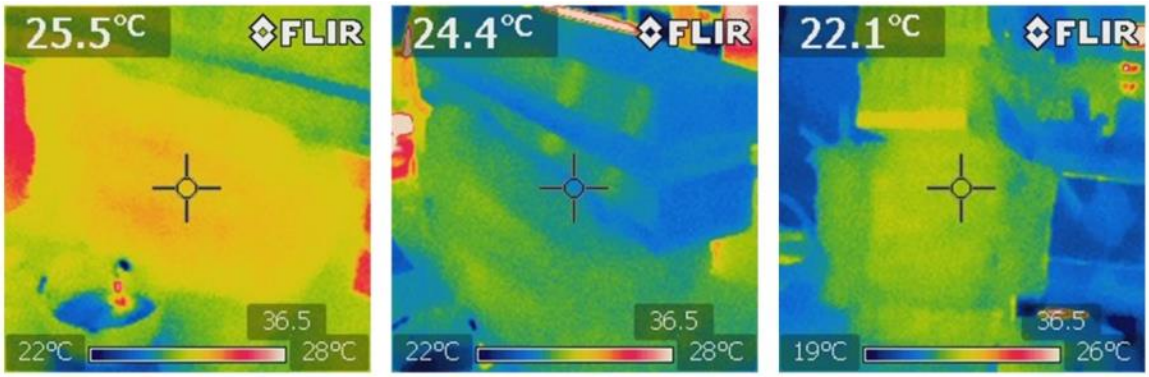

Figure 53: IR pictures of single later in-plane thermal conductivity measurement test-bed

Results

All the samples presented in

Table 11 were tested using the above-explained test-bed and the results are presented in Table 12. The uncertainties of the results are calculated based on appendix A.

Table 12: In-plane thermal conductivity measurement secifications and results

Sample	Power [W]	ΔT, ΔT' [˚C]	Thermal Conductivity [W/m. ˚C]	Uncertainty [%]
GT-1	6	36.4, 49.4	340	7.7
GT-2	6	23.8, 36.4	345	6.9
GT-3	6	41.1, 57.7	600	6.4
GT-4	6	25.3, 37.6	505	7
Battery-1	4	58, 65	21	8.2

4.5.3. A semi-analytical method for measurement of in-plane thermal conductivity

In-plane thermal conductivity measurement of thin plates due to their low thickness and somehow fragility is not as convenient as the measurement of their through-plane thermal conductivity. Besides, through-plane measurement instrument are more global and widespread whereas the possibility to measure the in-plane is an added option which most of these instrument lack. As such, in this study, an algorithm is presented through which by having the through-plane thermal conductivity of a material and performing a simple single heat transfer experiment the in-plane thermal conductivity can be calculated iteratively using Eq. (27). In the following the detailed steps of the algorithm are explained.

Algorithm:

1. The through-plane thermal conductivity of the plate sample is measured.
2. A rectangular shape of known dimensions is cut from the sample and one rectangular source and one sink of smaller size is attached to arbitrary locations.
3. The whole plate is insulated properly and a known amount of heat flux is applied to the source.
4. After reaching steady state, temperatures difference between two arbitrary spots on the plate, A and B, is measured.

5. An in-plane thermal conductivity value for the plate is assumed.
6. Based on the geometrical characteristics of the test setup and the input power of the source as well as the known through-plane and assumed in-plane thermal conductivities, temperatures of spots A and B are solved using Eq. (27).
7. The modeled temperature difference between A and B is compared with the experimental value:
   - If $(\Delta T)_{model} < (\Delta T)_{experimental}$ then the assumed in-plane thermal conductivity is decreased by ε.
   - If $(\Delta T)_{model} > (\Delta T)_{experimental}$ then the assumed in-plane thermal conductivity is increased by ε.
8. The loop starts over from step 5 until the desired accuracy is achieved.

The flowchart in Figure 54 demonstrates the above-mentioned algorithm.

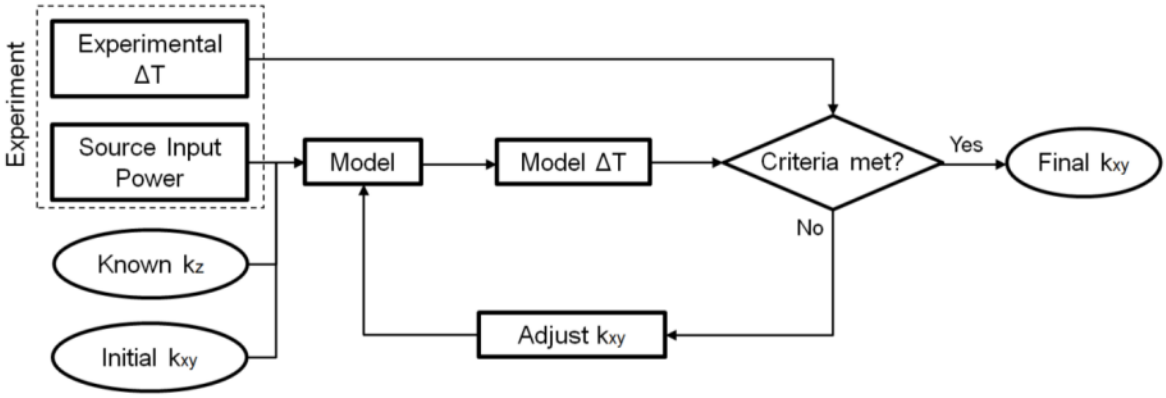

Figure 54: Semi-experimental method for in-plane thermal conductivity measurement (flowchart)

For samples which have two different thermal conductivities in in-plane direction (*x* and *y* directions) the same algorithm with small changes in steps 4 and 7 can be applied. The changes are as follow:

Step 4: After reaching steady state, temperatures of three spots on the plate, A, B and C, are measured. These three point should be chosen in a way that AB and AC be in the directions of x and y.

Step 7: the modeled temperature differences of AB and AC are compared with the experimental values:

- If $\begin{cases} AB: (\Delta T)_{model} < (\Delta T)_{experimental} \\ AC: (\Delta T)_{model} < (\Delta T)_{experimental} \end{cases}$ then $\begin{cases} k_x = k_x - \varepsilon \\ k_y = k_y - \varepsilon \end{cases}$

- If $\begin{cases} AB: (\Delta T)_{model} < (\Delta T)_{experimental} \\ AC: (\Delta T)_{model} > (\Delta T)_{experimental} \end{cases}$ then $\begin{cases} k_x = k_x - \varepsilon \\ k_y = k_y + \varepsilon \end{cases}$

- If $\begin{cases} AB: (\Delta T)_{model} > (\Delta T)_{experimental} \\ AC: (\Delta T)_{model} < (\Delta T)_{experimental} \end{cases}$ then $\begin{cases} k_x = k_x + \varepsilon \\ k_y = k_y - \varepsilon \end{cases}$

- If $\begin{cases} AB: (\Delta T)_{model} > (\Delta T)_{experimental} \\ AC: (\Delta T)_{model} > (\Delta T)_{experimental} \end{cases}$ then $\begin{cases} k_x = k_x + \varepsilon \\ k_y = k_y + \varepsilon \end{cases}$

Sample results

To obtain the temperature at two points, A and B, an experimental setup is built (section 4.3.2). Four graphite samples that were tested in section 4.5.2 are tested with this method. Points A and B are chosen to be at the distance of 5cm diagonally. The through-plane thermal conductivity of these materials was tested previously in LAEC. Table 13 shows the specification of the sample and experiment as well as the final results for in-plane thermal conductivities.

Table 13: Results of in-plane thermal conductivity of four samples using the new approach

Sample	k_z [W/m.˚C]	Q_{source} [W]	ΔT_{AB} [˚C]	k_{xy} [W/m.˚C] (results)	relative difference with direct measurement [%]
GT-1	0.1 – 2	2	5	~280	18
GT-2	0.1 – 2	2	4.2	~290	16
GT-3	0.1 – 2	2	6.1	~440	27
GT-4	0.1 – 2	2	3.9	~420	16

The differences could be associated with measurement errors, not well-uniformed heat flux at the heat source and sink, and thermal leakage due to imperfect insulation.

4.6. Conclusion

In the first part of this chapter, thermal spreaders were investigated and thermal spreading resistance for intermediary spreaders in cooling systems was comprehensively studied. An analytical model for temperature distribution inside anisotropic plates subjected to multiple heat sources and heat sinks was presented. Using this solution, a model for spreading resistance for such spreader plates was defined. The presented model was validated both numerically and experimentally. In the experimental procedure, a rectangular graphite sample was exposed to a square heat source at one corner and to a same size square heat sink on the back at the other corner. After applying a known heat flow at the heat source and attaining steady state (appendix B), the temperature at a number of locations were measured and compared to the model values. The maximum observed relative difference was found to be 5%. After validating the analytical model, a comprehensive parametric study on the effect of thermo-physical properties of the plate on thermal resistance was performed. The influence of anisotropy and geometrical parameters such as spreader, sources and sinks size and aspect ratio was investigated in detail and critical values were discussed.

In the second part of the chapter, the importance and challenges of the measurement of in-plane thermal conductivity of anisotropic thin layers was discussed and a smart and simple method for measurement of this characteristic was proposed. The proposed method which is named Two-Length Method is based on extracting the thermal resistance of a 1-D heat transfer in a known length of material by subtracting the bulk thermal resistance of two different lengths of samples exposed to a constant heat flow. A multi-layer test-bed for this purpose was designed and built. Several anisotropic samples were tested and thermal conductivity values were reported. Finally, a semi-analytical approach for calculating in-plane thermal conductivity was proposed. In this approach, the experimental data for through-plane thermal conductivity of a material and the specification of a simple test on that material are plugged into the analytical model, and then through an iterative process the in-plane thermal conductivity is determined.

Chapter 5. Conclusion and future works

A fully passive heat pipe-integrated cooling mechanism for outdoor telecommunication equipment was proposed, designed, analysed and tested. Experimental, analytical and numerical studies were performed in order to design an optimum cooling system for outdoor power enclosures produced by industrial partner, Alpha Technologies Ltd. As it was explained in Chapter 1, the active cooling systems of Alpha enclosures suffer from a number of drawbacks including non-uniform cooling of hotspots, the requirement for parasitic power and regular maintenance, noise, and cost. Figure 55 shows the performance of active cooling system of 1.2kW rectifier that is currently used in telecommunication equipment of Alpha enclosures.

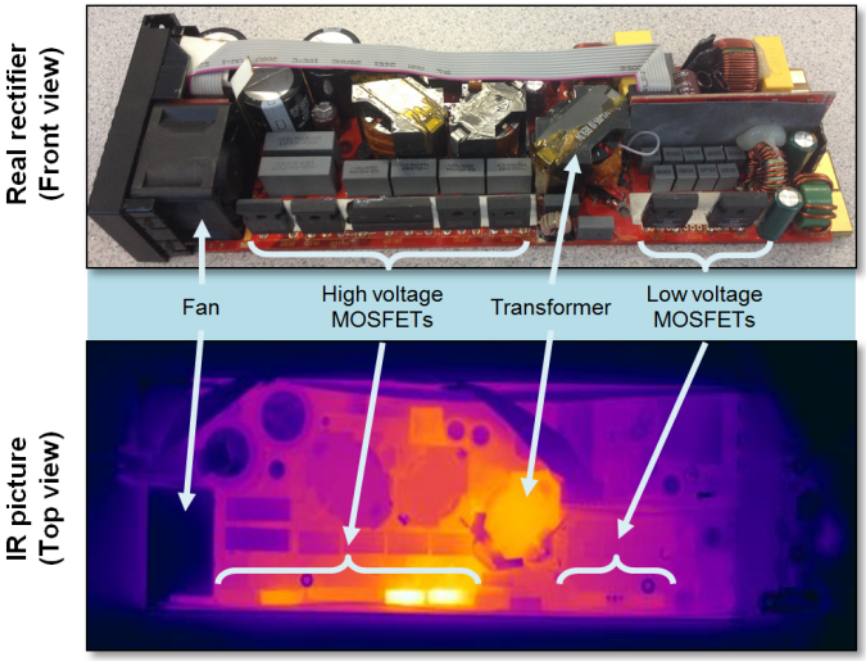

Figure 55: IR picture of an active-cooled 1.2KW rectifier functioning under 25% load

In the new design which is schematically shown in Figure 56, the fans, heat sinks, and air-to-air heat exchanger were replaced with a series of heat spreaders, heat

pipes, and a finned-wall cabinet. The new design needs no parasitic power, no maintenance and can provide more uniform temperature distribution in the rectifier module. The comparison of the forced cooling mechanism performance with the new passive cooling mechanism for a specific working condition, and three different ambient temperatures is shown in Figure 57.

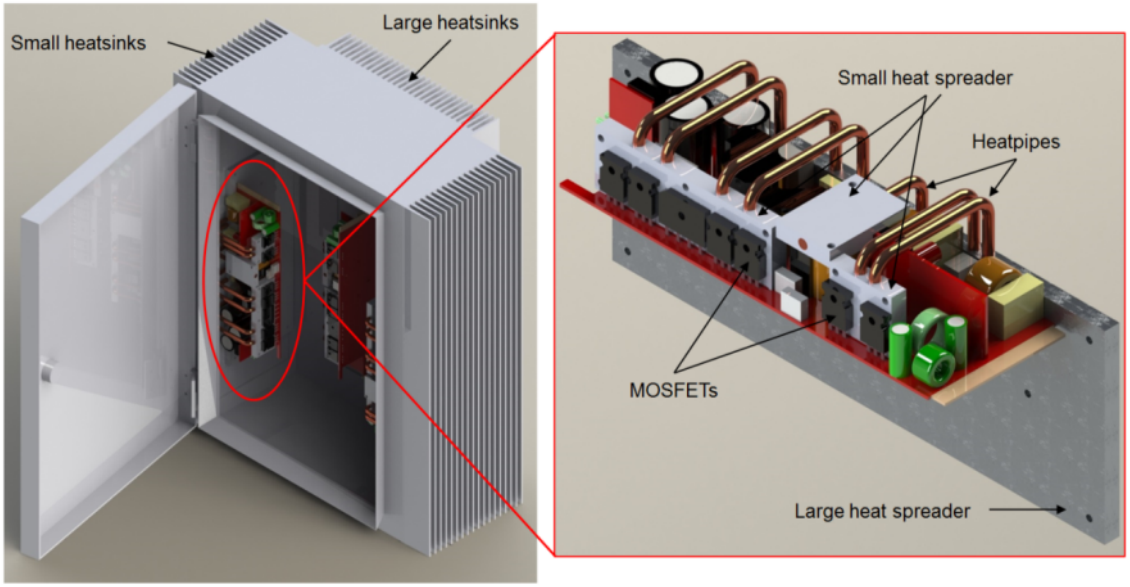

Figure 56: The new heat pipe-integrated passive cooling mechanism for 1.2KW rectifiers of Alpha's telecommunication equipment

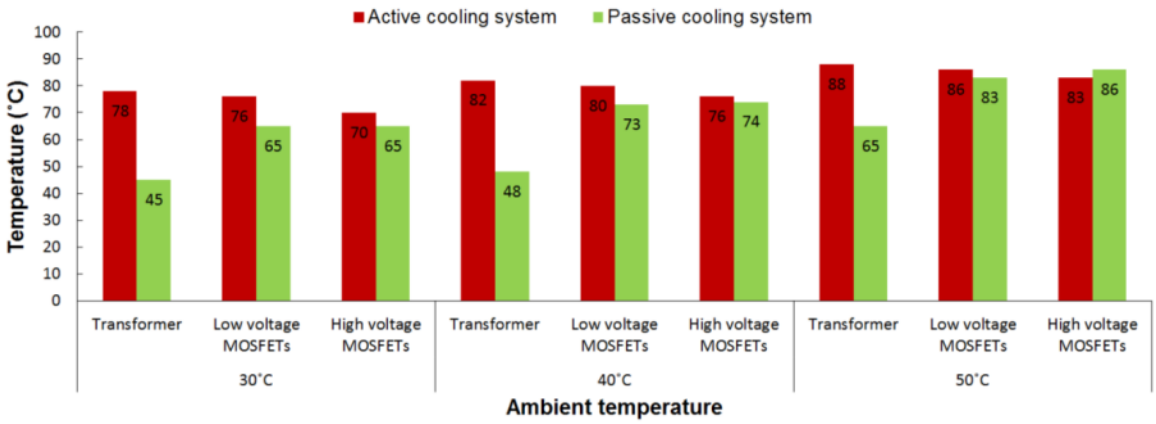

Figure 57: Performance comparison between active and new passive cooling mechanism of Alpha's rectifiers for a specific working condition

In order to reduce the cost of simulation and modeling of such thermal systems, a simplified yet accurate modeling approach was proposed. In this approach, a new

analytical methodology is developed that can accurately predict the dynamic thermal responses of multi-component systems. The passive cooling solution components including: heat spreaders, heat pipes and heat sinks, are modeled individually with a network of resistances and capacitances which represents the transient thermal behavior of that compartment. Then the corresponding R and C blocks are appropriately assembled to form a network to represent the thermal system. Analytical solutions for the resistance of different components were derived and implemented. Using these analytical solutions eliminates the need for numerical simulation of large components with highly non-uniform temperature distribution. According to the proposed approach, any type of thermal system with any number of components can be represented with an equivalent thermal circuit. By analyzing the equivalent thermal circuit, the model is capable of predicting the temperature distribution of the system in both transient and steady state condition for any loading scenario. This characteristic gives comprehensiveness and robustness to the modeling approach.

To validate the present RC model, a two-path passive cooling test-bed consisting of two heat sources connected to a heat sink using two heat pipes and two spreaders is built. The experiments are conducted under different dynamic thermal loading scenarios; and the temperatures at 16 locations, distributed along the heat path, are measured and recorded. The comparison between the proposed model and the experimental data shows an excellent agreement with maximum relative difference of 4.5%.

The following highlights the findings of this project:

- A passive cooling solution for telecommunication equipment was presented, offering a number of advantages over active systems, including; No need for parasitic power, no need for regular maintenance, no noise, feasibility to completely seal the equipment from its environment, higher efficiency, etc.
- A new system-level modeling approach for analysing transient and steady state thermal cooling systems was introduced and experimentally validated.
- Thermal resistance and capacitance of different components of passive cooling systems including, heat spreaders, heat pipes, heat sinks, convection and radiation are analytically derived and integrated to form an RC network representing the thermal behaviour of the system (Table 9).
- Temperature distribution inside anisotropic rectangular spreaders with multiple heat sources and sinks on top and bottom surfaces was analytically modeled.

The model was validated both numerically and experimentally with maximum relative errors of less than 0.1% and 5% respectively.

- A parametric study on the thermal resistance of spreaders was performed which can be referred to as a guideline for engineering thermal spreader design.
- A novel test-bed for measuring in-plane thermal conductivity of anisotropic materials was built and tested for different materials.

Future work

The following directions can be considered as the continuation of this dissertation:

1. Performing an optimization analysis for the proposed passive cooling solution to design an optimum arrangement of heat spreaders and heat pipes as intermediary components of cooling path.
2. Investigating the effect of enclosure geometry and equipment arrangement inside the enclosure on the thermal performance of the passive cooling mechanism.
3. Performing a comprehensive study on modeling thermal contact resistance and its transient behaviour and integrating it with the present model.
4. Executing a more detailed analysis of the heat pipe and investigating the resistive behaviour of evaporation, condensation, vapor flow and non-uniform heat flux profiles.
5. Considering the effect of convective heat transfer on the surface of heat spreaders instead of the adiabatic assumption in the proposed model.

References

[1] "Status of the power electronics industry by Yole Développement," 2012.

[2] B. Wunderle and B. Michel, "Progress in reliability research in the micro and nano region," *Microelectron. Reliab.*, vol. 46, no. 9–11, pp. 1685–1694, Sep. 2006.

[3] S. Gurrum and S. Suman, "Thermal Issues in Next-Generation Integrated Circuits," *IEEE Trans. Device Mater. Reliab.*, vol. 4, no. 4, pp. 709–714, 2004.

[4] E. Suhir, "Thermal Stress Failures in Electronics and Photonics: Physics, Modeling, Prevention," *J. Therm. Stress.*, vol. 36, no. 6, pp. 537–563, Jun. 2013.

[5] Y. A. Cengel, "Cooling of electronic equipment," in *Heat and Mass Transfer: AParactical Approach*, 2007.

[6] "Military Handbook Reliability Prediction of Electronic Equipment, MIL-HDBK-217F," 1992.

[7] S. Arrhenius, *Über die Reaktionsgeschwindigkeit bei der Inversion von Rohrzucker durch Säuren*. Wilhelm Engelmann, 1889, p. 248.

[8] S. V Garimella, L. Yeh, and T. Persoons, "Thermal Management Challenges in Telecommunication Systems and Data Centers," *IEEE Trans. COMPONENTS*, vol. 2, no. 8, pp. 1307–1316, 2012.

[9] B. Canis, "Battery Manufacturing for Hybrid and Electric Vehicles : Policy Issues," 2013.

[10] A. A. Pesaran, "Battery Thermal Management in EVs and HEVs : Issues and Solutions," in *Advanced Automotive Battery Conference*, 2001, pp. 1–10.

[11] L. R. Inc, "Thermal Management for LEDs and Power Electronics Grows to $ 4 . 8 Billion in 2020," 2014.

[12] "Available at: www.bccresearch.com/report/thermal-management-technologies-market." .

[13] G. Moore, "Cramming more components onto integrated circuits," *J. Electron.*, vol. 86, no. 1, pp. 114–117, 1965.

[14] B. K. Bose, *Power Electronics And Motor Drives: Advances and Trends*. 2006, pp. 1–100.

[15] D. O. Neacsu, “Integrated circuits for power electronics applications,” in *2010 IEEE International Symposium on Industrial Electronics*, 2010, pp. 4121–4169.

[16] R. J. McGlen, R. Jachuck, and S. Lin, “Integrated thermal management techniques for high power electronic devices,” *Appl. Therm. Eng.*, vol. 24, no. 8–9, pp. 1143–1156, Jun. 2004.

[17] Z. Zuo, L. R. Hoover, and A. L. Phillips, “Advanced thermal architecture for cooling of high power electronics,” *IEEE Trans. Components Packag. Technol.*, vol. 25, no. 4, pp. 629–634, Dec. 2002.

[18] M. Marz, “Thermal management in high-density power converters,” in *IEEE International Conference on ICIT*, 2003, pp. 1196–1201.

[19] M. Gerber and M. Marz, “System integration in automotive power systems,” in *Power Electronics and Applications*, 2005, pp. 1–10.

[20] M. a. Ebadian and C. X. Lin, “A Review of High-Heat-Flux Heat Removal Technologies,” *J. Heat Transfer*, vol. 133, no. 11, p. 110801, 2011.

[21] I. Mudawar, “Assessment of high-heat-flux thermal management schemes,” *Trans. Components Packag. Technol. IEEE*, vol. 24, no. 2, pp. 122–141, 2001.

[22] Y. Mitsutake and M. Monde, “Ultra High Critical Heat Flux During Forced Flow Boiling Heat Transfer With an Impinging Jet,” *J. Heat Transfer*, vol. 125, no. 6, p. 1038, 2003.

[23] Ericsson, “Traffic and Market Report on the Pulse of the Networked Society,” 2012.

[24] N. Beratlis and M. K. Smith, “Optimization of Synthetic Jet Cooling for Microelectronics Applications,” in *19th IEEE SEMI-THERM Symposium*, 2003, pp. 66–73.

[25] T. Cader and D. Tilton, “Implementing Spray Cooling Thermal Management in High Heat Flux Applications,” in *International Society Conference on Thermal Phenomena*, 2004, pp. 699–701.

[26] T. Açikalin, S. M. Wait, S. V. Garimella, and A. Raman, “Experimental Investigation of the Thermal Performance of Piezoelectric Fans,” *Heat Transf. Eng.*, vol. 25, no. 1, pp. 4–14, Jan. 2004.

[27] H. Oprins, S. Member, G. Van Der Veken, C. C. S. Nicole, C. J. M. Lasance, A. Member, and M. Baelmans, “On-Chip Liquid Cooling With Integrated Pump Technology,” *IEEE Trans. Components Packag. Technol.*, vol. 30, no. 2, pp. 209–217, 2007.

[28] a. Miner and U. Ghoshal, “Cooling of high-power-density microdevices using liquid metal coolants,” *Appl. Phys. Lett.*, vol. 85, no. 3, p. 506, 2004.

[29] S. C. Mohapatra and D. Loikits, “Advances in Liquid Coolant Technologies for Electronics Cooling,” in *21st IEEE SEMI-THERM Symposium*, 2005.

[30] P. Bagnoli, C. Casarosa, and M. Ciampi, “Thermal resistance analysis by induced transient (TRAIT) method for power electronic devices thermal characterization. I. Fundamentals and theory,” in *IEEE Transaction on Power Electronics*, 1998, vol. 13, no. 6, pp. 1208–1219.

[31] S. P. Gurrum, Y. K. Joshi, and J. Kim, “Thermal Management of High Temperature Pulsed Electronics Using Metallic Phase Change Materials,” *Numer. Heat Transf. Part A Appl.*, vol. 42, no. 8, pp. 777–790, Dec. 2002.

[32] F. L. Tan and S. C. Fok, “Numerical Investigation of Phase Change Material-Based Heat Storage Unit on Cooling of Mobile Phone,” *Heat Transf. Eng.*, vol. 33, no. 6, pp. 494–504, Apr. 2012.

[33] S. Moghaddam, M. Rada, a. Shooshtari, M. Ohadi, and Y. Joshi, “Evaluation of analytical models for thermal analysis and design of electronic packages,” *Microelectronics J.*, vol. 34, no. 3, pp. 223–230, Mar. 2003.

[34] X. Luo, Z. Mao, J. Liu, and S. Liu, “An analytical thermal resistance model for calculating mean die temperature of a typical BGA packaging,” *Thermochim. Acta*, vol. 512, no. 1–2, pp. 208–216, Jan. 2011.

[35] S. Liu, B. Leung, A. Neckar, S. O. Memik, G. Memik, and N. Hardavellas, “Hardware/software techniques for DRAM thermal management,” in *Proceedings of HPCA*, 2011, pp. 515–525.

[36] R. Zhao, L. Gosselin, M. Fafard, and D. P. Ziegler, “Heat transfer in upper part of electrolytic cells: Thermal circuit and sensitivity analysis,” *Appl. Therm. Eng.*, vol. 54, no. 1, pp. 212–225, May 2013.

[37] a. A. El-Nasr and S. M. El-Haggar, “Effective thermal conductivity of heat pipes,” *Heat Mass Transf.*, vol. 32, no. 1–2, pp. 97–101, Nov. 1996.

[38] J. Zuo and A. Faghri, “A network thermodynamic analysis of the heat pipe,” *Int. J. Heat Mass Transf.*, vol. 41, no. 11, pp. 1473–1484, 1998.

[39] H. Shabgard and A. Faghri, “Performance characteristics of cylindrical heat pipes with multiple heat sources,” *Appl. Therm. Eng.*, vol. 31, no. 16, pp. 3410–3419, Nov. 2011.

[40] F. Romary and A. Caldeira, “Thermal modelling to analyze the effect of cell temperature on PV modules energy efficiency,” in *Proceeding of Power Electronics and Applications (EPE 2011)*, 2011, vol. 48, pp. 1 – 9.

[41] P. G. Del Valle and D. Atienza, “Emulation-based transient thermal modeling of 2D/3D systems-on-chip with active cooling,” *Microelectronics J.*, vol. 42, no. 4, pp. 564–571, Apr. 2011.

[42] M. Barcella, W. Huang, K. Skadron, and M. Stan, “Architecture-Level Compact Thermal R-C Modeling,” 2002.

[43] M. R. Stan, K. Skadron, M. Barcella, W. Huang, K. Sankaranarayanan, and S. Velusamy, “HotSpot: a dynamic compact thermal model at the processor-architecture level,” *Microelectronics J.*, vol. 34, no. 12, pp. 1153–1165, Dec. 2003.

[44] P. Magnone, C. Fiegna, G. Greco, G. Bazzano, S. Rinaudo, and E. Sangiorgi, “Numerical simulation and modeling of thermal transient in silicon power devices,” *Solid. State. Electron.*, vol. 88, pp. 69–72, Oct. 2013.

[45] P. Cova, M. Bernardoni, N. Delmonte, and R. Menozzi, “Dynamic electro-thermal modeling for power device assemblies,” *Microelectron. Reliab.*, vol. 51, no. 9–11, pp. 1948–1953, Sep. 2011.

[46] B. López-Walle, M. Gauthier, and N. Chaillet, “Dynamic modelling for thermal micro-actuators using thermal networks,” *Int. J. Therm. Sci.*, vol. 49, no. 11, pp. 2108–2116, Nov. 2010.

[47] M. Miana and C. Cortés, “Transient thermal network modeling applied to multiscale systems. Part II: application to an electronic control unit of an automobile,” *IEEE Trans. Adv. Packag.*, vol. 33, no. 4, pp. 938–952, 2010.

[48] M. Miana and C. Cortés, “Transient thermal network modeling applied to multiscale systems. Part I: definition and validation,” *IEEE Trans. Adv. Packag.*, vol. 33, no. 4, pp. 924–937, 2010.

[49] A. P. Ramallo-González, M. E. Eames, and D. a. Coley, “Lumped parameter models for building thermal modelling: An analytic approach to simplifying complex multi-layered constructions,” *Energy Build.*, vol. 60, pp. 174–184, May 2013.

[50] A. Buonomano and A. Palombo, “Building energy performance analysis by an in-house developed dynamic simulation code: An investigation for different case studies,” *Appl. Energy*, vol. 113, pp. 788–807, Jan. 2014.

[51] A. Athienitis, “Modeling and Simulation of Passive and Active Solar Thermal Systems,” in *Comprehensive Renewable Energy*, vol. 3, Elsevier Ltd., 2012, pp. 357–418.

[52] K. Skadron, M. R. Stan, W. Huang, S. Velusamy, K. Sankaranarayanan, and D. Tarjan, “Temperature-Aware Microarchitecture : Extended Discussion and Results,” 2003.

[53] K. Skadron and M. Stan, “Temperature-aware microarchitecture: Modeling and implementation,” *ACM Trans. …*, vol. 1, no. 1, pp. 94–125, 2004.

[54] W. Huang and S. Ghosh, “HotSpot: A compact thermal modeling methodology for early-stage VLSI design,” *Very Large Scale Integr. Syst. IEEE Trans.*, vol. 14, no. 5, pp. 501–513, 2006.

[55] W. Huang, M. Stan, K. Skadron, K. Sankaranarayanan, S. Ghosh, and S. Velusamy, “Compact thermal modeling for temperature-aware design,” in *Proceedings of the 41st annual Design Automation Conference. ACM*, 2004, pp. 878–883.

[56] A. G. Kokkas, “Thermal Analysis of Multiple-Layer Structures,” *IEEE Trans. Electron Devices*, vol. ED-21, no. 11, pp. 674–681, 1974.

[57] V. Kadambi and N. Abuaf, “An Analysis of the Thermal Response of Power Chip Packages,” *IEEE Trans. Electron Devices*, vol. ED-32, no. 6, pp. 1024–1033, 1985.

[58] J. Albers, “An exact recursion relation solution for the steady-state surface temperature of a general multilayer structure,” *IEEE Trans. Components, Packag. Manuf. Technol. Part A*, vol. 18, no. 1, pp. 31–38, Mar. 1995.

[59] M. M. Yovanovich, Y. S. Muzychka, and J. R. Culham, “Spreading Resistance of Isoflux Rectangles and Strips on Compound Flux Channel,” *J. Thermophys. Heat Transf.*, vol. 13, no. 4, pp. 495–500, 1999.

[60] J. R. Culham, M. M. Yovanovich, and T. F. Lemczyk, “Thermal Characterization of Electronic Packages Using a Three-Dimensional Fourier Series Solution,” *J. Electron. Packag.*, vol. 122, no. 3, pp. 233–239, 2000.

[61] Y. S. Muzychka, J. R. Culham, and M. M. Yovanovich, “Thermal Spreading Resistances In Rectangular Flux Channels Part II - Edge Cooling,” in *36th AIAA Thermophysics Conference*, 2003.

[62] Y. S. Muzychka, J. R. Culham, and M. M. Yovanovich, “Thermal Spreading Resistance of Eccentric Heat Sources on Rectangular Flux Channels,” *J. Electron. Packag.*, vol. 125, no. 2, pp. 178–185, 2003.

[63] Y. S. Muzychka, “Influence Coefficient Method for Calculating Discrete Heat Source Temperature on Finite Convectively Cooled Substrates,” *IEEE Trans. Components Packag. Technol.*, vol. 29, no. 3, pp. 636–643, Sep. 2006.

[64] S. Karmalkar, P. V. Mohan, and B. P. Kumar, “A unified compact model of electrical and thermal 3-D spreading resistance between eccentric rectangular and circular contacts,” *IEEE Electron Device Lett.*, vol. 26, no. 12, pp. 909–912, Dec. 2005.

[65] B. Dan, J. F. Geer, and B. G. Sammakia, “Heat Conduction in a Rectangular Tube With Eccentric Hot Spots,” *J. Therm. Sci. Eng. Appl.*, vol. 3, no. 4, p. 041002, 2011.

[66] T. M. Ying and K. C. Toh, “A heat spreading resistance model for anisotropic thermal conductivity materials in electronic packaging,” in *The Seventh Intersociety Conference on Thermal and Thermomechanical Phenomena in Electronic Systems (Cat. No.00CH37069)*, 2000, pp. 314–321.

[67] T. T. Lam, W. D. Fischer, and P. S. Cabral, “Analysis of Thermal Resistance of Orthotropic Materials Used for Heat Spreaders,” *J. Thermophys. Heat Transf.*, vol. 18, no. 2, pp. 203–208, Apr. 2004.

[68] Y. S. Muzychka, M. M. Yovanovich, and J. R. Culham, “Thermal Spreading Resistance in Compound and Orthotropic Systems,” *J. Thermophys. Heat Transf.*, vol. 18, no. 1, pp. 45–51, Jan. 2004.

[69] Y. S. Muzychka, “Spreading Resistance in Compound Orthotropic Flux Tubes and Channels with Interfacial Resistance,” *J. Thermophys. Heat Transf.*, vol. 28, no. 2, pp. 313–319, Apr. 2014.

[70] Y. S. Muzychka, M. M. Yovanovich, and J. R. Culham, “Thermal Spreading Resistances in Rectangular Flux Channels Part I - Geometric Equivalences,” in *36th AIAA Thermophysics Conference*, 2003.

[71] M. M. Yovanovich, “Thermal Resistances of Circular Source on Finite Circular Cylinder With Side and End Cooling,” *J. Electron. Packag.*, vol. 125, no. 2, p. 169, 2003.

[72] Y. Rahmani and H. Shokouhmand, “Assessment of Temperature-Dependent Conductivity Effects on the Thermal Spreading/Constriction Resistance of Semiconductors,” *J. Thermophys. Heat Transf.*, vol. 26, no. 4, pp. 638–643, Oct. 2012.

[73] Y. S. Muzychka, “Thermal Spreading Resistance in Compound Orthotropic Circular Disks and Rectangular Channels with Interfacial Resistance,” in *44th AIAA Thermophysics*, 2013, pp. 1–11.

[74] B. Suman, S. De, and S. DasGupta, “Transient modeling of micro-grooved heat pipe,” *Int. J. Heat Mass Transf.*, vol. 48, no. 8, pp. 1633–1646, Apr. 2005.

[75] B. Suman, “A steady state model and maximum heat transport capacity of an electrohydrodynamically augmented micro-grooved heat pipe,” *Int. J. Heat Mass Transf.*, vol. 49, no. 21–22, pp. 3957–3967, Oct. 2006.

[76] Y. Zhang and A. Faghri, “Advances and Unsolved Issues in Pulsating Heat Pipes,” *Heat Transf. Eng.*, vol. 29, no. 1, pp. 20–44, Jan. 2008.

[77] “Available at: http://www.engr.uconn.edu/me/cms/people/9-people/people/50-amirjournals.” .

[78] N. Zhu and K. Vafai, “Analysis of cylindrical heat pipes incorporating the e□ffects of liquid-vapor coupling and non-Darcian transport-a closed form solution,” *Int. J. Heat Mass Transf.*, vol. 42, pp. 3405–3418, 1999.

[79] M. Aghvami and A. Faghri, “Analysis of flat heat pipes with various heating and cooling configurations,” *Appl. Therm. Eng.*, vol. 31, no. 14–15, pp. 2645–2655, Oct. 2011.

[80] C. Ferrandi, F. Iorizzo, M. Mameli, S. Zinna, and M. Marengo, “Lumped parameter model of sintered heat pipe: Transient numerical analysis and validation,” *Appl. Therm. Eng.*, vol. 50, no. 1, pp. 1280–1290, Jan. 2012.

[81] K. Sadik and Y. Yener, “One-Dimentional Steady-State Heat Conduction,” in *Heat Conduction*, 3rd ed., Washington, DC: Taylor & Francis, 1993, pp. 45–93.

[82] “http://www.mathworks.com/.” .

[83] “http://www.linear.com/designtools/software/.”

[84] “http://cirlab.det.unifi.it/Sapwin/.”

[85] Z. J. Zuo and A. Faghri, “Boundary element approach to transient heat pipe analysis,” *Numer. Heat Transf.*, vol. 32, pp. 205 – 220, 1997.

[86] F. Incropera, D. DeWitt, and T. Bergrnan, *Fundamentals of Heat and Mass Transfer (The 6th Edition)*, 6th ed. 2007, pp. 559–780.

[87] “Available at: http://www.frostytech.com/.” .

[88] W. Kuo, T. Wu, H. Lu, and T. Lo, “Microstructures and Mechanical Properties of Nano-Flake Graphite Composites,” in *16th International Conference on Composite Materials*, 2007.

[89] L. Dai, “Functionalization of Graphene for Efficient Energy Conversion and Storage,” *Acc. Chem. Res.*, vol. 46, no. 1, pp. 31–42, 2013.

[90] D. D. L. Chung and Y. Takizawa, “Performance of Isotropic and Anisotropic Heat Spreaders,” *J. Electron. Mater.*, vol. 41, no. 9, pp. 2580–2587, Jun. 2012.

[91] J. Norley, J. Tzeng, and G. Getz, “The Development of a Natural Graphite Heat-Spreader,” in *Seventeenth IEEE SEMI*, 2001, pp. 107–110.

[92] Y. Taira, S. Kohara, and K. Sueoka, “Performance improvement of stacked graphite sheets for cooling applications,” *2008 58th Electron. Components Technol. Conf.*, pp. 760–764, May 2008.

[93] Panasonic Electronic Devices Co., “Pyrolitic Graphite Sheet.” [Online]. Available: http://www.panasonic.com/industrial/demo/en_demo.asp.

[94] K. F. Kelly and W. E. Billups, “Synthesis of soluble graphite and graphene.,” *Acc. Chem. Res.*, vol. 46, no. 1, pp. 4–13, Jan. 2013.

[95] P. J. Oliver, “Partial Differential Equations in Three – Dimensional Space,” in *Introduction to Partial Differential Equations*, 2012, pp. 972–1023.

[96] “COMSOL Multiphysics 4.2a.” [Online]. Available: http://www.comsol.com/4.2a/.

[97] E. Sadeghi, N. Djilali, and M. Bahrami, “A novel approach to determine the in-plane thermal conductivity of gas diffusion layers in proton exchange membrane fuel cells,” *J. Power Sources*, vol. 196, no. 7, pp. 3565–3571, Apr. 2011.

[98] M. S. Ismail, T. Damjanovic, D. B. Ingham, L. Ma, and M. Pourkashanian, “Effect of polytetrafluoroethylene-treatment and microporous layer-coating on the in-plane permeability of gas diffusion layers used in proton exchange membrane fuel cells,” *J. Power Sources*, vol. 195, no. 19, pp. 6619–6628, Oct. 2010.

[99] N. Zamel, X. Li, J. Shen, J. Becker, and A. Wiegmann, “Estimating effective thermal conductivity in carbon paper diffusion media,” *Chem. Eng. Sci.*, vol. 65, no. 13, pp. 3994–4006, Jul. 2010.

[100] N. Alhazmi, M. S. Ismail, D. B. Ingham, K. J. Hughes, L. Ma, and M. Pourkashanian, “The in-plane thermal conductivity and the contact resistance of the components of the membrane electrode assembly in proton exchange membrane fuel cells,” *J. Power Sources*, vol. 241, pp. 136–145, Nov. 2013.

[101] C. . Heusch, H.-G. Moser, and A. Kholodenko, “Direct measurements of the thermal conductivity of various pyrolytic graphite samples (PG,TPG) used as thermal dissipation agents in detector applications,” *Nucl. Instruments Methods Phys. Res. Sect. A*, vol. 480, no. 2–3, pp. 463–469, Mar. 2002.

[102] M. Bahrami, J. R. Culham, M. M. Yovanovich, and G. E. Schneider, “Thermal Contact Resistance of Nonconforming Rough Surfaces, Part 1: Contact Mechanics Model,” *J. Thermophys. Heat Transf.*, vol. 18, no. 2, pp. 209–217, Apr. 2004.

Appendix A

Uncertainty analysis

Uncertainties are classified into two groups; Random and systematic. The random uncertainty can be treated statistically but the systematic one which comes from the accuracy of the instrument cannot be treated much. The more an experiment is repeated the more the random uncertainty will be diminished but the systematic error which is an inherent characteristic of the experimental setup will remain unchanged. So, in the best case, the total uncertainty of an experiment is equal to its systematic uncertainty. In most of the experiments where the results are reported based on only one test, it is already assumed that the random error equal to zero and the reported uncertainty includes only the systematic one. There is not a clear theory that tells how to combine in general the two random and systematic uncertainties. But there is an approximation which says that these two have to combine in quadrature which for a function *K* is given in Eq.(51),

$$\delta k_{tot} = \sqrt{(\delta k_{sys})^2 + (\delta k_{ran})^2} \tag{51}$$

After finding the total uncertainty, the function K is shown as follows,

$$K = \overline{K}_n + \delta k_{tot} \tag{52}$$

Where, $\overline{K}_n$ is the average of *K* for *n* repetitions of the experiment and δk_{ran} is the standard deviation. For the measurement uncertainty, δk_{sys} of the function *K* which is a function of *m* parameters, the following general relation is used,

$$\delta k_{sys} = \sqrt{\left(\frac{\partial K}{\partial X_1}\delta x_1\right)^2 + \left(\frac{\partial K}{\partial X_2}\delta x_2\right)^2 + \ldots + \left(\frac{\partial K}{\partial X_m}\delta x_m\right)^2} \tag{53}$$

If the function K is the product of *m* independent variables in the form of $K = X_1^{s_1} X_2^{s_2} ... X_m^{s_m}$, the general form of uncertainty, Eq.(53), will be reduced to the percentage uncertainty in the following form,

$$\frac{\delta k_{sys}}{K} = \sqrt{\left(s_1 \frac{\delta x_1}{X_1}\right)^2 + \left(s_2 \frac{\delta x_2}{X_2}\right)^2 + ... + \left(s_m \frac{\delta x_m}{X_m}\right)^2} \tag{54}$$

During the experimental part of this study, different parameters such as, temperature, voltage, current and length were directly measured. All the measurement tools have an uncertainty which is reported in Table A.1. Based on those measurements, some secondary parameters such as power, thermal resistance, thermal conductivity and thermal capacitance were calculated. The uncertainties of the secondary parameters are calculated based on Eq.(53), and their corresponding functions are listed in Table A.1.

Table A.1: Experimental parameters uncertainty

Parameter	Description	Measurement type	Function	Maximum uncertainty
T	Temperature	direct	-	±0.5˚C
V	Voltage	direct	-	AC (VARIAC): ±0.1V DC (Chroma): ±0.01V
I	Current	direct	-	DC (Chroma): ±0.01A Ammeter: ±0.01A
L	Length	direct	-	Caliper: 0.00001m Ruler: 0.0005m
P	Power	indirect	V×I	-
R	Resistance	indirect	Eq. (1)	-
C	Capacitance	indirect	Eq. (2)	-
k	Thermal conductivity	indirect	Eq. (50)	-

Appendix B

Steady state criterion

A criterion for achieving steady state condition is established. According to this criterion, when the slope of temperature over time becomes less than 1 [˚C/hrs], the system can be considered steady state (Eq.(55)).

$$\text{Steady state criteria: } \frac{\partial T}{\partial t} = \frac{\text{Temp. diff. variation}}{\text{One hour}} \leq 1 \left[\frac{^{\circ}C}{hr}\right] \tag{55}$$